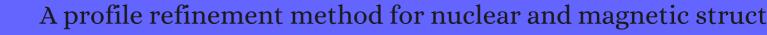
## CITATION REPORT List of articles citing



DOI: 10.1107/s0021889869006558 Journal of Applied Crystallography, 1969, 2, 65-71.

Source: https://exaly.com/paper-pdf/9835749/citation-report.pdf

Version: 2024-04-23

This report has been generated based on the citations recorded by exaly.com for the above article. For the latest version of this publication list, visit the link given above.

The third column is the impact factor (IF) of the journal, and the fourth column is the number of citations of the article.

#	Paper	IF	Citations
2270	Spin structure and magnetic anisotropy of Cr5S6 and rhombohedral Cr2S3. <b>1971</b> , 32, 581-590		42
2269	The crystallographic and magnetic structures of La1\(\text{\text{B}}\)BaxMn1\(\text{\text{M}}\)MexO3 (Me = Mn or Ti). <b>1971</b> , 3, 238-242	<u>-</u>	338
2268	Preparation, crystal structure, and magnetic structure of LiCrS2 and LiVS2. <b>1971</b> , 3, 590-595		109
2267	Magnetic and crystallographic structures of MexNbS2 and MexTaS2. <b>1971</b> , 3, 154-160		109
2266	Magnetic Structure, Magnetization, and Short-Range Spin Correlations in the Ising Linear-Chain Antiferromagnet CsCoCl312H2O. <b>1972</b> , 6, 2669-2676		19
2265	Neutron-diffraction determination of magnetic structures. <b>1972</b> , 8, 161-182		29
2264	The crystallographic and magnetic structure of Ni(IO3)2.2D2O. <b>1972</b> , 57, 215-220		6
2263	Magnetic structure and space group of the garnet Ca3Fe2(GeO4)3. <b>1972</b> , 10, 529-531		26
2262	Magnetic structure and space group of the garnet Ca3Cr2(GeO4)3. <b>1972</b> , 11, 645-647		18
2261	Rhombohedral Magnetic Structure in Spessartite Type Garnets. <b>1973</b> , 55, K159-K163		31
2260	Crystal structures and magnetic structures of some metal(I) chromium(III) sulfides and selenides. <b>1973</b> , 6, 574-582		175
2259	The magnetic structure of KCrS2. <b>1973</b> , 6, 384-386		43
2258	The crystal structure of Ni5TiB2O10. <b>1973</b> , 8, 1285-1292		25
2257	Location of hydrogen atoms in ADP by neutron powder profile refinement. <b>1973</b> , 246, 90-1		40
2256	Cubic-tetragonal-orthorhombic-rhombohedral ferroelectric transitions in perovskite potassium niobate: neutron powder profile refinement of the structures. <b>1973</b> , 6, 2559-2572		355
2255	Structure of rhombohedral ferroelectric barium titanate. <b>1973</b> , 6, 215-218		70
2254	Magnetic properties of NdZn. <b>1974</b> , 4, 1517-1521		12

2253	Studies of the magnetic structure of Fe3P. <b>1974</b> , 7, 1344-1352	65
2252	Magnetic properties and magnetic structure of ∃-NaFeO2. <b>1974</b> , 23, 683-688	13
2251	The Magnetic Structure of Tm2Fe17. <b>1974</b> , 24, K125-K127	20
2250	A neutron-diffraction study on the structural relationships of RCo5 hydrides. <b>1974</b> , 35, 301-306	57
2249	Neutron diffraction study of the crystal and magnetic structure of the ionic ferromagnet Cs2CrCl4. <b>1974</b> , 15, 313-316	20
2248	Preparation of compounds A2CuCl4NBrx (A=K,Rb,NH4,Tl; x=0,1,2) and crystal structures of compounds Rb2CuCl4NBrx with ordered distribution of the anions. <b>1974</b> , 9, 345-352	26
2247	The structures of some titanium-niobium oxides by powder neutron diffraction. <b>1974</b> , 338, 311-326	32
2246	A neutron diffraction study of the hydrides of the early lanthanide elements at room temperature. <b>1974</b> , 7, 2409-2416	88
2245	Was tragen heute die Beugungsmethoden zur modernen Erkenntnis Ber chemische Bindung, Dynamik und kooperative Eigenschaften der kristallisierten Materie bei?. <b>1975</b> , 79, 935-943	1
2244	The study of covalency by magnetic neutron scattering. <b>1975</b> , 1-87	20
2243	The structures of fluorides X. Neutron powder diffraction profile studies of UF6 at 193°K and 293°K. <b>1975</b> , 14, 378-382	20
2242	The structures of fluorides XIII: The orthorhombic form of tungsten hexafluoride at 193°K by neutron diffraction. <b>1975</b> , 15, 360-365	21
2241	Etude par diffraction neutronique de la forme haute pression de FeOOH. <b>1975</b> , 17, 1505-1510	30
2240	X-ray and neutron diffraction study of intermediate phases in nonstoichiometric cerium dioxide. <b>1975</b> , 15, 344-351	64
2239	Determination of the ratios of polytypes in a silicon carbide grit using neutron diffraction. <b>1975</b> , 10, 189-192	4
2238	Magnetic order in the pseudo-binary system Th(Fe1⊠Nix)5. <b>1975</b> , 29, 595-600	26
2237	Magnetic order and magnetic history effects in ThCo5xNi5Bx. <b>1975</b> , 30, 177-186	29
2236	Design for a conventional high-resolution neutron powder diffractometer. <b>1975</b> , 127, 361-370	72

2235	Structure and order parameters in the pressure-induced continuous transition in TeO2. <b>1975</b> , 12, 1899-1907	71
2234	Magnetic properties of some light rareBarth compounds with CsCl structure. <b>1975</b> , 46, 1352-1354	36
2233	Recent structural studies of the KH2PO4-KD2PO4 system. <b>1976</b> , 14, 591-593	23
2232	Role of crystallography. <b>1976</b> , 29, 34-42	2
2231	Crystal structure of Ba2Bi3+Bi5+O6. <b>1976</b> , 19, 969-973	365
2230	The structures of fluorides. XV. Neutron diffraction-kubic harmonic profile analysis of the body-centered cubic phase of sulfur hexafluoride at 193°K. <b>1976</b> , 18, 241-246	32
2229	Metamagnetism of CoMnSi. <b>1976</b> , 35, K69-K72	26
2228	Crystal and magnetic structure of NiMnGe. <b>1976</b> , 38, 721-729	134
2227	Multicomponent profile refinement of time-of-flight neutron diffraction data. <b>1976</b> , 137, 331-337	46
2226	D1A, a high resolution neutron powder diffractometer with a bank of mylar collimators. <b>1976</b> , 137, 463-471	140
2225	Synthesis and crystal structure of (ThCu3)(Mn3+2Mn4+2)O12, a new ferrimagnetic perovskite-like compound. <b>1976</b> , 19, 45-51	66
2224	Isotope effects in the bonds of €CrOOH and €CrOOD. <b>1976</b> , 19, 299-304	36
2223	Crystallographic and magnetic structure of CoCl2[6D2O and CoBr2[6D2O. 1976, 14, 2119-2125	11
2222	Magnetic properties and structure of chromium niobium oxide and iron tantalum oxide. <b>1976</b> , 9, 2601-2610	19
2221	The structural phase transition in octafluoronaphthalene. <b>1977</b> , 10, 1133-1149	4
2220	The magnetic structure of ErFe3. <b>1977</b> , 7, 1885-1890	23
2219	On the use of Guinier-H⁄gg film data for structure analysis. <b>1977</b> , 145, 310-320	21
2218	Neutron diffraction study of the structure and phase transitions of alkali cyanide crystals. <b>1977</b> , 66, 5147-514	9 <sub>74</sub>

2217	The structures of fluorides⊠VII. <b>1977</b> , 39, 1989-1991	16
2216	Crystal and magnetic structure of KFeO2. <b>1977</b> , 38, 1117-1123	33
2215	Neutron powder profile studies of the gamma uranium trioxide phases. <b>1977</b> , 20, 9-19	48
2214	Preparation and crystal structure of 町a2N. <b>1977</b> , 20, 205-207	32
2213	Isotope effects in the bonds of ⊞-CrOOH and ⊞-CrOOD. <b>1977</b> , 21, 325-329	50
2212	Profile analysis of powder neutron diffraction data: Its scope, limitations, and applications in solid state chemistry. <b>1977</b> , 21, 253-275	109
2211	Neutron scattering study of the magnetism of Rb2CrCl4, a two-dimensional easy-plane ferromagnet. <b>1977</b> , 86-88, 657-659	20
2210	The crystal structure of the intercalates SnTaS2 and SnNbS2. <b>1977</b> , 12, 1057-1062	24
2209	Synthesis and structures of compounds NaxVSe2. <b>1977</b> , 12, 1103-1110	14
2208	The cation distribution in Zn2Mg(PO4)2 determined by X-ray profile-fitting refinements. <b>1977</b> , 12, 563-568	21
2207	Structural studies of the (La, Sr) CrO3 system. <b>1977</b> , 12, 463-471	132
2207	Structural studies of the (La, Sr) CrO3 system. <b>1977</b> , 12, 463-471  The structure refinement of boehmite (-A100H) and the study of its structural variability based on Guinier-H\(\bar{G}\)g powder data. <b>1977</b> , 12, 1213-1219	
,	The structure refinement of boehmite (-A100H) and the study of its structural variability based on Guinier-Hgg powder data. <b>1977</b> , 12, 1213-1219	132
2206	The structure refinement of boehmite (-A100H) and the study of its structural variability based on Guinier-Hgg powder data. <b>1977</b> , 12, 1213-1219  Calcium hydride and deuteride studied by neutron diffraction and NMR. <b>1977</b> , 20, 93-101	132 25
2206 2205 2204	The structure refinement of boehmite (-A100H) and the study of its structural variability based on Guinier-Hgg powder data. 1977, 12, 1213-1219  Calcium hydride and deuteride studied by neutron diffraction and NMR. 1977, 20, 93-101	132 25 64
2206 2205 2204	The structure refinement of boehmite (-A100H) and the study of its structural variability based on Guinier-H2g powder data. 1977, 12, 1213-1219  Calcium hydride and deuteride studied by neutron diffraction and NMR. 1977, 20, 93-101  Etude par diffraction neutronique de l'oxyhydroxyde de chrome ©CrOOH. 1977, 43, 81-88  Strukturparameter von TlPd3O4 aus einem Neutronen-Pulverdiagramm. 1978, 443, 19-22	132 25 64
2206 2205 2204 2203	The structure refinement of boehmite (-A100H) and the study of its structural variability based on Guinier-Hgg powder data. 1977, 12, 1213-1219  Calcium hydride and deuteride studied by neutron diffraction and NMR. 1977, 20, 93-101  Etude par diffraction neutronique de l'oxyhydroxyde de chrome €CrOOH. 1977, 43, 81-88  Strukturparameter von TlPd3O4 aus einem Neutronen-Pulverdiagramm. 1978, 443, 19-22  On the Structure of Bismuthsesquioxide: The ⊕, ∰and ⊕phase. 1978, 444, 151-166	132 25 64 10 8

2199	Magnetic and specific heat measurements on polycrystalline samples of some rare-earth zirconium sulphides. <b>1978</b> , 93, 1-23	14
2198	Highlights of synchrotron radiation. <b>1978</b> , 43, 337-375	11
2197	Oxydes de plomb. IV. Evolution structurale de l'oxyde Pb3O4 entre 240 et 5°K et mbanisme de la transition. <b>1978</b> , 23, 327-339	36
2196	X-ray powder profile refinement of zirconium in #hombohedral boron. <b>1978</b> , 26, 275-279	30
2195	A spherical sample container for neutron powder diffractometry. <b>1978</b> , 151, 201-203	
2194	Hydrogen molybdenum bronzes. <b>1978</b> , 7, 679-686	11
2193	Deuterium storage in FeTi. Measurement of desorption isotherms and structural studies by means of neutron diffraction. <b>1978</b> , 13, 931-946	73
2192	Structural studies on Li1NTa3O8NFx solid solutions by full-profile refinements of guinier-hgg X-ray film data. <b>1978</b> , 13, 1371-1378	1
2191	Residual stress measurements on chromium films by x-ray diffraction using the sin2[method. <b>1978</b> , 53, 65-71	20
2190	On the profile of X-ray diffraction lines in GUINIER powder diagrams. <b>1978</b> , 13, 569-575	2
	On the profile of X-ray diffraction lines in GUINIER powder diagrams. 1978, 13, 569-575  A neutron powder diffraction study of palladium tetrafluoride. 1978, 17, 748-749	22
2189		
2189	A neutron powder diffraction study of palladium tetrafluoride. <b>1978</b> , 17, 748-749	22
2189 2188 2187	A neutron powder diffraction study of palladium tetrafluoride. <b>1978</b> , 17, 748-749  Tetrachlorophosphonium oxotetrachlorochromate(V). <b>1978</b> , 17, 749-751	22
2189 2188 2187 2186	A neutron powder diffraction study of palladium tetrafluoride. 1978, 17, 748-749  Tetrachlorophosphonium oxotetrachlorochromate(V). 1978, 17, 749-751  Debye-Waller factor and thermal expansion of arsenic, antimony and bismuth. 1978, 11, 1043-1051	22 11 39
2189 2188 2187 2186 2185	A neutron powder diffraction study of palladium tetrafluoride. 1978, 17, 748-749  Tetrachlorophosphonium oxotetrachlorochromate(V). 1978, 17, 749-751  Debye-Waller factor and thermal expansion of arsenic, antimony and bismuth. 1978, 11, 1043-1051  The crystal structure of uranium pentabromide by powder neutron diffraction. 1978, 40, 1055-1057	22 11 39
2189 2188 2187 2186 2185	A neutron powder diffraction study of palladium tetrafluoride. 1978, 17, 748-749  Tetrachlorophosphonium oxotetrachlorochromate(V). 1978, 17, 749-751  Debye-Waller factor and thermal expansion of arsenic, antimony and bismuth. 1978, 11, 1043-1051  The crystal structure of uranium pentabromide by powder neutron diffraction. 1978, 40, 1055-1057  Neutron and X-ray diffraction investigation of deuterium storage in La7Ni3. 1978, 60, 1-9	22 11 39 13 63

2181	Neutron diffraction study of gamma iron titanium deuteride. <b>1979</b> , 9, L61-L66	61
2180	A qualitative x-ray powder diffraction study of the structures of strontium-barium zirconate solid solutions at room temperature. <b>1979</b> , 1, 49-60	1
2179	Magnetic and structural phase transitions in BaMnF4. <b>1979</b> , 19, 5754-5772	106
2178	Magnetic structure of TbFe3. <b>1979</b> , 50, 2006-2007	11
2177	The uses of pulsed neutron sources for research in magnetism and other areas of condensed matter physics. <b>1979</b> , 50, 1952-1957	5
2176	A neutron diffraction study of the structure of the antiferromagnet CopNi1BO. <b>1979</b> , 50, 7578	12
2175	The crystal growth and atomic structure of As2(Se, S)3 compounds. 1979, 39, 111-132	27
2174	Disordered structure of Na2CO3 at 400°C. <b>1979</b> , 96, 89-95	6
2173	Non-stoichiometry in anion-excess ReO3 phases; the structure of Zr0.8Yb0.2F3.2O0.3(MX3.5) by powder neutron diffraction. <b>1979</b> , 27, 163-178	19
2172	The distribution of the deuterium atoms in the deuterated hexagonal laves-phase ZrMn2D3. <b>1979</b> , 31, 47-50	120
2171	The distribution of the deuterium atoms in the deuterated cubic laves-phase ZrV2D4[5. <b>1979</b> , 32, 1087-1090	77
2170	Die Kristallstruktur von Li8PbO6. <b>1979</b> , 449, 102-104	5
2169	Die Kristallstruktur von Na2Pt(OD)6. <b>1979</b> , 453, 5-8	12
2168	Structure of lithiumBodium Balumina by powder neutron diffraction. <b>1979</b> , 278, 438-439	21
2167	Crystal growth and structure of BiVO4. <b>1979</b> , 14, 1571-1581	332
2166	Alkali metal location and tungsten off-center displacement in hexagonal potassium and cesium tungsten bronzes. <b>1979</b> , 14, 667-674	35
2165	A neutron diffraction study of the ferrimagnetic spinel NiCo2O4. <b>1979</b> , 14, 1013-1024	69
2164	A structural study of the hexagonal potassium tungsten bronze, K0.26WO3. <b>1979</b> , 14, 1397-1402	27

2163	Improved resolution and powder neutron diffraction research on the KSN-2 diffractometer. <b>1979</b> , 29, 846-852	7
2162	The structure and ferroelastic phase transition of BiVO4. <b>1979</b> , 1, 155-169	108
2161	Elastic and inelastic neutron studies of hydrogen molybdenum bronzes. <b>1979</b> , 28, 185-193	102
2160	Deuterium	14
2159	Structural phase transitions of FeTi-deuterides. <b>1979</b> , 14, 1281-1294	52
2158	The magnetic properties of CsCrCl3, an antiferromagnetic chain compound with single-ion anisotropy. <b>1979</b> , 14, 166-168	14
2157	Neutron powder diffraction studies of two-dimensional magnetic oxides. <b>1979</b> , 14, 159-162	50
2156	The magnetic structure of non-stoichiometric ferrous oxide. <b>1979</b> , 12, 337-345	94
2155	Preferential ordering of Mn and Fe Atoms in Y6(Fe1⊠Mnx)23. <b>1980</b> , 41, 1105-1109	19
2154	A neutron diffraction investigation of deuterated Pd3P0.80. <b>1980</b> , 32, 321-327	27
2153	Neutron Powder Diffraction Studies of Fluorite and Pyrochlore NdxZr1🛭 O2🗸/2 Solid Solutions with 0.25. <b>1980</b> , 101, 765-774	26
2152	Magnetic ordering in the chain compound KFeS2. <b>1980</b> , 57, K25-K30	19
2151	Crystal and magnetic structures of PrCo2Ge2 and HoCo2Ge2. <b>1980</b> , 58, 67-70	44
2150	Disorder in KNiCl3 as observed by electron diffraction. <b>1980</b> , 58, 481-488	17
2149	Structures of the high temperature phases of rubidium nitrate. <b>1980</b> , 58, 525-531	27
2148	Crystallographic and magnetic structure of RbCoCl3 🛮 2 D2O. <b>1980</b> , 98, 205-208	1
2147	On magnetic properties of UPb3 [A neutron diffraction study. <b>1980</b> , 102, 188-191	8
2146	A neutron diffraction study of H, Na-Y zeolites. <b>1980</b> , 41, 1089-1095	93

2145	Magnetic structure of NdB6. <b>1980</b> , 41, 1319-1321	67
2144	Neutron diffraction experiments on CsCrI3 at 300, 77, and 1.2 K. <b>1980</b> , 34, 65-70	16
2143	Neutron powder diffraction study of the structures of CeTaO4, CeNbO4, and NdTaO4. <b>1980</b> , 35, 167-175	43
2142	Ordering in solid solutions. <b>1980</b> , 35, 267-271	14
2141	Neutron powder diffraction and magnetic measurements on CsMnI3. <b>1980</b> , 35, 367-375	43
2140	Low temperature phase transitions and magnetic structure of PrB6. <b>1980</b> , 36, 861-868	53
2139	Crystal structure and magnetic properties of copper formate anhydrate [∃-Cu(HCOO)2]. <b>1980</b> , 34, 699-703	16
2138	The lineshapes in pulsed neutron powder diffraction. <b>1980</b> , 171, 107-113	21
2137	Temperature dependence of the crystal and magnetic structures of BiFeO3. <b>1980</b> , 13, 1931-1940	846
2136	LaAg x In1⊠. <b>1980</b> , 37, 39-45	22
2136 2135	LaAg x In1\( \text{N}. 1980, 37, 39-45\)  The cation distribution between five- and six-coordinated sites in some (Mg,)3(PO4)2) solid solutions. 1980, 15, 1183-1191	22
2135	The cation distribution between five- and six-coordinated sites in some (Mg,)3(PO4)2) solid	
2135	The cation distribution between five- and six-coordinated sites in some (Mg,)3(PO4)2) solid solutions. <b>1980</b> , 15, 1183-1191	25
2135	The cation distribution between five- and six-coordinated sites in some (Mg,)3(PO4)2) solid solutions. <b>1980</b> , 15, 1183-1191  Neutron diffraction investigation of Zr3Y4O12. <b>1980</b> , 15, 1419-1423	25
2135 2134 2133	The cation distribution between five- and six-coordinated sites in some (Mg,)3(PO4)2) solid solutions. 1980, 15, 1183-1191  Neutron diffraction investigation of Zr3Y4O12. 1980, 15, 1419-1423  Neutron and electron diffraction of the FeTi? D(H) - □ phase. 1980, 15, 627-634	25 25 23
2135 2134 2133 2132	The cation distribution between five- and six-coordinated sites in some (Mg,)3(PO4)2) solid solutions. 1980, 15, 1183-1191  Neutron diffraction investigation of Zr3Y4O12. 1980, 15, 1419-1423  Neutron and electron diffraction of the FeTi? D(H) - 🖟 phase. 1980, 15, 627-634  Crystallography of human tooth enamel: Initial structure refinement. 1980, 15, 17-29  Etude par diffraction de neutrons des structures magnEiques de TbBe 13 🖺 basse tempEature.	25 25 23 54
2135 2134 2133 2132 2131	The cation distribution between five- and six-coordinated sites in some (Mg,)3(PO4)2) solid solutions. 1980, 15, 1183-1191  Neutron diffraction investigation of Zr3Y4O12. 1980, 15, 1419-1423  Neutron and electron diffraction of the FeTi? D(H) - II phase. 1980, 15, 627-634  Crystallography of human tooth enamel: Initial structure refinement. 1980, 15, 17-29  Etude par diffraction de neutrons des structures magnEiques de TbBe 13 Ibasse tempEature. 1980, 41, 123-133	<ul><li>25</li><li>25</li><li>23</li><li>54</li><li>19</li></ul>

2127	X-Ray Diffraction Profile Analysis for the Determination of the Crystal Structure of BaTiO3. <b>1980</b> , 19, 1757-1762	9
2126	Cubic-to-tetragonal phase transition in RbCaF3 investigated by diffraction experiments with neutrons, x rays, and Irays from a MEsbauer source. <b>1980</b> , 21, 1209-1218	46
2125	野ESnF2 phase transition: neutron diffraction and NMR study. <b>1980</b> , 41, 1019-1024	17
2124	Structural studies of RbH2PO4in its paraelectric and ferroelectric phases. <b>1980</b> , 13, 4841-4853	55
2123	A neutron powder diffraction study of (V,Cr)3C2🛭. <b>1980</b> , 76, 145-151	10
2122	Structural investigation of Th6Mn23D16 by neutron diffraction. <b>1980</b> , 74, 97-102	25
2121	The deuterium site occupation in ZrV2Dx as a function of the deuterium concentration. <b>1980</b> , 73, 355-362	76
2120	Magnetic Properties of the NiMnGe1⊠Six system. <b>1980</b> , 15-18, 483-484	1
2119	The crystal structure of s-triazine at 5K. <b>1981</b> , 14, L929-L931	11
2118	Crystal structure of magnesium heptaboride Mg2B14. <b>1981</b> , 82, 325-334	49
2117	Application of the Rietveld Method for Structure Refinement with Powder Diffraction Data. <b>1981</b> , 1-23	7
2116	Investigations of crystal and magnetic properties of the Mn5⊠FexGe3 intermetallic compounds. <b>1981</b> , 23, 149-155	9
2115	Crystal and magnetic structure of CoMnGe, CoFeGe, FeMnGe and NiFeGe. <b>1981</b> , 25, 176-186	76
2114	Neutron diffraction study of antiferromagnetism in YbVO4. <b>1981</b> , 23, 254-256	14
2113	Preferred orientation correction in powder pattern-fitting <b>1981</b> , 10, 211-221	38
2112	Hydrogen Atom Positions in Dickite. <b>1981</b> , 29, 316-319	21
2111	An alternative to the Rietveld profile refinement method. <b>1981</b> , 157, 101-117	9
2110	Determination of orientational order in submonolayer butane films adsorbed on graphite by elastic neutron diffraction. <b>1981</b> , 78, 504-508	38

2109	Phenomenological and structural study of a low-temperature phase transition in the PbZrO3?PbTiO3 system. <b>1981</b> , 37, 248-255	41
2108	The six-layer structure of BaSn0.9Fe5.47O11. <b>1981</b> , 40, 290-300	13
2107	An order-disorder transition in Sr2IrD5: Evidence for square pyramidal IrD5 units from powder neutron diffraction data. <b>1981</b> , 40, 352-360	36
2106	Reversible high temperature exchange of carbonate and hydroxyl ions in tooth enamel and synthetic hydroxyapatite. <b>1981</b> , 9, 1-26	29
2105	A program for refining crystal structures from the profile of x-ray powder diagrams. <b>1981</b> , 22, 249-252	2
2104	Structural investigations of polycrystalline diaspore samples by X-ray powder diffraction. <b>1981</b> , 7, 138-140	20
2103	Crystal and magnetic structure of the NiMnGeSin System. 1981, 64, 367-378	65
2102	Crystal and magnetic structure of the NiMn1ETitGe system. <b>1981</b> , 66, 45-52	16
2101	Structural aspects of lithium insertion in oxides: Li x ReO 3 and Li 2 FeV 3 O 8. <b>1981</b> , 5, 323-326	32
2100	Deuterium sites in the defect pyrochlore DTaWO 6 : Location from neutron powder diffraction data. <b>1981</b> , 5, 455-458	12
2099	Neutron TOF diffraction studies of FeV2S4 and Fe2VS4. <b>1981</b> , 105, 223-229	8
2098	The canted ferrimagnetic structure of Nd5Ge4 by neutron diffraction. 1981, 42, 583-586	19
2097	Neutron powder diffraction on RbCrl3 and magnetic measurements on RbCrl3 and CsCrl3. <b>1981</b> , 38, 199-210	8
2096	Neutron powder diffraction on ∃-Tl4CrI6 and 町l4CrI6. <b>1981</b> , 38, 239-245	4
2095	Pattern-fitting structure refinement of tin(II) oxide. <b>1981</b> , 38, 381-385	68
2094	Neutron powder diffraction and magnetic measurements on TlMnI3 and TlFeI3. <b>1981</b> , 37, 189-203	6
2093	The structure of LaTaO4 at 300°C by neutron powder profile analysis. <b>1981</b> , 36, 139-147	41
2092	Structure de SnPb2O4 [quatre tempfatures: relation entre dilatation et agitation thermiques. <b>1981</b> , 36, 81-90	35

2091 The cooperative Jahn-Teller distorted structure of RbCuCl3. <b>1981</b> , 39, 168-172	15
2090 The structure of quartz at 25 and 590°C determined by neutron diffraction. <b>1981</b> , 36, 371-380	189
2089 Neutron powder diffraction and magnetic measurements on RbTil3, RbVI3, and CsVI3. <b>1981</b> , 37, 308-317	16
Magnetic ordering in CoMnSn studied by neutron diffraction and 119Sn MBsbauer spectroscopy. <b>1981</b> , 38, 875-877	22
2087 Crystals and magnetic structure of RMn2Si2 (R = Pr, Nd, Y) and YMn2Ge2. <b>1981</b> , 39, 863-866	73
2086 Order-disorder phase transition in ZrV2D3.6. <b>1981</b> , 38, 637-641	61
2085 Crystal and magnetic structure of Ni2Mn5Bi4 and Cu4Mn3Bi4. <b>1981</b> , 38, 41-43	9
2084 Optimization of Computer Controlled X-Ray Stress Analysis. <b>1981</b> , 30, 509-513	7
2083 The crystal structures of Ba2LaRuO6 and Ca2LaRuO6. <b>1981</b> , 16, 397-405	15
X-ray and neutron diffraction studies of the incommensurate structural transition in $\mathfrak{m}$ hBr4. <b>1981</b> , 16, 1421-1427	8
The synthesis, structure and physical properties of a non-stoichiometric sodium chromium selenide, Na0.34Cr1.15Se2. <b>1981</b> , 16, 729-739	6
2080 Neutron diffraction and magnetic studies of ErFe3. <b>1981</b> , 52, 2052-2054	15
2079 Structural and magnetic properties of Y(Mn1\(\mathbb{H}\)Fex)12. <b>1981</b> , 52, 2077-2078	82
$_{2078}$ The structures and the improper ferroelastic phase transition of RbAlF4. <b>1981</b> , 36, 407-410	2
2077 A powder neutron diffraction study of stoichiometric silver beta alumina at 4.2K. <b>1981</b> , 14, 1545-1554	17
2076 Structural Studies on Nonstoichiometric Oxides Using X-Ray and Neutron Diffraction. <b>1981</b> , 399-433	10
Neutron diffraction study of long-range antiferromagnetic order and crystal structure of uranium (III) tri-iodide. <b>1981</b> , 14, 1847-1854	15
Structural phase transitions in ferroelastic RbAlF4. I. DSC, X-ray powder diffraction investigations and neutron powder profile refinement of the structures. <b>1982</b> , 15, 183-196	52

Neutron-diffraction study of magnetically ordered Tb2Fe3Si5. <b>1982</b> , 25, 4702-4710	37
Frustration effects in the disordered system CsMnFeF6, studied by neutron scattering, ac susceptibility, and magnetization measurements. <b>1982</b> , 26, 6150-6158	23
2071 Neutron Scattering: Some Recent Applications to Inorganic Chemistry. <b>1982</b> , 2, 39-67	1
Gamma-lithium iodate structure at 515 K and the $\oplus$ -LilO3 to $\oplus$ LilO3, $\oplus$ LilO3 to $\oplus$ LilO3 phase transitions. <b>1982</b> , 77, 4222-4226	11
Neutron diffraction studies of Nd2(CoxFe1\( \text{N}\))17 alloys: Preferential site occupation and magnetic structure. <b>1982</b> , 53, 250-256	113
2068 A neutron diffraction study of Cr3(11B0.44C0.56)C0.85 and Cr3C(C0.52N0.48)*. <b>1982</b> , 160, 275-284	10
Crystal Structure Determination of Antiferroelectric PbZrO3 Application of Profile Analysis Method to Powder Method of X-ray and Neutron Diffraction 1982, 51, 3583-3591	94
Neutronenstreuung Œine Methode zur Untersuchung der Struktur und Dynamik von Mineralien. <b>1982</b> , 86, 1049-1054	
2065 The structure and dynamics of crystalline 2,4-hexadiyne. <b>1982</b> , 45, 1015-1034	6
2064 Magnetic properties of the Ce1-xLaxMn2Si2 system. <b>1982</b> , 27, 49-54	64
2063 Crystal structure and thermal expansion of ⊞-quartz SiO2 at low temperatures. <b>1982</b> , 53, 6751-6756	131
2062 Structure and phase relations in metal hydrides studied by neutron diffraction. <b>1982</b> , 88, 1-8	24
2061 Crystal and magnetic structure of Co Ni1-MnGe system. <b>1982</b> , 27, 281-292	87
2060 The Intercalation Chemistry of 卧lumina. <b>1982</b> , 181-227	4
An Evaluation of Some Profile Models and the Optimization Procedures Used in Profile Fitting.  1982, 26, 73-80	1
2058 Accuracy and Precision of Intensities in X-Ray Polycrystalline Diffraction. <b>1982</b> , 26, 35-44	3
2057 Resistance du nitrure de silicium a l'irradiation par neutrons rapides. <b>1982</b> , 17, 851-862	4
2056 The crystal structures of lead dioxides from the positive plate of the lead/acid battery. <b>1982</b> , 17, 769-784	58

2055	NH4AlF4: Determination of the ordered and disordered structures by neutron powder profile refinement. <b>1982</b> , 17, 391-397	35
2054	Gamma-ray crystallography and related techniques. <b>1982</b> , 193, 285-292	7
2053	Crystalline phase composition of positive plates in lead/acid traction batteries under simulated electric vehicle service. <b>1982</b> , 8, 175-196	21
2052	Structure and ionic conductivity of Bi2O3 substituted with lanthanide oxides. <b>1982</b> , 43, 1129-1136	45
2051	A neutron powder diffraction study of the lithium insertion compound LiMoO2 from 4월40K. <b>1982</b> , 43, 657-666	32
2050	Neutron profile refinement of the structures of Li2SnO3 and Li2ZrO3. <b>1982</b> , 45, 170-179	91
2049	The structure of dehydrated Na zeolite A () by neutron profile refinement. 1982, 44, 245-253	33
2048	Residual Stresses [Measurement and Causes in Machining Processes. 1982, 31, 491-510	326
2047	Computer simulation of X-ray powder patterns with a microcomputer. <b>1982</b> , 6, 33-37	2
2046	Comparison of neutron diffraction and EPR results on the cubic crystal structures of piezoelectric Bi4Y3O12(Y = Ge, Si). <b>1982</b> , 44, 657-661	49
2045	Spin state equilibria and the semiconductor to metal transition of LaCoO3. <b>1982</b> , 44, 1213-1216	74
2044	Correlation in the statistical analysis of a reverse fourier neutron time-of-flight experiment. <b>1982</b> , 192, 397-406	5
2043	The structure of the hollandite type phase of synroc b in the temperature range 20🛭 060°c. <b>1982</b> , 110, 173-177	17
2042	The structures of lithium-inserted metal oxides: LiReO3 and Li2ReO3. <b>1982</b> , 42, 251-262	72
2041	Crystal structure and luminescence of compounds A3BC10O20. <b>1982</b> , 41, 39-43	19
2040	Localization of hydrogen in the layer oxide HTiNbO5. <b>1982</b> , 41, 57-62	31
2039	Evolution structurale d'oxydes isomorphes MeX2O4: Relation entre dilatation, vibrations et rigidite. <b>1982</b> , 43, 12-28	35
2038	Strong Zn2+/Mn2+ cation ordering among five- and six-coordinated sites in E(Zn0.75Mn0.25)3(PO4)2. <b>1982</b> , 1, 349-353	8

2037	Structure refinement of yttrium ⊞-sialon from X-ray powder profile data. <b>1982</b> , 1, 533-535	48
2036	Magnetic Properties of the CoxNi1-x MnGe System in the Hexagonal Phase. <b>1982</b> , 69, K49-K54	2
2035	Adsorption sites in Na-A zeolites. Neutron diffraction study of NaA-methane and NaA-acetylene systems. <b>1982</b> , 2, 260-266	24
2034	Modifications structurales du nitrure de silicium en fonction de la temperature. <b>1983</b> , 18, 921-934	45
2033	The structure of cesium-exchanged zeolite-RhO at 293K and 493K determined from high resolution neutron powder data. <b>1983</b> , 18, 841-852	44
2032	The high-temperature paraelastic structure of LaNbO4. <b>1983</b> , 18, 749-756	58
2031	Neutron diffraction studies of NiCoP4O12 and NiZnP4O12. <b>1983</b> , 18, 765-773	9
2030	The structure of dehydrated zeolite 3A (Si/Al = 1.01) by neutron profile refinement. <b>1983</b> , 47, 123-131	28
2029	Preparation and characterization of the system BaBrxCl2⊠: The structure of BaBrCl. <b>1983</b> , 48, 351-356	20
2028	The structures of the lithium inserted metal oxides Li0.2ReO3 and Li0.36WO3. <b>1983</b> , 50, 121-128	46
2027	Fast ion transport in the NASICON analog Na3Sc2(PO4)3: Structure and conductivity. <b>1983</b> , 9-10, 839-844	41
2026	Calculated X-ray powder diffraction data for phases encountered in lead/acid battery plates. <b>1983</b> , 9, 55-71	28
2025	Neutron diffraction study of the Ni2Mn1-xCrxSn system. <b>1983</b> , 76, K117-K120	1
2024	Crystallographic studies of some olivine-related (Ni, Mg)3(PO4)2 solid solutions. <b>1983</b> , 10, 10-15	5
2023	Full-profile analysis of the structure of (NH4)XVXMo1🖸O3. 1983, 23, 590-593	2
2022	A powder neutron diffraction investigation of vacancy ordering and covalence in Fe2O3. <b>1983</b> , 49, 325-333	187
2021	Magnetic properties of PrX2 compounds (X = Pt, Rh, Ru, Ir) studied by hyperfine specific heat, magnetization and neutron-diffraction measurements. <b>1983</b> , 119, 215-227	12
2020	Application of synchrotron radiation to high resolution powder diffraction and rietveld refinement. <b>1983</b> , 208, 573-578	60

2019	Growth and characterization of AgI polytypes. <b>1983</b> , 7, 451-492	13
2018	Antiferromagnetic ordering in DyCo2Si2 and TmCo2Si2. <b>1983</b> , 48, 55-56	27
2017	Neutron diffraction study of RECo2Si2 intermetallics. 1983, 45, 145-148	57
2016	Magnetic properties of NdCo2Ge2, ErCo2Ge2 and PrFe2Ge2 compounds. <b>1983</b> , 45, 149-152	38
2015	The magnetic structure of HoCo2Si2. <b>1983</b> , 44, 875-877	12
2014	ComposE isomorphes MeX2O4: Dilatation thermique anisotrope et ordre magnEique dans MnSb2O4. <b>1983</b> , 47, 132-142	28
2013	The structures of lithium inserted metal oxides: Li2FeV3O8. <b>1983</b> , 48, 309-317	12
2012	Neutron and X-ray diffraction study on polymorphism in lithium orthotantalate, Li3TaO4. <b>1983</b> , 48, 420-430	14
2011	The crystal structures and magnetic properties of Ba2LaRuO6 and Ca2LaRuO6. 1983, 46, 234-244	130
2010	Les antimonites antiferromagnetiques MnSb2O4 et NiSb2O4. <b>1983</b> , 49, 14-19	27
	Les antimonites antiferromagnetiques MnSb2O4 et NiSb2O4. <b>1983</b> , 49, 14-19  A neutron powder diffraction study of the liphase in the Fe?W?C system. <b>1983</b> , 49, 118-122	11
2009	A neutron powder diffraction study of the liphase in the Fe?W?C system. 1983, 49, 118-122  Magnetic ordering and exchange effects in the antiferromagnetic solid solutions MnxNi1\( \text{N} \text{O} \). 1983,	11
2009 2008	A neutron powder diffraction study of the [phase in the Fe?W?C system. 1983, 49, 118-122  Magnetic ordering and exchange effects in the antiferromagnetic solid solutions MnxNi1 20. 1983, 27, 6964-6967	11 195
2009 2008 2007 2006	A neutron powder diffraction study of the hase in the Fe?W?C system. 1983, 49, 118-122  Magnetic ordering and exchange effects in the antiferromagnetic solid solutions MnxNi1NO. 1983, 27, 6964-6967  The antiferromagnetic structure of ErCo2Si2 by neutron diffraction. 1983, 30, 355-358	11 195 17
2009 2008 2007 2006	A neutron powder diffraction study of the hase in the Fe?W?C system. 1983, 49, 118-122  Magnetic ordering and exchange effects in the antiferromagnetic solid solutions MnxNi1NO. 1983, 27, 6964-6967  The antiferromagnetic structure of ErCo2Si2 by neutron diffraction. 1983, 30, 355-358  Magnetic ordering in HoRu2Si2, HoRh2Si2, TbRh2Si2 and TbIr2Si2 by neutron diffraction. 1983, 39, 268-274	11 195 17 77
2009 2008 2007 2006	A neutron powder diffraction study of the liphase in the Fe?W?C system. 1983, 49, 118-122  Magnetic ordering and exchange effects in the antiferromagnetic solid solutions MnxNi1NO. 1983, 27, 6964-6967  The antiferromagnetic structure of ErCo2Si2 by neutron diffraction. 1983, 30, 355-358  Magnetic ordering in HoRu2Si2, HoRh2Si2, TbRh2Si2 and TbIr2Si2 by neutron diffraction. 1983, 39, 268-274  Crystal and magnetic structure of the CoMn1NTixSi system. 1983, 38, 99-104	11 195 17 77 20

2001	The effect of stoichiometric variations on the magnetic structure of Y6Mn23. <b>1983</b> , 94, 221-225	5
2000	Deuterium site occupation and magnetism in Ho6Fe23Dx, compounds. <b>1983</b> , 94, 95-105	37
1999	Crystal structure of YbD2 and its temperature dependence determined by neutron diffraction. <b>1983</b> , 94, 151-155	16
1998	Neutron scattering investigations of Be2ZrH1.5 and Be2ZrD1.5. <b>1983</b> , 89, 201-204	26
1997	A review of the magnetic structures and properties of the R6M23 compounds and their hydrides. <b>1983</b> , 95, 1-15	16
1996	Powder neutron diffraction study of nickel-titanium martensite. <b>1983</b> , 13, L77-L81	72
1995	Structural phase transitions and superconducting transition temperatures of hexagonal MxWO3compounds. <b>1983</b> , 16, 5217-5232	17
1994	Crystal Structure of Ferroelectric PbZr0.9Ti0.1O3 Studied by X-Ray and Neutron Diffraction Profile Analysis Method. <b>1983</b> , 52, 913-919	22
1993	Deuterium site occupation in the oxygen-stabilized 🛭 carbides Zr3V3ODx. I. Preparation and neutron powder diffraction. <b>1983</b> , 79, 4522-4531	51
1992	Structure of the Oxygen Point Defect in SnMo6S8 and PbMo6S8. <b>1983</b> , 51, 1911-1914	50
1991	Crystal structures of solid bromoform. <b>1983</b> , 79, 1495-1504	30
1990	Neutron powder diffraction study of phase transitions and structures of (KCN)x(KBr)1☑ mixed crystals. <b>1983</b> , 28, 3506-3511	56
1989	Neutron-diffraction study of polycrystalline H2SO4 and H2SeO4. <b>1983</b> , 28, 3501-3505	15
1988	The validity of the Rietveld method. <b>1983</b> , 164, 157-158	2
1987	De Gruyter. <b>1983</b> , 165, 175-190	26
1986	Helimagnetism of CuxZn1⊠Cr2Se4 (for 0.0∕‱0.1). <b>1983</b> , 3, 105-120	16
1985	Applications of neutron scattering in chemistry. <b>1983</b> , 1-84	4
1984	Hydrogen Atom Positions in Kaolinite by Neutron Profile Refinement. <b>1983</b> , 31, 352-356	50

1983	Atom Positions in Highly Ordered Kaolinite. <b>1983</b> , 31, 357-366	52
1982	The effect of local disorder on the magnetic, electric and thermal properties of RE(Fe1-xAlx)2(RE=Gd, Dy). <b>1984</b> , 14, 981-1004	31
1981	Structural transitions and ionic conduction in Na2UBr6. <b>1984</b> , 17, 4587-4600	7
1980	Neutron-diffraction study of magnetically ordered Er2Fe3Si5. <b>1984</b> , 29, 271-277	19
1979	Neutron-diffraction study of ⊞- and ∰oxygen. <b>1984</b> , 29, 1387-1393	117
1978	Magnetic ordering in CeM2Si2 (M=Ag,Au,Pd,Rh) compounds as studied by neutron diffraction. <b>1984</b> , 29, 2664-2672	186
1977	Magnetic structure of Er6Fe23. <b>1984</b> , 56, 1224-1226	12
1976	Crystal structure of rubidium cyanide at 4 K determined by neutron powder diffraction. <b>1984</b> , 29, 2168-2170	39
1975	The structure of koechlinite bismuth molybdatell controversy resolved by neutron diffraction. <b>1984</b> , 56, 219-237	39
1974	The temperature dependence of the crystal structures of the solid halogens, bromine and chlorine. <b>1984</b> , 53, 929-939	85
1973	Application of diffraction techniques in studies of lead/acid battery performance. <b>1984</b> , 11, 19-32	16
1972	Magnetic structures of PrCO2Si2 and TbCo2Si2 compounds. <b>1984</b> , 45, 689-693	19
1971	The antiferromagnetic structures of TbCu2Ge2 and HoCu2Ge2 by neutron diffraction. <b>1984</b> , 45, 695-699	26
1970	Refinements of the six-layer structures of the R-type hexagonal ferrites BaTi2Fe4O11 and BaSn2Fe4O11. <b>1984</b> , 52, 302-312	44
1969	Neutron powder diffraction investigations of hydrogenated Pd3P0.80 and Pd6P. <b>1984</b> , 52, 327-329	6
1968	A neutron-diffraction study of the tetragonal crystal structures of some yttrium-holmium dicarbides. <b>1984</b> , 53, 376-381	24
1967	The crystal structures of the Chevrel phases Li3.3Mo6S8 and Li3.2Mo6Se8. <b>1984</b> , 54, 193-203	13
1966	The crystal and magnetic structures of Sr2YRuO6. <b>1984</b> , 52, 138-145	144

1965	The crystal structures of the lithium-inserted metal oxides Li0.5TiO2 anatase, LiTi2O4 spinel, and Li2Ti2O4. <b>1984</b> , 53, 64-75	267
1964	The structure of Li3.4Si0.7S0.3O4 by powder neutron diffraction. <b>1984</b> , 55, 14-22	7
1963	The structure of a carbon monoxide adduct of cobalt-exchanged zeolite A (Co5.25Na1.5?A 🛮 1.5CO) by neutron profile refinement. <b>1984</b> , 55, 209-217	14
1962	The structure of dehydrated zeolite 5A () by neutron profile refinement. <b>1984</b> , 51, 83-90	36
1961	Neutron and X-ray powder diffraction study of LixRuO2 and LixIrO2: The crystal structure of Li0.9RuO2. <b>1984</b> , 51, 104-117	29
1960	Crystal structure refinement of Sn3Sb2S6 by high-resolution neutron powder diffraction. <b>1984</b> , 19, 503-508	14
1959	The crystal structures of PbO.PbXO4 (X = S, Cr, Mo) at 5K by neutron powder profile refinement. <b>1984</b> , 19, 549-554	33
1958	Calibration Curve for Quantitative Analysis of the Monoclinic-Tetragonal ZrO2 System by X-Ray Diffraction. <b>1984</b> , 67, C-119-C-121	295
1957	XFIT: A package for simulating and fitting X-ray powder diffraction patterns. <b>1984</b> , 34, 145-151	2
1956	An X-ray structural analysis of cesium substitution in the barium hollandite phase of synroc. <b>1984</b> , 125, 236-243	33
1955	The crystal and magnetic structures of Ca2YRuO6 and the electronic properties of the series M2+2X3+Ru5+O6 (M = Ca, Sr, Ba; X = La, Y). <b>1984</b> , 54, 245-250	58
1954	Temperature dependence of the structure and bonding in deuterated Cu(II) Tutton's salt. <b>1984</b> , 51, 364-375	49
1953	The Simulation and Interpretation of the EPR Powder Spectra of Gd3+-Doped LaAlO3. <b>1984</b> , 122, 317-330	6
1952	Magnetic Properties of RhMnSi and CoTiSi. <b>1984</b> , 82, 195-200	6
1951	The systems Y2O3-Nb2O5 and Ho2O3-Nb2O5: the cubic solid-solution region. <b>1984</b> , 3, 492-494	8
1950	Rietveld refinements for calcium and yttrium containing ∃-sialons. <b>1984</b> , 19, 3115-3120	60
1949	A neutron powder diffraction study of the crystal and magnetic structures of ilvaite from 305 K to 5 K la mixed valence iron silicate with an electronic transition. <b>1984</b> , 11, 67-74	26
1948	TernÆe Verbindungen von Lithium mit Yttrium, Lanthan bzw. Neodym und 5b-Elementen im Bufgefllten[]CaAl2Si2-Typ. <b>1984</b> , 515, 151-158	27

1947	Synthese und Struktur von Na2PtH4, einem ternÆen Hydrid mit quadratisch planaren PtH42Baugruppen. <b>1984</b> , 516, 35-41	55
1946	Magnetic and crystallographic properties of several C1b type Heusler compounds. <b>1984</b> , 43, 249-255	101
1945	Magnetization, M₨bauer and neutron studies of 日- and 且iMnFeF6; Evidence of idle spin behaviour in a ferrimagnet. <b>1984</b> , 42, 217-232	21
1944	Dynamical properties of premartensitic NiTi. <b>1984</b> , 17, L529-L532	74
1943	A neutron powder diffraction study of the crystal structure of LaCuSi. <b>1984</b> , 97, L1-L3	15
1942	Framework structures in metal chalcogenides and the characterization of their bonding by magnetic properties. <b>1984</b> , 100, 241-247	36
1941	Magnetic and crystallographic structure of Th6Mn23Dx. <b>1984</b> , 96, 201-211	22
1940	Structural and magnetic phase transitions in ZrMn2D3. <b>1984</b> , 103, 267-275	20
1939	Phase transformations among three polymorphs of Mg2NiH4. <b>1984</b> , 103, 277-283	31
1938	Imaging the structures of zeolite L and synthetic mazzite. <b>1984</b> , 395, 153-164	34
1937	Neutron diffraction study of magnetic ordering in ErMn2Si2, ErMn2Ge2 and ErFe2Si2. <b>1984</b> , 40, 265-270	44
1936	Relationships between crystal structure and magnetic properties in Nd2Fe14B. <b>1984</b> , 29, 4176-4178	776
1935	Crystallographic studies of olivine-related sarcopside-type solid solutions. <b>1984</b> , 166, 159-176	7
1934	The crystal structure of calcium metaarsenate, CaAs2O6. <b>1985</b> , 173, 313-317	4
1933	A Neutron Powder Diffraction Investigation of Deuterated Pd15P2*. <b>1985</b> , 145, 43-49	9
1932	Diffraction methods for biological macromolecules. Least squares refinement. <b>1985</b> , 115, 23-41	
1931	Crystal structures of stable and metastable iron-containing carbides. <b>1985</b> , 30, 17-44	7
1930	The Impact of New Diffraction Techniques in Zeolite Structural Chemistry. <b>1985</b> , 24, 239-248	1

1929	Neutron powder diffraction study of the Debye-Waller factor in TiC and TiN compounds and comparison with X-ray results. <b>1985</b> , 88, 157-163	8
1928	Exchange and Dipolar Interactions in TbF3. <b>1985</b> , 89, 571-580	4
1927	Phase transition in tetracyanoethylene at high pressure by X-ray diffraction. <b>1985</b> , 92, K23-K27	5
1926	Localizing active sites in zeolitic catalysts: neutron powder profile analysis and computer simulation of deuteropyridine bound to gallozeolite-L. <b>1985</b> , 318, 611-614	113
1925	Ho Be13 commensurate and incommensurate magnetic structures. <b>1985</b> , 130, 366-371	9
1924	Structural and magnetic properties of Mn1ETitAs. 1985, 46, 275-286	14
1923	Neutron structure refinement of $\square$ and $\square$ ithium lodate: Comparison between $\square$ , $\square$ and $\square$ hases. <b>1985</b> , 56, 133-147	21
1922	An X-ray and neutron powder diffraction study of the Ca2+xNd8⊠(SiO4)6O2Ū.5x system. <b>1985</b> , 60, 145-158	45
1921	Anhydrous deuterium 軸lumina: Powder neutron diffraction studies at 4.2, 298, 573, and 720 K. <b>1985</b> , 60, 214-229	5
1920	Structures isomorphes MeX2O4 <b>E</b> volution structurale entre 2 K et 300 K de l'antimonite FeSb2O4: Elasticit[et ordre magnEique anisotropes. <b>1985</b> , 60, 78-86	36
1919	Magnetic order in AVX3 (A = Rb, Cs, (CD3)4 N; X = Cl, Br, I): A neutron diffraction study. <b>1985</b> , 56, 343-354	31
1918	Monoxyde quadratique PbO⊞(I): Description de la transition structurale ferroe∶lastique. <b>1985</b> , 57, 343-350	81
1917	The spiral magnetic structure of #chromium(III) orthophosphate (#CrPO4). <b>1985</b> , 57, 357-361	40
1916	A study of the mixed Na1⊠Lix zeolite A system by powder X-ray diffraction. <b>1985</b> , 58, 325-334	12
1915	Monoxyde PbO∄(II): lasticitlet vibrations anisotropes; modlisation; constantes lastiques. <b>1985</b> , 58, 87-97	3
1914	Magnetic and structural properties of Cr1ETitAs. <b>1985</b> , 59, 9-22	10
1913	Evolution structure entre 2 et 300 K de l'oxyde MnSb2O4: Proprie te se lastiques et magne tiques anisotropes. <b>1985</b> , 59, 123-131	17
1912	Frustrated magnetic structures: II. Antiferromagnetic structure of the ordered modified pyrochlore NH4FellFellIF6 at 4.2 K. <b>1985</b> , 53, 559-563	28

1911	Magnetic structure of the canted 1D-antiferromagnet NaBaFe2F9. <b>1985</b> , 55, 887-890	1
1910	The determination of the Bi valence state in BaBiO3 by neutron powder diffraction data. <b>1985</b> , 56, 829-831	48
1909	Spin reorientation in Tm2Fe14B. <b>1985</b> , 56, 181-183	33
1908	Structural characterisation of synthetic gallium mazzite. <b>1985</b> , 20, 125-136	27
1907	Powder neutron diffraction study of the crystal and magnetic structures of ferromagnetic mixed anion salts Rb2CrCl4NXx. <b>1985</b> , 20, 197-201	6
1906	The structure and magnetic properties of chromium(III) molybdate. <b>1985</b> , 58, 221-225	19
1905	Neutron-diffraction study of RECuSi (RE = Tb, Dy, Ho) intermetallic compounds. <b>1985</b> , 56, 1043-1045	22
1904	Estimation of iron oxides in soil clays by profile refinement combined with differential X-ray diffraction. <b>1985</b> , 20, 15-27	24
1903	Crystal Structure of Kaolinite: Dimethylsulfoxide Intercalate. <b>1985</b> , 33, 490-500	103
1902	DyBe13magnetic structure: neutron diffraction and Mossbauer study. <b>1985</b> , 15, 181-192	12
1901	Triangular antiferromagnetic ordering and phase transitions in uranium trichloride-neutron diffraction and neutron spectroscopy study. <b>1985</b> , 18, 2909-2921	14
1900	Order-disorder transition and structure of the ordered vacancy compound Nb6C5: powder neutron diffraction studies. <b>1985</b> , 18, 809-823	51
1899	Magnetic structure of DyFe 3. <b>1985</b> , 2, 253-256	4
1898	X-ray structural determination of modified PZT. <b>1985</b> , 3, 133-139	3
1897	Neutron-diffraction studies of UBe13and ThBe13. <b>1985</b> , 32, 6042-6044	28
1896	Lattice-parameter changes and triclinic distortions in LixMo6Se8 for 0. <b>1985</b> , 31, 484-489	33
1895	Digital processing of X-ray diffraction patterns from oriented fibers. <b>1985</b> , 24, 193-227	28
1894	Phase diagrams and magnetic excitations in holmium phosphide. <b>1985</b> , 31, 456-469	22

## (1986-1985)

1893	The equilibrium low-temperature structure of ice. <b>1985</b> , 82, 424-428	201
1892	Phase transitions in proustite: I structural studies. <b>1985</b> , 6, 1-24	14
1891	Crystal and magnetic structure of Pr2Fe14B and Dy2Fe14B. <b>1985</b> , 57, 2343-2345	73
1890	Crystal structure of low cristobalite at 10, 293, and 473 K: Variation of framework geometry with temperature. <b>1985</b> , 57, 1045-1049	120
1889	A neutron diffraction study of the (phase Ti9Fe3(Ti0.7Fe0.3)O3. 1985, 113, 103-111	8
1888	Hydrogen positions in TbBrD2. <b>1985</b> , 113, 149-155	22
1887	Refinement of the crystal and magnetic structure of PrFeO3 AT T = 8 K. <b>1985</b> , 111, 109-111	16
1886	Magnetic properties of TbCl3 determined by neutron scattering. <b>1985</b> , 111, 177-184	4
1885	The magnetic structure of TlFe3Te3. <b>1985</b> , 106, 301-303	10
1884	Darstellung und kristallstruktur von Li4Re6S11. <b>1985</b> , 105, 303-310	35
1883	X-ray diffraction study on the formation of Ititanium hydride. <b>1986</b> , 20, 213-216	26
1882	A neutron diffraction and magnetization study of PdMnTe. <b>1986</b> , 123, 169-173	3
1881	Magnetic structure of DyFe3. <b>1986</b> , 118, 269-273	5
1880	A neutron powder diffraction study of Ta2C and W2C. <b>1986</b> , 120, 239-245	34
1879	Stoichiometry and oxygen structure of Fe sillenite. <b>1986</b> , 4, 194-197	13
1878	25. Diskussionstagung der Arbeitsgemeinschaft Kristallographie der Deutschen Mineralogischen Gesellschaft, der Deutschen Physikalischen Gesellschaft und der Gesellschaft Deutscher Chemiker 10. bis 12. MÆz 1986 in Gie&n. <b>1986</b> , 174, 1-201	3
1877	Preferential site occupation and magnetic structure of Nd2(CoxFe1☑)14B systems. <b>1986</b> , 60, 4224-4229	127
1876	Site Occupation and Local Vibration of Hydrogen Isotopes in Hexagonal Ti5Si3 H(D)1−x. 1986, 27, 639-647	17

1875 Orientational disorder in cubic CsNO2 by neutron powder diffraction. <b>1986</b> , 177, 93-102	4
1874 Texture Correction in Phase Analysis and Thin Film Studies. <b>1986</b> , 1, 28-32	6
1873 High Temperature Studies of Stoichionetric Cerium Dioxide. <b>1986</b> , 82, 95	
$_{1872}$ The crystal structures and phase transition of methyl bromide. <b>1986</b> , 57, 919-930	22
1871 Heights of Overlapping X-ray Reflections and Phase Analysis. <b>1986</b> , 21, 873-879	1
1870 Zeolite structure refinements using powder data. <b>1986</b> , 6, 325-333	29
Neutron powder diffraction study and physical characterization of zeolite D-ZKB deep-bed calcined at 500°C and 650°C. <b>1986</b> , 6, 378-387	18
Determination of the structure of Y(HCOO)3 by the neutron time-of-flight diffraction method. <b>1986</b> , 59, 95-97	11
1867 Structural properties of ZrTe5 and HfTe5 as seen by powder diffraction. <b>1986</b> , 60, 91-93	74
1866 Nuclear and magnetic structures of ND4MnFeF6 at 4.2 K. <b>1986</b> , 58, 165-169	
Ordered magnetic frustration 🛭 Antiferromagnetic structure of the hexagonal bronzoid	42
HTB?FeF3; Comparison with the non frustrated rhombohedral form. <b>1986</b> , 58, 171-176	42
HTB?FeF3; Comparison with the non frustrated rhombohedral form. <b>1986</b> , 58, 171-176  Adiabatic calorimetry and neutron diffraction studies of phases and phase transitions in [Ni(ND3)6](NO3)2. <b>1986</b> , 138, 295-304	6
Adiabatic calorimetry and neutron diffraction studies of phases and phase transitions in	6
Adiabatic calorimetry and neutron diffraction studies of phases and phase transitions in [Ni(ND3)6](NO3)2. <b>1986</b> , 138, 295-304	6
Adiabatic calorimetry and neutron diffraction studies of phases and phase transitions in [Ni(ND3)6](NO3)2. <b>1986</b> , 138, 295-304  Neutron diffraction study of crystal and magnetic structures of $\oplus$ -FeC2O4?2D2O. <b>1986</b> , 138, 315	6
Adiabatic calorimetry and neutron diffraction studies of phases and phase transitions in [Ni(ND3)6](NO3)2. 1986, 138, 295-304  Neutron diffraction study of crystal and magnetic structures of \(\text{H}\)-FeC2O4?2D2O. 1986, 138, 315  1862 Chemical physics employing neutron crystallographic methods. 1986, 137, 159-168  Synthesis, structure and low temperature magnetism of the new lithium and sodium insertion	5-322 14
Adiabatic calorimetry and neutron diffraction studies of phases and phase transitions in [Ni(ND3)6](NO3)2. 1986, 138, 295-304  Neutron diffraction study of crystal and magnetic structures of \(\text{H}\)-FeC2O4?2D2O. 1986, 138, 315  Chemical physics employing neutron crystallographic methods. 1986, 137, 159-168  Synthesis, structure and low temperature magnetism of the new lithium and sodium insertion compounds: LiFe(II)ClMoO4 and NaFe(II)ClMoO4. 1986, 47, 741-750	6 5-322 14 4

The structure of the lithium-inserted metal oxide LiV2O5. <b>1986</b> , 65, 63-71	102
1856 Powder neutron diffraction study of ZrTiO4, Zr5Ti7O24, and FeNb2O6. <b>1986</b> , 64, 30-46	82
Synthesis, structural characterization, and magnetic properties of the dimer compounds Cs3Cr2X9, X = Cl, Br, I. <b>1986</b> , 64, 90-101	17
1854 Structural and magnetic properties of MnAs0.90P0.10. <b>1986</b> , 64, 123-133	15
1853 Thermal parameters for lithium halides. <b>1986</b> , 64, 217-219	
1852 Structural and dynamical studies of EBi2O3 oxide ion conductors. <b>1986</b> , 63, 8-15	95
1851 Structural consequences of the coupled substitution of Eu,S in calcium sulfoapatite. <b>1986</b> , 63, 267-277	27
1850 The crystal structure and magnetic properties of the synthetic langbeinite KBaFe2(PO4)3. <b>1986</b> , 62, 16-25	47
Neutron powder diffraction study of tetragonal crystal structures of cerium-neodymium dicarbides. <b>1986</b> , 62, 172-176	11
The structure of a dehydrated partially magnesium exchanged zeolite a ( $\sim$ Mg2Na8?A) by neutron profile refinement. <b>1986</b> , 62, 184-190	6
A neutron powder diffraction study of the low- and high-temperature structures of Bi12PbO19. <b>1986</b> , 62, 290-296	21
1846 Refinement of the structure of PEEK fibre in an orthorhombic unit cell. <b>1986</b> , 27, 861-865	58
Darstellung und Kristallstruktur der isotypen Verbindungen Ca2Os3B5 und Eu2Os3B5. <b>1986</b> , 533, 30-36	8
Zur Charakterisierung der magnetischen Eigenschaften von NaMnP, NaMnAs, NaMnSb, NaMnBi, LiMnAs und KMnAs Ber Neutronenbeugungsexperimente. <b>1986</b> , 539, 175-182	38
1843 Mg2lrB2⊠, ein Magnesium-Iridiumborid mit W2CoB2 -verwandter Struktur. <b>1986</b> , 543, 89-96	7
1842 Magnetic Properties of ZrMnSi, ZrMnGe, and HfMnSi Intermetallics. <b>1986</b> , 94, 207-211	2
Nature of isomorphism in crystals of bismuth-zinc and bismuth-cadmium double oxides with the sillenite structure. <b>1986</b> , 26, 569-574	
1840 Structure refinement by the complete-profile powder method. <b>1986</b> , 26, 606-618	2

1839	Structural properties of VP1☑ As x ; 0.00?x?1.00. <b>1986</b> , 117, 773-781	6
1838	Structure of oxygen clathrate hydrate by neutron powder diffraction. <b>1986</b> , 4, 235-240	33
1837	The structural chemistry of zeolites as viewed by powder neutron diffraction. <b>1986</b> , 136, 213-217	2
1836	The structure of the low temperature phase of lithium metal. <b>1986</b> , 136, 481-484	6
1835	Structure of high-pressure KNO3-IV. <b>1986</b> , 136, 503-506	11
1834	Crystal structure determination by powder neutron diffraction at the spallation neutron source, ISIS. <b>1986</b> , 320, 46-48	62
1833	Structure determination of ⊞-CrPO4 from powder synchrotron X-ray data. <b>1986</b> , 322, 620-622	73
1832	Mechanism for the Dehydroxylation of Kaolinite, Dickite, and Nacrite from Room Temperature to 455°C. <b>1986</b> , 69, 61-65	22
1831	Crystal structure of the inverse weberite ZnFeF5(H2O)2, magnetic and m\sbauer study of the antiferromagnet ZnFeF5(H2O)2 and ferrimagnet Mn FeF5(H2O)2. <b>1986</b> , 61, 283-290	20
1830	Structural and magnetic properties of Mn1 <b>E</b> NitAs. <b>1986</b> , 61, 61-80	11
1829	Mn3O4 commensurate and incommensurate magnetic structures. <b>1986</b> , 58, 128-134	74
1828	Paramagnetic scattering experiments on MnAs1 $\overline{B}$ Px, x = 0.06, 0.12 and 0.18. <b>1986</b> , 62, 241-246	8
1827	Crystal structure and magnetic properties of some new hexagonal ferrites (Ba2Sn2MeFe10⊠GaxO22) with the QS-structure. <b>1986</b> , 62, 367-380	12
1826	Martensitic-like transformations in CrMn1 [As. <b>1986</b> , 58, 287-296	10
1825	Crystal and magnetic structure of Ce2Fe14B and Lu2Fe14B. <b>1986</b> , 54-57, 570-572	33
1824	Neutron diffraction studies of some hexagonal ferrites: BaFe12O19, BaMg2?W and BaCo2?W. <b>1986</b> , 62, 57-67	116
1823	A new form of FeF3 with the pyrochlore structure: Soft chemistry synthesis, crystal structure, thermal transitions and structural correlations with the other forms of FeF3. <b>1986</b> , 21, 971-978	66
1822	Structural characterization of dehydrated gallium zeolite L. <b>1986</b> , 21, 661-672	39

1821	Structure of the lithium insertion compound Li2Fe2(MoO4)3 from neutron powder diffraction data. <b>1986</b> , 21, 719-726	35
1820	A study of decomposition methods for refinement of H+-ZSM5 zeolite with powder diffraction data. <b>1986</b> , 176, 183-192	4
1819	Fluorocomplexes of niobium IV - Part V. The magnetic structure of MnNbF6. <b>1986</b> , 58, 71-74	9
1818	Powder neutron diffraction study of zeolite Na?ZKI; an application of new functions for peak shape and asymmetry. <b>1986</b> , 6, 449-454	18
1817	Zeolite Structural Investigations by High Resolution Solid State MAS NMR. <b>1986</b> , 361-368	8
1816	Powder neutron diffraction studies of the mixed ilmenite system Fe0.6Co0.4TiO3. <b>1986</b> , 19, 1273-1282	2
1815	Ordered magnetic frustration. IV. The two magnetic structures of the inverse weberite Fe2F5(H2O)2: an example of the thermal evolution of the frustration character. <b>1986</b> , 19, 1081-1095	24
1814	Effect of stacking faults on diffraction: The structure of lithium metal. <b>1986</b> , 34, 3586-3603	93
1813	Magnetic structure of the heavy-fermion compound U2Zn17. <b>1986</b> , 33, 3614-3617	72
1812	Neutron scattering studies of the spin reorientation in Er2Fe14B. <b>1986</b> , 59, 93-96	44
1811	Order parameter and critical exponent for the pressure-induced phase transitions in ReO3. <b>1986</b> , 33, 4793-4798	76
1810	Magnetic properties of La(FexAl1-x)13 determined via neutron scattering and M\(\mathbb{B}\)sbauer spectroscopy. <b>1986</b> , 34, 169-173	76
1809	Crystal structures and phase transition of the cyanospinel K2Hg(CN)4. <b>1986</b> , 85, 6004-6009	18
1808	The crystal structure of LaNi5D7. <b>1986</b> , 16, 675-685	73
1807	The zeolite cage structure. <b>1986</b> , 231, 1093-9	160
1806	Applications of Total Pattern Fitting to a Study of Crystallite Size and Strain in Zinc Oxide Powder. <b>1986</b> , 1, 211-221	125
1805	Magnetic frustration in the mixed garnets (FexCr1-x)2Ca3(GeO4)3: the phase diagram and relaxation of the antiferromagnetic long-range order. <b>1987</b> , 20, 2565-2583	13
1804	A New Method for Analyzing Powder Diffraction Patterns: Confirmation of a Predicted Phase of SF6. <b>1987</b> , 236, 1463-5	12

1803	Magnetic ordering of the linear chain system manganese oxalate dihydrate investigated by means of neutron diffraction and bulk magnetic measurements. <b>1987</b> , 20, 2247-2259	16
1802	Data Collection Strategies for Constant Wavelength Rietveld Analysis*. <b>1987</b> , 2, 146-162	54
1801	Synchrotron X-Ray Powder Diffraction. <b>1987</b> , 12, 16-20	2
1800	Magnetic Structure of Intermetallic Compound EMn5Ge2. <b>1987</b> , 56, 4107-4112	5
1799	Structural phase transitions in ferroelastic TlAlF4: DSC investigations and structures determinations by neutron powder profile refinement. <b>1987</b> , 20, 2885-2900	17
1798	Neutron diffraction study of ⊞-iron titanium cerium hydride. <b>1987</b> , 4, 105-108	2
1797	The magnetic structure of DHCP Ce0.75Y0.25and cerium. <b>1987</b> , 17, L101-L104	16
1796	De Gruyter. <b>1987</b> , 180, 123-129	5
1795	Crystal structure of the high-temperature superconductor La1.85Sr. 1987, 35, 6716-6720	233
1794	Structure of the single-phase high-temperature superconductor YBa2Cu3O7[1 1987, 51, 57-59	614
1793	Structure and crystal fields of PrBr3 and PrCl3: A neutron study. <b>1987</b> , 61, 3426-3428	17
1792	Diffusivity and neutron scattering study of the Li-defect conversion in MgF2. <b>1987</b> , 36, 6657-6663	
1791	Oxygen ordering in the crystal structure of the 93-K superconductor YBa2Cu3O7 using powder neutron diffraction at 298 and 79.5 K. <b>1987</b> , 35, 8770-8773	174
1790	Neutron study of the crystal structure and vacancy distribution in the superconductor Ba2YCu. <b>1987</b> , 35, 8778-8781	294
1789	Synthesis and Structural Characterization of a Hydrated Gallosilicate Zeolite with the Nat-Framework. <b>1987</b> , 111, 147	10
1788	Neutron Diffraction Studies of Magnetic Materials. <b>1987</b> , 96, 241	1
1787	High Temperature Superconductors in the La1+xBa2-xCu3Oy System. <b>1987</b> , 99, 101	4
1786	De Gruyter. <b>1987</b> , 181, 151-160	13

1785	De Gruyter. <b>1987</b> , 179, 281-304	15
1784	Orientational ordering and the low temperature structure of SF6. <b>1987</b> , 62, 1127-1141	36
1783	Structure of the 100 K Superconductor Ba 2 YCu 3 O 7 between (5 □300) K by Neutron Powder Diffraction. <b>1987</b> , 3, 1301-1307	530
1782	A new study of the structure of LaNi5D6.7 using a modified Rietveld method for the refinement of neutron powder diffraction data. <b>1987</b> , 129, 65-76	108
1781	Neutron powder diffraction and inelastic scattering study of the structures of Zr2Pd, Zr2PdD1.70 and Zr2PdD1.96. <b>1987</b> , 129, 77-91	23
1780	The accommodation of strain and particle size broadening in rietveld refinement; its application to de-deuterided LaNi5 alloy. <b>1987</b> , 129, 105-114	44
1779	Crystallographic and magnetic structure of Ni2MnSn and NiMn2Sn. <b>1987</b> , 128, 167-171	64
1778	Structural properties of Ni1ERhtBi3. <b>1987</b> , 128, 177-183	32
1777	Temperature dependence of the crystal structure of the ceramic superconducting La1.85Sr0.15CuO4: a powder neutron diffraction study. <b>1987</b> , 20, L429-L434	56
1776	New Opportunities in Synchrotron X-ray Crystallography. <b>1987</b> , 238, 312-9	21
1775	Crystal and magnetic structures of Fe0.25TiSe2 and Fe0.48TiSe2. <b>1987</b> , 22, 1131-1138	38
1774	Vibrational and electronic spectra of 🗖 n2Co(PO4)2. <b>1987</b> , 61, 441-444	4
1773	Locations of deuterobenzene molecules in the synthetic zeolite ZSM-5 at 77 K by powder neutron diffraction. <b>1987</b> , 7, 311-318	38
1772	Neutron diffraction study of卧sialon. <b>1987</b> , 6, 1101-1102	31
1771	Magnetic structure and cation distribution in (Fe,Mn)2SiO4 (olivine) by neutron diffraction. <b>1987</b> , 15, 54-58	16
1770	Magnetic order in grunerite, Fe7Si8O22(OH)2A quasi-one dimensional antiferromagnet with a spin canting transition. <b>1987</b> , 14, 36-44	9
1769	BindungsverhÆtnisse in den kristallinen Phasen von Rubidiumhydroxid und -deuterohydroxid, RbOH und RbOD. <b>1987</b> , 544, 28-54	35
1768	Die Kristallstruktur von Bariumhydrid, ermittelt <b>B</b> er Neutronenbeugungsexperimente an BaD2. <b>1987</b> , 545, 69-74	47

1767	Ordered Magnetic Frustration. XI. Refinement of the Crystal and Frustrated Magnetic Structures of the Direct Weberite Na2NiCrF7 by Neutron Powder Diffraction. <b>1987</b> , 553, 163-171	16
1766	BindungsverhÆtnisse in kristallinen Phasen von Kaliumdeuterohydroxid, KOD. <b>1987</b> , 553, 187-195	28
1765	Thermal Vibrations in Substoichiometric Vanadium Nitrides. Dynamical Deformation Effect. <b>1987</b> , 143, 471-476	5
1764	Quantitative analysis of a Fe3O4 + Li x Fe3O4 sample by the X-ray Rietveld method. <b>1987</b> , 22, 1001-1005	5
1763	Aluminophosphate molecular sieve AlPO4-11: partial refinement from powder data using a pulsed neutron source. <b>1987</b> , 7, 160-162	107
1762	Gallosilicate sodalite <b>f</b> urther syntheses and structural details. <b>1987</b> , 7, 569-573	34
1761	The $x$ ray anomalous dispersion corrections and their use for the characterization of materials. <b>1987</b> , 14, 1-46	4
1760	Some applications of pattern fitting to powder diffraction data. <b>1987</b> , 14, 185-211	22
1759	Structural phase transition at 150K in the high-temperature superconductor La1.85Sr0.15CuO4. <b>1987</b> , 63, 35-40	83
1758	Temperature behaviour of the tetrafluoroaluminates K1\(\mathbb{R}\)ExalF4. Evolution of the shear structural phase transition. <b>1987</b> , 61, 539-541	13
1757	Topochemical reduction of the high temperature superconductor YBa2Cu3O7: The structure of YBa2Cu3O6 by neutron diffraction. <b>1987</b> , 64, 497-500	31
1756	Electron microscopy and neutron diffraction studies of Ba2YCu3O7II compounds. 1987, 64, 1037-1041	28
1755	Measurement of the cation partitionings in FexV3 $mathbb{M}$ S4 (x = 1.0 and 2.0) by powder neutron diffraction. <b>1987</b> , 48, 607-612	15
1754	Structure systematics in A3Mo2X9, X = Cl, Br, I, from Rietveld refinement of X-ray powder data. <b>1987</b> , 69, 162-170	44
1753	The antiferromagnetic structures of KFeS2, RbFeS2, KFeSe2, and RbFeSe2 and the correlation between magnetic moments and crystal field calculations. <b>1987</b> , 70, 262-270	92
1752	An investigation of the low oxidation state chemistry of rhenium in the BaO?Re?Re2O7 phase diagram. <b>1987</b> , 71, 61-69	10
1751	Preparation and crystal structure of superconducting Y2FeC4 and isotypic lanthanoid iron carbides. <b>1987</b> , 70, 19-28	38
1750	The homogeneity ranges, order-disorder transition, and structures of the nonstoichiometric monosulfides of zirconium. <b>1987</b> , 70, 88-92	11

1749	Ordered magnetic frustration. <b>1987</b> , 66, 242-250	12
1748	Further aspects of the structure and magnetism of the layered compound Fe(III)ClMoO4: Māsbauer spectroscopy, susceptibility, and powder neutron diffraction studies. <b>1987</b> , 66, 105-115	5
1747	The crystallographic and magnetic structure of Ni2O3H. <b>1987</b> , 71, 418-425	11
1746	BaLa4Cu5O13+[], an oxygen-deficient perovskite built up from corner-sharing CuO6 octahedra and CuO5 pyramids. <b>1987</b> , 68, 143-152	78
1745	A neutron-diffraction study of the tetragonal-monoclinic crystal structures of some uranium-thorium dicarbides. <b>1987</b> , 68, 219-226	25
1744	Crystal structure of Nd(OH)2NO3 ©H2O completely solved and refined from X-ray powder diffraction. <b>1987</b> , 68, 292-299	38
1743	The structure of a carbon monoxide adduct of zeolite 5A. <b>1987</b> , 68, 351-359	4
1742	Nolution structurale sous pression de NiSb2O4: Compressibilit\( \bar{8}\) anisotropes et ordre magnetique. <b>1987</b> , 67, 98-103	6
1741	Structural refinement of delithiated LiVO2 by neutron diffraction. <b>1987</b> , 67, 285-290	31
1740	Superconductivity in lanthanum barium cuprate perovskites. <b>1987</b> , 85, 632-638	35
1739	Neutron diffraction study of age-hardened U-0.75 wt% Ti alloy. <b>1987</b> , 150, 85-92	4
1738	The squared modulated magnetic structure of HoRu2Ge2. <b>1987</b> , 68, 90-94	17
1737	The Magnetic structure of Ulr. <b>1987</b> , 67, 323-330	36
1736	Magnetic order in the ternary compound NdRu2Ge2. <b>1987</b> , 69, 305-310	16
1735	Electronic and magnetic properties of rare-earth ions in REBa2Cu3O7-x (RE=Dy, Ho, Er). <b>1987</b> , 68, L139-L144	135
1734	Ordered magnetic frustration: IX. Magnetic structure of Ba2Ni3F10 at 2.5 K. <b>1987</b> , 66, 213-218	11
1733	Ordered magnetic frustration: X. Magnetic structure of ⊞-KCrF4 at 1.5 K. <b>1987</b> , 66, 219-224	19
1732	Thermal, magnetic and structural aspects of transitions in Mn0.63Cr0.37As. Thermodynamic properties from 10 to 350 K. <b>1987</b> , 65, 37-52	10

1731	Neutron scattering in intermetallics. <b>1987</b> , 70, 88-96	34
1730	Molecular field model for ?-Mn5Ge2. <b>1987</b> , 70, 252-254	
1729	The crystal structure of La 2 NiRuO 6. <b>1987</b> , 22, 1623-1627	21
1728	Neutron powder diffraction study of orthorhombic Ba 2 YCu 3 O 6.5. <b>1987</b> , 22, 1733-1740	36
1727	A new modification of ReO3-type MoO3 and the deuterated intercalation compound from which it is derived: D0.99M0O3. <b>1987</b> , 22, 803-811	33
1726	The structure and properties of Ba2YCu3O6. <b>1987</b> , 22, 1007-1013	150
1725	Structure of La1.5Ba1.5Cu3O7.3. <b>1987</b> , 22, 1563-1571	24
1724	Characterization of guest molecules adsorbed on zeolites of known structure by combined x-ray powder profile refinements and conventional difference-fourier techniques. Part II - Localization of the n-hexane, TPA and p-xylene guests in a pentasil type zeolite. <b>1987</b> , 22, 489-496	18
1723	The ordered perovskite system Ln2NiRuO2. <b>1987</b> , 22, 535-542	27
1722	First success of powder methods. <b>1987</b> , 325, 109-110	7
1722 1721		7
ĺ		
1721	Structural Aspects of the Lattice Thermal Expansion of Hexagonal Cordierite. <b>1987</b> , 70, 175-182  Synthese von TiNF und Strukturbestimmung durch Pulverdiffraktometrie mit	47
1721 1720	Structural Aspects of the Lattice Thermal Expansion of Hexagonal Cordierite. 1987, 70, 175-182  Synthese von TiNF und Strukturbestimmung durch Pulverdiffraktometrie mit Synchrotronstrahlung. 1988, 100, 1013-1013  Uniforme heterogene Katalysatoren Edie Rolle der FestkEperchemie bei der	13
1721 1720 1719	Structural Aspects of the Lattice Thermal Expansion of Hexagonal Cordierite. 1987, 70, 175-182  Synthese von TiNF und Strukturbestimmung durch Pulverdiffraktometrie mit Synchrotronstrahlung. 1988, 100, 1013-1013  Uniforme heterogene Katalysatoren Elie Rolle der Festkiperchemie bei der Katalysatorentwicklung. 1988, 100, 1735-1753  Synthesis of TiNF and Structure Determination by Powder Diffraction using Synchrotron Radiation.	47 13 38
1721 1720 1719 1718	Structural Aspects of the Lattice Thermal Expansion of Hexagonal Cordierite. 1987, 70, 175-182  Synthese von TiNF und Strukturbestimmung durch Pulverdiffraktometrie mit Synchrotronstrahlung. 1988, 100, 1013-1013  Uniforme heterogene Katalysatoren idie Rolle der Festkiperchemie bei der Katalysatorentwicklung. 1988, 100, 1735-1753  Synthesis of TiNF and Structure Determination by Powder Diffraction using Synchrotron Radiation. 1988, 27, 929-930  Uniform Heterogeneous Catalysts: The Role of Solid-State Chemistry in their Development and Design. 1988, 27, 1673-1691	47 13 38 14
1721 1720 1719 1718	Structural Aspects of the Lattice Thermal Expansion of Hexagonal Cordierite. 1987, 70, 175-182  Synthese von TiNF und Strukturbestimmung durch Pulverdiffraktometrie mit Synchrotronstrahlung. 1988, 100, 1013-1013  Uniforme heterogene Katalysatoren idie Rolle der Festkiperchemie bei der Katalysatorentwicklung. 1988, 100, 1735-1753  Synthesis of TiNF and Structure Determination by Powder Diffraction using Synchrotron Radiation. 1988, 27, 929-930  Uniform Heterogeneous Catalysts: The Role of Solid-State Chemistry in their Development and Design. 1988, 27, 1673-1691	47 13 38 14 141

Neutron poweder diffraction investigation of ⊞nd ⊯opper chloride in the temperature range 8586 K. <b>1988</b> , 28-30, 284-293	5
1712 Structure of the proton conductor, cubic HSbO3tkH2O. <b>1988</b> , 28-30, 601-606	3
1711 Aluminate sodalites 🖪 family with strained structures and ferroic phase transitions. <b>1988</b> , 15, 419-426	50
1710 Darstellung und Struktur ternÆer Platinhydride A3PtH5 mit A? K, Rb oder Cs. <b>1988</b> , 566, 31-38	32
1709 La3Ba3Cu6O14+x: A single phase or a mixture?. <b>1988</b> , 107, 73-84	11
1708 Neutron Powder Diffraction of Nb2BN1-x. <b>1988</b> , 71, C450-C452	14
1707 Bismuth valence order-disorder study in BaBiO3 by powder neutron diffraction. <b>1988</b> , 65, 1363-1369	111
The ab-initio crystal structure determination of UPd2Sn by synchrotron X-ray powder diffraction.  1706 1988, 67, 831-835	25
Magnetic structure and Missbauer spectroscopy of the canted 1D-antiferromagnet Ba2CoFeF9.  1705  1988, 66, 987-991	1
1704 Crystal structure and magnetic properties of pseudoternary NdRh2⊠RuxSi2 compounds. <b>1988</b> , 65, 261-	-265 9
1704 Crystal structure and magnetic properties of pseudoternary NdRh2\(\mathbb{R}\) RuxSi2 compounds. <b>1988</b> , 65, 261- 1703 CePd2Si2: A reduced-moment antiferromagnet. <b>1988</b> , 66, 103-107	- <b>265</b> 9
1703 CePd2Si2: A reduced-moment antiferromagnet. <b>1988</b> , 66, 103-107	52 8
CePd2Si2: A reduced-moment antiferromagnet. <b>1988</b> , 66, 103-107  Crystal and magnetic structures of the ferrimagnet Ba2Ni7F18. <b>1988</b> , 65, 185-188	52 8
1703 CePd2Si2: A reduced-moment antiferromagnet. 1988, 66, 103-107  1702 Crystal and magnetic structures of the ferrimagnet Ba2Ni7F18. 1988, 65, 185-188  1701 Neutron diffraction and magnetic anisotropy study of Y-Fe-Ti intermetallic compounds. 1988, 66, 465-4  1700 Ba2U2O7: Crystal structure and phase relationships. 1988, 49, 551-554  1699 A neutron powder diffraction study of Ba2YCu3O7. 1988, 49, 47-52	52 8 469 115
CePd2Si2: A reduced-moment antiferromagnet. <b>1988</b> , 66, 103-107  Crystal and magnetic structures of the ferrimagnet Ba2Ni7F18. <b>1988</b> , 65, 185-188  Neutron diffraction and magnetic anisotropy study of Y-Fe-Ti intermetallic compounds. <b>1988</b> , 66, 465-4  Ba2U2O7: Crystal structure and phase relationships. <b>1988</b> , 49, 551-554	52 8 469 115
1703 CePd2Si2: A reduced-moment antiferromagnet. 1988, 66, 103-107  1702 Crystal and magnetic structures of the ferrimagnet Ba2Ni7F18. 1988, 65, 185-188  1701 Neutron diffraction and magnetic anisotropy study of Y-Fe-Ti intermetallic compounds. 1988, 66, 465-4  1700 Ba2U2O7: Crystal structure and phase relationships. 1988, 49, 551-554  1699 A neutron powder diffraction study of Ba2YCu3O7. 1988, 49, 47-52  A low-temperature powder neutron diffraction study of the antiferromagnetic phase of	52 8 469 115 17

1695	The chemical bonds in MeSb2O4 (Me = Mn, Ni, Fe, Zn) isomorphous compounds: Thermal expansion, force constants, energies. <b>1988</b> , 73, 305-316	14
1694	La8NSrxCu8O20: An oxygen-deficient perovskite built of CuO6, CuO5, and CuO4 polyhedra. <b>1988</b> , 73, 514-519	112
1693	YBaCuFeO5+⊞ A novel oxygen-deficient perovskite with a layer structure. <b>1988</b> , 73, 531-535	196
1692	The structures of the Bcarbides Ni6Mo6C, Co6Mo6C, and Co6Mo6C2. <b>1988</b> , 75, 296-304	43
1691	Structure determination of LISICON solid solutions by powder neutron diffraction. <b>1988</b> , 75, 390-396	23
1690	Structure and bonding in Li2MoO3 and Li2MoO3 (0 <i>版</i> 加.7). <b>1988</b> , 76, 87-96	75
1689	The crystal and magnetic structures of Sr2CoFeO5. <b>1988</b> , 76, 334-339	44
1688	Superconducting Tl2Ba2CuO6: The orthorhombic form. <b>1988</b> , 76, 432-436	41
1687	Neutron powder diffraction structure and electrical properties of the defect pyrochlores Pb1.5M2O6.5 (M = Nb, Ta). <b>1988</b> , 77, 322-335	28
1686	The magnetic properties of the synthetic langbeinite KBaCr2(PO4)3. <b>1988</b> , 75, 21-29	37
1685	Novel defect pyrochlores ABi2B5O16 (A = Cs, Rb; B = Ta, Nb). <b>1988</b> , 75, 188-196	14
1684	The structural and magnetic properties of SrMnO3: A reinvestigation. <b>1988</b> , 74, 60-66	134
1683	Carbon species in the crystal structures of uranium-transition-element carbides,UMC2. <b>1988</b> , 74, 304-313	7
1682	Ber Metallalkyl- und -aryl-Verbindungen: XXXVII. Strukturverfeinerung von Methylkalium. Darstellung von KCD3 und Neutronenbeugungsuntersuchung bei 1.35 und 290 K. <b>1988</b> , 358, 1-14	28
1681	Neutron-diffraction evidence for 3D long-range antiferromagnetic ordering in DyBa2Cu3O6.95 and for antiferromagnetic correlations in HoBa2Cu3O6.8. <b>1988</b> , 152, 145-153	69
1680	High-temperature charge-density studies of CeO2⊠ using x-ray and neutron diffraction techniques. <b>1988</b> , 150, 241-249	7
1679	Magnetic order in the ternary compound TmCu2Si2. 1988, 75, 303-308	19
1678	The magnetic structure of NaMnFeF6. <b>1988</b> , 74, 158-164	4

1677 Fluorocomplexes of niobium IV. <b>1988</b> , 74, 165-176	8
1676 Structural and magnetic properties of Mn1EFetAs (0.00 Æ Æ0.20). 1988, 73, 318-326	5
1675 Crystal structure and magnetic properties of NaFe1NAlxO2 solid solutions. 1988, 75, 73-78	2
1674 Magnetic structure of NaFe0.25Al0.75O2. <b>1988</b> , 72, 215-218	
1673 L'oxynitrure de silicium: Si2N2O. <b>1988</b> , 23, 1087-1099	10
1672 Structural anomalies of YBa2Cu3O6.9 at the superconducting transition temperature. <b>1988</b> , 23, 1439-1445	29
1671 The solid phases of sulphur hexafluoride by powder neutron diffraction. <b>1988</b> , 184, 123-145	33
1670 Low-temperature structural distortion in CuS. <b>1988</b> , 184, 111-121	82
1669 Crystallographic study of tetragonal, superconducting YBa2(Cu0.93Fe0.05)3O7. <b>1988</b> , 71, 43-52	125
Probing structural changes during the onset of catalytic activity byin situ X-ray diffractometry. <b>1988</b> , 1, 191-194	27
E. P. R. and neutron diffraction investigation of the order of the ammonium ions in Rbx(NH4)1-x A1F4 single crystals. <b>1988</b> , 80, 19-22	
1666 A neutron diffraction study of amorphous boron. <b>1988</b> , 104, 249-252	17
1665 Magnetic structure and properties of equiatomic rare earth germanides. <b>1988</b> , 139, 221-231	18
1664 Darstellung und kristallstruktur des Natrium-Iridiumborids NaIr3B4. <b>1988</b> , 143, 49-57	3
1663 Time-of-flight neutron powder diffraction study of the LaNi5D3 structure. <b>1988</b> , 143, 315-324	30
1662 On the stabilization of Zr5Al3 in the Mn5Si3-type structure by interstitial oxygen. <b>1988</b> , 137, 55-59	7
1661 Crystallographic and magnetic structure of TbFe10V2 and ErFe10V2. <b>1988</b> , 144, 209-214	40
Reinvestigation of the oxygen stabilized Ti2Ni-type phase Ti4Fe2O0.4 by neutron diffraction. <b>1988</b> , 144, 275-281	9

1659	Neutron diffraction study of the crystallographic and magnetic structure of Nd2Fe14C. 1988, 144, L33-L37	30
1658	A single-crystal and synchrotron powder X-ray refinement of the structure of SrNb8O14, a new oxoniobate containing Nb6 octahedra. <b>1988</b> , 142, 123-133	29
1657	Komplexe platinhydride A2PtH4 MIT A? Na, K, Rb oder Cs. <b>1988</b> , 142, 243-252	50
1656	Note on the crystallographic and magnetic structure of YFe10V2. <b>1988</b> , 138, L11-L14	92
1655	Magnetic structure and preferential site occupation in manganese- and chromium-substituted Y2Fe14B compounds. <b>1988</b> , 136, 375-383	21
1654	Magnetic anisotropy and crystal structure of intermetallic compounds of the ThMn12 structure. 1988, 64, 5084-5087	62
1653	Ammonium perchlorate structure and dynamics at low temperatures. <b>1988</b> , 88, 5106-5122	25
1652	Ab-initio structure determination of LiSbWO6 by X-ray powder diffraction. <b>1988</b> , 23, 447-452	2050
1651	Crystal and magnetic structures of ternary metal hydrides: A comprehensive review. <b>1988</b> , 87-138	46
1650	Neutron diffraction and magnetic investigations of Ga substituted MnAl permanent magnet materials. <b>1988</b> , 63, 4616-4619	16
1649	Structure refinements of superconducting Tl2Ba2CaCu2O8 and Tl2Ba2Cu3O10 from neutron diffraction data. <b>1988</b> , 38, 6624-6630	151
1648	Neutron diffraction study of alpha -MnC2O. <b>1988</b> , 38, 9035-9039	5
1647	Neutron-powder-diffraction study of nuclear and magnetic structure in YBa2Cu3-xCoxO7+y with $x=0.84$ and $y=0.32$ . <b>1988</b> , 38, 6575-6582	84
1646	Triple-shell symmetry in alpha -(Al,Si)-Mn. <b>1988</b> , 37, 3906-3913	34
1645	Neutron-diffraction study of NdBa2Cu3O7+x with x=0.06 and 0.18. <b>1988</b> , 38, 11861-11864	15
1644	Superconducting and Magnetic Behavior in La2-xNaxCuO4. <b>1988</b> , 240, 495-7	65
1643	Structure of icosahedral clusters in cubic Al5.6Li. <b>1988</b> , 37, 8495-8498	48
1642	Site-selective doping and superconductivity in (La1-yPry)(Ba2-xLax)Cu3O7+ delta. <b>1988</b> , 38, 6667-6676	39

1641	Application of the Rietveld Refinement Procedure in Assaying Powdered Mixtures. 1988, 3, 2-6	216
1640	The magnetic structure of alpha -CoC2O4.2D2O investigated by means of neutron diffraction. <b>1988</b> , 21, 5273-5285	11
1639	Neutron Diffraction Study of Nonstoichiometry in Ba1.5La1.5Cu3Oy. <b>1988</b> , 27, L824-L826	19
1638	Structural characterization of La2 $\blacksquare$ MxCuO4 (M = Sr,Ba) samples by synchrotron x-ray and neutron powder diffraction techniques. <b>1988</b> , 3, 1327-1335	9
1637	Semi-Quantitative X-Ray Diffraction Analysis of Fly Ash by the Reference Intensity Ratio Method. <b>1988</b> , 136, 67	9
1636	A high-resolution NMR and synchrotron x-ray powder diffraction study of zeolite ZSM-11. <b>1988</b> , 3, 563-569	24
1635	A Practical Method for the Determination of the Instrumental Full Width at Half Maximum. <b>1988</b> , 3, 84-85	1
1634	A Neutron Diffraction Study of Non-Stoichiometric Mn1☑ O. <b>1988</b> , 138, 53	3
1633	Local structural variations in YBa2Cu. <b>1988</b> , 37, 9373-9381	63
1632	Using X-ray Powder Diffraction to Determine the Structure of VPI-5 - A Molecular Sieve with the Largest Known Pores. <b>1988</b> , 32, 507-514	5
1631	Verification of the Triclinic Crystal Structure of Kaolinite. <b>1988</b> , 36, 225-232	113
1630	Rietveld Refinement of Non-Hydrogen Atomic Positions in Kaolinite. <b>1989</b> , 37, 289-296	193
1629	Electron Diffraction Evidence for C-Centering of Non-Hydrogen Atoms in Kaolinite. <b>1989</b> , 37, 563-565	9
1628	Structure Refinements in Chemistry and Physics. A Comparative Study Using the Rietveld and the Two- Step Method. <b>1989</b> , 33, 261-268	2
1627	Neutron Scattering Methods for Materials Science. <b>1989</b> , 166, 15	1
1626	Structural properties of liquid alkali-metal-lead alloys: NaPb, KPb, RbPb, and CsPb. <b>1989</b> , 40, 6018-6029	68
1625	Neutron-powder-diffraction study of the structure and antiferromagnetic ordering in Pr2CuO4. <b>1989</b> , 40, 6998-7004	78
1624	Structural characteristics of Sr1⊠LaxTi3+□as a function of oxygen partial pressure at 1400 °C. <b>1989</b> , 65, 1492-1498	67

1623	Synthesis and properties of nonstoichiometric samples of YBa2Cu3O7-x; 0.04 . <b>1989</b> , 39, 254-258	40
1622	Microstructure, lattice parameters, and superconductivity of YBa2(Cu1-xFex)3O7- delta for 0 . <b>1989</b> , 39, 6667-6680	227
1621	Support for the Haldane conjecture: Gap for magnetic excitations in the quasi-one-dimensional S=1 Heisenberg antiferromagnet AgVP2S6. <b>1989</b> , 39, 4820-4823	36
1620	Thermal-neutron scattering lengths and capture by even calcium isotopes. <b>1989</b> , 39, 1297-1306	19
1619	Structural properties of the superconductor LaBa2Cu3-yO7-z in the solid solution system La1+xBa2-xCu3-yO7-z. <b>1989</b> , 40, 6771-6786	57
1618	Neutron powder diffraction study in the mixed molecular system (NaCN)1-x(KCN)x. <b>1989</b> , 39, 6186-6193	19
1617	Neutron-diffraction study of ErBa2Cu3Ox in the composition range 6.1 . <b>1989</b> , 40, 4472-4477	54
1616	Neutron Rietveld Analysis of Anion and Cation Disorder in the Fast-Ion Conducting Pyrochlore System Y2(ZrxTi1☑)2O7. <b>1989</b> , 166, 81	17
1615	Crystal Structure and Thermal Conductivity of Gd3(Ga1-xAlx)5O12Garnets. 1989, 28, 1644-1647	15
1614	De Gruyter. <b>1989</b> , 186,	
1613	Neutron powder diffraction study of a Na,Cs-Rho zeolite. <b>1989</b> , 187, 253-266	15
1612	Cyanogen: structure, dynamics and inter-molecular potentials. <b>1989</b> , 1, 5827-5835	5
1611	Exchange striction and exchange constants in Bi2CuO4. <b>1989</b> , 1, 7045-7053	24
1610	Crystal Structures of Superconducting LnBaAeCu3Oy(Ln=La, Nd; Ae=Ca, Sr). <b>1989</b> , 28, 754-757	12
1609	A neutron powder diffraction study of Rbx(NH4)1-xAlF4mixed compounds. 1989, 1, 1577-1588	1
1608	Neutron Powder Diffraction Study of the Structures of La1.9Ca1.1Cu2O6 and La1.9Sr1.1Cu2O6+ $\square$ 1989, 166, 187	1
1607	Perovskite threefold superlattices: A structure determination of the A3M3O8 phase. <b>1989</b> , 24, 423-430	42
1606	Structural and magnetic properties of FeNbO4-II. <b>1989</b> , 24, 523-527	23

## (1989-1989)

1605	Thermal expansion of NaTi2(PO4)3 studied by rietveld method from X-ray diffraction data. <b>1989</b> , 24, 611-618	57
1604	New barium tantalum sulphides Part 2. Ba3Ta2S8. <b>1989</b> , 24, 625-631	6
1603	Powder X-ray diffraction data and crystal structures of ternary sulphides, Ba2TiS4, Ba3TiS5 and tetragonal BaCu2S2. <b>1989</b> , 24, 1337-1345	21
1602	New barium tantalum sulphides Part 4. Ba16.5Ta9S39. <b>1989</b> , 24, 1491-1499	5
1601	Properties and structures of R2⊠AxCuO4 phases: R = La, Pr and Nd; A = Sr, Pb and Cd. <b>1989</b> , 24, 321-330	44
1600	Modulated structure and weak ferromagnetism in Nd3Ge5 studied by neutron diffraction and magnetic measurements. <b>1989</b> , 82, 99-108	15
1599	Crystallographic and magnetic structure of TbSi1.67 and TbSi1.67-🛭 <b>1989</b> , 79, 231-241	18
1598	Helicoidal magnetic structure of Ru2FeSi. <b>1989</b> , 80, 195-199	12
1597	Crystal and magnetic structure of the sulfur spinels Cu0.45Co0.55Cr2S4 - xSex. <b>1989</b> , 80, 311-317	2
1596	Magnetic structure of the TbNiC2 ternary carbide. <b>1989</b> , 81, 163-167	31
1596 1595	Magnetic structure of the TbNiC2 ternary carbide. <b>1989</b> , 81, 163-167  Crystal structures of high-T c oxides. <b>1989</b> , 76, 413-444	241
1595	Crystal structures of high-T c oxides. <b>1989</b> , 76, 413-444  Monoclinic symmetry in LaSrCu0.5Co0.5O4½ found by neutron, Guinier-and synchrotron-X-ray	241
1595 1594	Crystal structures of high-T c oxides. 1989, 76, 413-444  Monoclinic symmetry in LaSrCu0.5Co0.5O4½ found by neutron, Guinier-and synchrotron-X-ray powder structure analysis. 1989, 75, 439-445	241
1595 1594 1593	Crystal structures of high-T c oxides. 1989, 76, 413-444  Monoclinic symmetry in LaSrCu0.5Co0.5O4½ found by neutron, Guinier-and synchrotron-X-ray powder structure analysis. 1989, 75, 439-445  Elastic and quasielastic neutron scattering studies in KBr:KCN mixed crystals. 1989, 75, 81-99	241 4 16
1595 1594 1593 1592	Crystal structures of high-T c oxides. 1989, 76, 413-444  Monoclinic symmetry in LaSrCu0.5Co0.5O4½ found by neutron, Guinier-and synchrotron-X-ray powder structure analysis. 1989, 75, 439-445  Elastic and quasielastic neutron scattering studies in KBr:KCN mixed crystals. 1989, 75, 81-99  Magnetic properties and antiferromagnetic Cu ordering in Pr2CuO4. 1989, 77, 185-191  The crystal structure of the prototypic ceramic superconductor BaPbO3: An X-ray and neutron	241 4 16 58
1595 1594 1593 1592 1591	Crystal structures of high-T c oxides. 1989, 76, 413-444  Monoclinic symmetry in LaSrCu0.5Co0.5O4® found by neutron, Guinier-and synchrotron-X-ray powder structure analysis. 1989, 75, 439-445  Elastic and quasielastic neutron scattering studies in KBr:KCN mixed crystals. 1989, 75, 81-99  Magnetic properties and antiferromagnetic Cu ordering in Pr2CuO4. 1989, 77, 185-191  The crystal structure of the prototypic ceramic superconductor BaPbO3: An X-ray and neutron diffraction study. 1989, 75, 297-302  A comparison of the catalytic performance of the layered oxychlorides of bismuth, lanthanum and	241 4 16 58 25

1587 Structure refinement of La1.9Ca1.1Cu2O6 with neutron powder diffraction data. <b>1989</b> , 157, 89-92	69
1586 Crystal structure of synthetic mordenites. <b>1989</b> , 9, 170-176	65
1585 . <b>1989</b> , 25, 2154-2157	8
$_{15}8_{4}$ Rietveld refinement of Y2O3 using the Pearson VII profile shape function. <b>1989</b> , 24, 607-611	29
1583 Lokalisierung von para-Xylol in Yb-Faujasit (Zeolith Y) durch Neutronenbeugung. <b>1989</b> , 101, 786-787	6
1582 Residual stress and stress distribution in a WC-Ni composite. <b>1989</b> , 119, 127-134	47
1581 Neutron scattering characterization of magnetic materials. <b>1989</b> , 3, 387-391	
Neutron diffraction refinement and high resolution X-ray study of crystal structure of LiND4SO4 (DLAS). <b>1989</b> , 156-157, 118-120	6
1579 Fe3F8(H2O)2: Magnetic structures at 40 and 2 K and Monte Carlo simulation. <b>1989</b> , 156-157, 327-328	3
Preferential site occupation in Y and La substituted Pr2Fe14B intermetallic compounds. <b>1989</b> , 156-157, 747-750	5
1577 Antiferromagnetism of UNi2P2 and UNiAs2 by neutron diffraction. <b>1989</b> , 156-157, 829-831	21
Neutron powder diffraction study of Pb2Sr2YCu3O8, the prototype of a new family of superconductors. <b>1989</b> , 157, 272-278	115
Structural phase relations in the La2MJLnxSryCuO4II, the Ln2MCexCuO4II and the Ln2MSryCuO4II systems: A powder neutron diffraction study. <b>1989</b> , 161, 21-33	20
1574 Dynamics of Fe in superconducting YBa2(Cu1NFex)3Oy by neutron scattering. <b>1989</b> , 159, 124-130	17
1573 Metal ordering and oxygen displacements in (Nd, Sr, Ce)2CuO4 Jy. <b>1989</b> , 158, 440-448	71
Neutron and low temperature X-ray powder diffraction and thermal expansion measurements on La1.85Sr0.15Cu1 $\&$ ZnxO4 $\&$ 1989, 158, 458-464	5
1571 Alkali-metal substituted La2CuO4: Structures of La2⊠MxCuO4 (M = Na, K;x 🛈.2). <b>1989</b> , 158, 465-470	20
EXAFS and neutron diffraction studies of local and average structures for YBa2Cu2.8Zn0.2O7 <b>1989</b> , 157, 483-490	74

1569	The superconductors (Tl, Pb)Sr2CaCu2O7 and (Tl, Pb)Sr2Ca2Cu3O9: Neutron powder diffraction, high resolution electron microscopy and X-ray absorption studies. <b>1989</b> , 159, 245-254	59
1568	High resolution synchrotron X-ray powder diffraction study of the structure of TI2 Ba 2 CaCu 2 O 8. <b>1989</b> , 162-164, 530-531	1
1567	The magnetic structure of Pd3MnD0.53. <b>1989</b> , 71, 623-626	12
1566	New investigation on magnetic and neutron diffraction properties of Y2Cu2O5 and related oxides. <b>1989</b> , 72, 459-463	35
1565	Neutron diffraction study of substituted YBa2Cu2.85M0.15O7-🛭 <b>1989</b> , 70, 919-921	7
1564	A neutron powder diffraction study of the effect of pressure on the crystal structure of La2CuO4. <b>1989</b> , 69, 261-264	20
1563	Structural singularities in the vicinity of superconductive transition in YBa2Cu3O7-b-material. <b>1989</b> , 70, 159-162	12
1562	Combined use of nuclear magnetic resonance, electron microscopy, and diffraction techniques as a probe of the uniqueness of zeolite structures: zeolites KZ-2, Theta-1, ZSM-22, and NU-10. <b>1989</b> , 9, 531-534	23
1561	Application of X-ray energy-dispersive diffraction for characterization of materials under high pressure. <b>1989</b> , 18, 93-138	43
1560	Methodologies to establish the structure and composition of new zeolitic molecular sieves. <b>1989</b> , 50, 449-467	30
1559	Magnetism of iron-sulfur tetrahedral frameworks in compounds with thallium I. Chain structures. <b>1989</b> , 50, 297-308	27
1558	Sur le systfhe BaFeO3Ӣ (0 1989, 80, 6-11	40
1557	Preparation and crystal structures of La2Cu1\( \text{LixO4}\) solid solutions and evidence for a new oxide with a defect K2NiF4 structure: La4Li2O7. <b>1989</b> , 80, 112-119	38
1556	Crystal structure and magnetism in CoSb2O6 and CoTa2O6. <b>1989</b> , 83, 20-30	64
1555	Crystal structure of Li3ThF7 solved by X-ray and neutron diffraction. <b>1989</b> , 80, 206-212	18
1554	Spin-glass behavior in Sr2FeRuO6 and BaLaNiRuO6: A comparison with antiferromagnetic BaLaZnRuO6. <b>1989</b> , 78, 281-293	120
1553	Single-crystal X-ray and powder neutron diffraction of ThB2C (ThB2C-type). <b>1989</b> , 78, 294-300	26
1552	Ordered magnetic frustration. <b>1989</b> , 78, 66-77	24

1551	The crystal and magnetic structures of Sr2LuRuO6, Ba2YRuO6, and Ba2LuRuO6. <b>1989</b> , 78, 108-116	151
1550	Refinement of the lithium distribution in Li2Ti3O7 using high-resolution powder neutron diffraction. <b>1989</b> , 78, 170-177	32
1549	Neutron powder investigation of praseodymium and cerium nitride fluoride solid solutions. <b>1989</b> , 83, 324-331	18
1548	Crystal structure determination and rietveld refinement of Zn(OH)(NO3) []H2O. <b>1989</b> , 81, 9-20	43
1547	The oxidation state of Pr in PrBa2Cu3O7. <b>1989</b> , 81, 121-128	88
1546	Structure and oxidation state relationships in ternary copper oxides. <b>1989</b> , 82, 21-29	105
1545	The structure of V9Mo6O40 determined by powder neutron diffraction. <b>1989</b> , 82, 65-69	16
1544	Neutron diffraction determination of full structures of anhydrous Li?X and Li?Y zeolites. <b>1989</b> , 82, 95-102	90
1543	Structure determinations of La2O2CO3-II and the unusual disordered phase La2O2.52(CO3)0.74Li0.52 using powder diffraction. <b>1989</b> , 82, 132-138	36
1542	Crystal and magnetic structures of LiCoF4: The first compound with a dirutile structure. <b>1989</b> , 79, 1-11	19
1541	Crystal structure and magnetism in MnSb2O6: Incommensurate long-range order. <b>1989</b> , 79, 263-276	36
1540	Powder neutron diffraction study of the thermal expansion of a K-substituted cordierite. <b>1989</b> , 24, 3976-3983	15
1539	Bindungsverh/tnisse in kristallinen Phasen von Caesiumhydrogensulfid, CsHS und CsDS. <b>1989</b> , 569, 117-130	11
1538	Neutronenbeugung an Li2CuO2. <b>1989</b> , 578, 18-26	13
1537	Thermal Expansion of Tungsten Carbide at Low Temperature. <b>1989</b> , 72, 515-517	31
1536	Effect of YO1.5 Dopant on Unit-Cell Parameters of ZrO2 at Low Contents of YO1.5. <b>1989</b> , 72, 662-664	46
1535	Crystal Structure of Orthorhombic Zirconia in Partially Stabilized Zirconia. <b>1989</b> , 72, 1757-1760	141
1534	The Structure of Y1Ba2Cu3O7-□ and its Derivatives. <b>1989</b> , 42, 135-212	103

1533	MFIT: Multiple spectra fitting program. <b>1989</b> , 2, 24-26	47
1532	Electrical resistivity and magnetic ordering of gadolinium and terbium bromide deuterides, LnBrDx (). <b>1989</b> , 152, 227-238	9
1531	Superstructure in the intermetallic compound TmNi2. <b>1989</b> , 153, 259-266	17
1530	Synthese ternÆer nitride von alkalimetallen: Verbindungen mit tantal, MTaN2 MIT M ? Na, K, RbundCs. <b>1989</b> , 146, 147-160	7°
1529	Hydrogen(deuterium)-stabilized and lithiumintercalated erbium monochloride: An X-ray singlecrystal and neutron powder diffraction study. <b>1989</b> , 156, 161-171	9
1528	Crystallographic and magnetic structure of ternary carbides of the type Nd2Fe17Cx. <b>1989</b> , 155, 15-21	101
1527	A neutron diffraction study of the atomic ordering in Er(Fe1 lkCox)3. <b>1989</b> , 149, 363-369	3
1526	Structure of the ⊞-phase of solid methanol. <b>1989</b> , 67, 575-581	105
1525	Crystal structures of methylene bromide and methylene iodide. <b>1989</b> , 68, 835-851	19
1524	Neutron Powder Diffraction: A Powerful Materials Research Technique. <b>1989</b> , 166, 41	1
1523	Powder Diffraction Data for Synthetic Pargasite, Scandian Pargasite and Their Fluorine Analogues: NaCa2Mg4(Al,Sc)Si6Al2O22(OH,F)2. <b>1989</b> , 4, 36-39	
1522	The Determination of Direction-Dependent Crystallite Size and Strain by X-Ray Whole-Powder-Pattern Fitting. <b>1989</b> , 4, 130-136	11
1521	Structure of ErBa2Cu3Ox in the Composition Range 6.1 1989, 166, 181	1
1520	Neutrons: The Kinder, Gentler Probe of Condensed Matter. <b>1989</b> , 166, 3	
1519	Neutron Irradiated Uranium Silicides Studied by Neutron Diffraction and Rietveld Analysis. <b>1989</b> , 166, 437	3
1518	The Effect of Sorbates and Elevated Temperatures on the Structures of Some Zeolite Catalysts. 1989, 46, 827-842	5
1517	Multitechnique Analysis of The Lattice Structures of Highly Siliceous Zeolites. <b>1989</b> , 545-557	2
1516	Structural and chemical varieties of dioptase, Cu6[Si6O18] [16H2O. <b>1989</b> , 187, 15-23	22

1515	Crystal structure and cation distribution of MnCrInS4 from synchrotron powder diffraction data. <b>1990</b> , 190, 277-285	2
1514	Bestimmung der Kristallstruktur von T-Na3PO4 mit R\(\textit{l}\)tgen- und Neutronenpulvertechniken. <b>1990</b> , 192, 233-243	26
1513	Use of Rietveld Pattern Fitting to Determine the Weight Fraction of Crystalline Material in Natural Low Quartz Specimens. <b>1990</b> , 5, 64-69	12
1512	Neutron Irradiated Uranium Silicides Studied by Neutron Diffraction and Rietveld Analysis. <b>1990</b> , 209, 579	1
1511	X-Ray Determination of Site Occupation Parameters in Ordered Ternaries Cu(AuxM1-xM = Ni,Pd. <b>1990</b> , 213, 369	6
1510	Rietveld Structure Refinement of Metastable Lithium Disilicate Using Synchrotron X-Ray Powder Diffraction Data From the Daresbury SRS 8.3 Diffractometer. <b>1990</b> , 5, 137-143	6
1509	QPDA IA User-Friendly, Interactive Program for Quantitative Phase and Crystal Size/Strain Analysis of Powder Diffraction Data. <b>1990</b> , 5, 195-199	16
1508	Synchrotron X-ray Rietveld analysis of .ALPHAhafnium phosphate <b>1990</b> , 6, 689-693	11
1507	Measurement of Phase Abundance in Magnesia-Partially-Stabilized Zirconia by Rietveld Analysis of X-ray Diffraction Data. <b>1990</b> , 73, 2822-2827	24
1506	Neutron Diffraction Studies of Phase Transformations between Tetragonal and Orthorhombic Zirconia in Magnesia-Partially-Stabilized Zirconia. <b>1990</b> , 73, 2828-2833	82
1505	<b>P</b> olymorph MethodDetermination of Monoclinic Zirconia in Partially Stabilized Zirconia Ceramics. <b>1990</b> , 73, 3096-3099	20
1504	Determination of valence and cation distributions by resonant powder X-ray diffraction. <b>1990</b> , 343, 46-49	47
1503	Extending the power of powder diffraction for structure determination. <b>1990</b> , 346, 731-734	56
1502	Role of oxygen in PrBa2Cu3O7-y: Effect on structural and physical properties. <b>1990</b> , 41, 6655-6667	162
1501	Several features of the dealumination of type Y zeolite using silicon tetrachloride and ethylenediaminetetraacetic acid. <b>1990</b> , 39, 861-866	1
1500	Magnetic ordering in PrFe2Ge2. <b>1990</b> , 86, 377-382	19
1499	Magnetic order in DyFe2Si2 compound. <b>1990</b> , 86, 383-386	15
1498	Magnetic structure of NdCo2Ge2 compound. <b>1990</b> , 86, 387-390	18

1497	The magnetic structure of the ferrimagnet NaCu3F7. <b>1990</b> , 87, 57-62	1
1496	Modulated structure and ferromagnetic ordering in PrGe1.60 studied by neutron diffraction and magnetic measurements. <b>1990</b> , 89, 47-55	11
1495	High-temperature crystal structures of orthorhombic and rhombohedral PrNiO3. <b>1990</b> , 25, 1091-1098	26
1494	Determination of the composition of BaNbO3 using profile refinement and phase analysis. <b>1990</b> , 25, 9-14	18
1493	Mixed oxides: The crystal structure of Ba3NiRuSbO9. <b>1990</b> , 25, 89-93	11
1492	The structure of the 🛭-phase CaZr4O9 in calcium stabilized zirconia. <b>1990</b> , 25, 435-442	12
1491	Polymorphism of the fast ionic conductor Li2MnBr4-neutron diffraction and differential scanning calorimetry. <b>1990</b> , 25, 451-456	11
1490	New barium tantalum sulphides Part 5. Ba2TaS5. <b>1990</b> , 25, 723-730	7
1489	Structural evolution study of substituted watites Fe1 Iz Iy (Ca, Mg)yO. <b>1990</b> , 51, 1131-1136	8
1488	Anisotropic thermal expansion of YBa2Cu4O8 in the temperature range 10🛭97 K. <b>1990</b> , 170, 56-58	15
1487	Growth of single crystals, thermal dependency of lattice parameters and Raman scattering in the Nd2-xCexCuO4-□system. <b>1990</b> , 170, 103-111	30
1486	Structure refinement and water location in the very large-pore molecular sieve VPI-5 by X-ray Rietveld techniques. <b>1990</b> , 10, 163-168	37
1485	Linear¶hain Antiferromagnetism in ∃-NiC2O4 🛛 2D2O. <b>1990</b> , 161, K99-K102	
1484	Determination of the Cationic Arrangement in Sn2F6 from neutron powder diffraction. <b>1990</b> , 590, 173-180	14
1483	The thermal expansion of ScAlO3 🖪 silicate perovskite analogue. <b>1990</b> , 17, 89-96	33
1482	The structural consequences of charge disproportionation in mixed-valence iron oxides. II. The crystal and magnetic structures of BaLaFe2O5.91 at 5 K. <b>1990</b> , 85, 38-43	21
1481	Structure and oxygen stoichiometry in Ln2⊠Sr1+xCu2O6Ӣ (Ln = La, Nd, Sm) phases. <b>1990</b> , 85, 88-99	36
1480	A structural study of the incorporation of silica into sodiumferrites, Na1 $\square$ [Fe1 $\square$ SixO2], x = 0 to 0.20. <b>1990</b> , 85, 202-219	20

1479	Properties of a new perovskite oxyde Sr2VO4. <b>1990</b> , 85, 321-325	81
1478	Synthesis and structural characterization of gallosilicates with the zeolite ANA-framework. <b>1990</b> , 10, 553-558	24
1477	Charting cation migration in a nickel exchanged zeolitic catalyst: An in situ rietveld X-ray study. <b>1990</b> , 2, 181-183	49
1476	Strukturbestimmung an NaCD3-Pulvern bei 1.5 und 300 K durch Neutronen- und Synchrotronstrahlenbeugung. <b>1990</b> , 102, 728-729	9
1475	New X-ray rietveld refinement of kaolinite from Keokuk, Iowa. <b>1990</b> , 25, 105-110	10
1474	Ber Metallalkyl- und -aryl-Verbindungen, 40 Strukturverfeinerung von Methyllithium durch Neutronenbeugung von (LiCD3)4 bei 1.5 und 290 K. <b>1990</b> , 123, 79-81	56
1473	A versatile double-axis multicounter neutron powder diffractometer. <b>1990</b> , 288, 477-485	135
1472	Ferromagnetic layers in Y2Cu2O5: a neutron diffraction study. <b>1990</b> , 149, 319-327	20
1471	F-electron localization/delocalization phenomena in PrBa2Cu3O7 and CmBa2Cu3O7. <b>1990</b> , 163, 655-658	21
1470	Structural studies of the T*-phases (La, Tb, Pb)2CuO4, (La, Tb, Sr)2CuO4. <b>1990</b> , 171, 468-478	5
1470 1469	Structural studies of the T*-phases (La, Tb, Pb)2CuO4, (La, Tb, Sr)2CuO4. <b>1990</b> , 171, 468-478  Formation mechanism of 110 K high-Tc superconducting phase in the Ca- and Cu-rich Bi-Pb-Sr-Ca-Cu-O system. <b>1990</b> , 169, 76-80	5 45
1469	Formation mechanism of 110 K high-Tc superconducting phase in the Ca- and Cu-rich	
1469	Formation mechanism of 110 K high-Tc superconducting phase in the Ca- and Cu-rich Bi-Pb-Sr-Ca-Cu-O system. <b>1990</b> , 169, 76-80	45
1469 1468 1467	Formation mechanism of 110 K high-Tc superconducting phase in the Ca- and Cu-rich Bi-Pb-Sr-Ca-Cu-O system. <b>1990</b> , 169, 76-80  A structural study of Ni-substituted Pb2Sr2YCu3O8+II <b>1990</b> , 165, 499-504  Crystal structure, atomic ordering and charge localization in Pb2Sr2Y1IICaxCu3O8+II (x=0, I=1.47).	45
1469 1468 1467	Formation mechanism of 110 K high-Tc superconducting phase in the Ca- and Cu-rich Bi-Pb-Sr-Ca-Cu-O system. <b>1990</b> , 169, 76-80  A structural study of Ni-substituted Pb2Sr2YCu3O8+E <b>1990</b> , 165, 499-504  Crystal structure, atomic ordering and charge localization in Pb2Sr2Y1\(\text{U}\)CaxCu3O8+E (x=0, \(\text{E}=1.47\). <b>1990</b> , 169, 401-412	45 2 45
1469 1468 1467 1466	Formation mechanism of 110 K high-Tc superconducting phase in the Ca- and Cu-rich Bi-Pb-Sr-Ca-Cu-O system. 1990, 169, 76-80  A structural study of Ni-substituted Pb2Sr2YCu3O8+1 1990, 165, 499-504  Crystal structure, atomic ordering and charge localization in Pb2Sr2Y1 CaxCu3O8+1 (x=0, 1=1.47). 1990, 169, 401-412  Sr-induced oxygen defects in La2 SrxCuO4-1 a neutron powder diffraction study. 1990, 172, 120-126	45 2 45 51
1469 1468 1467 1466	Formation mechanism of 110 K high-Tc superconducting phase in the Ca- and Cu-rich Bi-Pb-Sr-Ca-Cu-O system. 1990, 169, 76-80  A structural study of Ni-substituted Pb2Sr2YCu3O8+E 1990, 165, 499-504  Crystal structure, atomic ordering and charge localization in Pb2Sr2Y1ECaxCu3O8+E(x=0, E=1.47). 1990, 169, 401-412  Sr-induced oxygen defects in La2ESrxCuO4-Ea neutron powder diffraction study. 1990, 172, 120-126  The crystal structure of the La1.6Sr0.4CaCu2O6-Esuperconductor. 1990, 172, 138-142  Li2ZnI4: A neutron powder study. 1990, 87, 463-466	45 2 45 51 53

	The distorted perovskite : A novel example of 1:3 B-cation ordering. <b>1990</b> , 84, 16-22	18
1460	Crystallographic distortion and magnetic structure of terbium iron garnet at low temperatures. <b>1990</b> , 84, 39-51	26
1459	Crystal structure of the lithium ion conductor, Li3.4Ga0.2SiO4. <b>1990</b> , 88, 564-570	9
1458	The crystal and magnetic structures of Ba3NiRu2O9, Ba3CoRu2O9, and Ba3ZnRu2O9. 1990, 89, 174-183	65
1457	Low-temperature structures of CuO and AgO and their relationships to those of MgO and PdO. <b>1990</b> , 89, 184-190	69
1456	The crystal and magnetic structures of Sr2LaFe3O8. <b>1990</b> , 84, 237-244	51
1455	The structural consequences of charge disproportionation in mixed-valence iron oxides. I. The crystal structure of Sr2LaFe3O8.94 at room temperature and 50 K. <b>1990</b> , 84, 271-279	151
1454	A structural investigation of Ag0.167TiS2 by time-of-flight neutron powder diffraction. <b>1990</b> , 84, 355-364	6
1453	Persistence of the La2NiO4 crystal structure in La2-xBaxNiO4 samples with high Ba contents (x ? 1). <b>1990</b> , 76, 1327-1331	9
1452	UCr4Al8 and UMn4Al8: Neutron diffraction study. <b>1990</b> , 75, 929-933	12
		13
1451	The site preference of Cu substituted Zn and Ni in YBa2Cu3O7[1990, 75, 445-449	46
	The site preference of Cu substituted Zn and Ni in YBa2Cu3O7[1990, 75, 445-449	46
1450	The site preference of Cu substituted Zn and Ni in YBa2Cu3O7Ū1990, 75, 445-449  Neutron diffraction study of the magnetic structure of Er 2 BaNiO 5. 1990, 76, 467-474  Real time deuterium loading investigation in palladium using neutron diffraction. 1990, 75, 359-362	46 63
1450 1449	The site preference of Cu substituted Zn and Ni in YBa2Cu3O7Ū1990, 75, 445-449  Neutron diffraction study of the magnetic structure of Er 2 BaNiO 5. 1990, 76, 467-474  Real time deuterium loading investigation in palladium using neutron diffraction. 1990, 75, 359-362	46 63 4
1450 1449 1448 1447	The site preference of Cu substituted Zn and Ni in YBa2Cu3O7ll1990, 75, 445-449  Neutron diffraction study of the magnetic structure of Er 2 BaNiO 5. 1990, 76, 467-474  Real time deuterium loading investigation in palladium using neutron diffraction. 1990, 75, 359-362  Crystal and magnetic structure of Li2CuO2. 1990, 74, 779-784	46 63 4
1450 1449 1448 1447	The site preference of Cu substituted Zn and Ni in YBa2Cu3O7[1990, 75, 445-449  Neutron diffraction study of the magnetic structure of Er 2 BaNiO 5. 1990, 76, 467-474  Real time deuterium loading investigation in palladium using neutron diffraction. 1990, 75, 359-362  Crystal and magnetic structure of Li2CuO2. 1990, 74, 779-784  Phase Analysis of Metallic Plutonium-Containing Fuel Alloys Using Neutron Diffraction. 1990, 34, 447-457	46 63 4 108

1443 A neutron powder diffraction study of the #to Iphase transformation in NaFeO2. <b>1990</b> , 193, 51-69	23
Refinement of the crystal structure of the manganous antimonate Mn2Sb2O7 with neutron powder diffraction data by the profile decomposition method. <b>1990</b> , 190, 41-46	9
Unexpected effects of gold on the structure, superconductivity, and normal state of YBa2Cu3O7. <b>1990</b> , 57, 934-936	23
1440 Incorporation of gold into YBa2Cu3O7: Structure and Tc enhancement. <b>1990</b> , 42, 6200-6208	91
Three-dimensional magnetic properties of Bi2CuO4. <b>1990</b> , 2, 6989-6998	26
1438 Neutron Powder Diffraction. <b>1990</b> , 15, 49-55	5
1437 Investigation of magnetic ordering in UPdAs2by neutron diffraction. <b>1990</b> , 2, 3967-3972	10
1436 New microcrystalline catalysts. <b>1990</b> , 333, 173-207	69
On the preferential site occupation of Fe in RFe4Al8and related compounds. <b>1990</b> , 2, 1677-1681	46
1434 Crystal and magnetic structures of Bi2CuO4. <b>1990</b> , 2, 2205-2214	36
Faraday communications. HighIbw displacive transition in the all-silica form of the AlPO4-5 topology. <b>1990</b> , 86, 2341-2342	10
1432 Crystal-Chemistry of Transition Metal Hemicarbides. <b>1990</b> , 215-248	8
Neutron diffraction study of the Brown phase BaNd2CuO5. <b>1990</b> , 9, 401-404	30
High temperature methods for processing monazite: I. Reaction with calcium chloride and calcium carbonate. <b>1990</b> , 166, 197-210	26
On the preferential site occupation of T? Cr or Mn in rare earth compounds of the type RT4Al8. 1990, 166, 329-334	43
1428 A neutron diffraction study of Zr3PD3⊠. <b>1990</b> , 161, 269-278	15
Lithium-platinmetall-Al(Ga, In)-legierungen: Neue farbige tern/Ee intermetallische phasen. <b>1990</b> , 161, 303-312	17
Neutron diffraction determination of the Debye temperature of TraGa2/-x alloys (x = 0, 0.5, 1.75). <b>1990</b> , 158, 319-325	1

1425 Hydrogen-supported formation of G phase Cu16Zr6Al7 in the ternary system Cu?Zr?Al. <b>1990</b> , 159, 291-298	10
1424 Structure determination of Y0.95Ni2 by X-ray powder diffraction. <b>1990</b> , 161, L27-L31	48
Symmetry reduction and magnetic ordering in the defect ⊞-GdSi2-type compound TbSix, 1.75 ?x 1990, 162, 197-219	10
Neutron diffraction study of the structural and magnetic properties of the R2Fe17Hx(Dx) ternary compounds (R? Ce, Nd and Ho). <b>1990</b> , 162, 273-284	136
Magnetic structure of rare earth compounds of the type RFe10V2. <b>1990</b> , 162, 285-295	30
1420 Phase transitions and heterogeneous equilibria in the TaRu homogeneity range. <b>1990</b> , 157, 37-45	14
1419 Crystallographic and magnetic structure of Dy3Ge5 and DyGe1.9. <b>1990</b> , 163, 319-330	24
1418 Magnetic structure of ternary rare earth carbides of the type R2Fe17C. <b>1990</b> , 163, 353-359	27
1417 Crystal and magnetic structure of the permanent magnet material Lu2Fe14C. <b>1990</b> , 163, 361-368	12
Ber Metallalkyl- und -aryl-Verbindungen, 44 Darstellung und Struktur von Methylnatrium.  1416 Strukturbestimmung an NaCD3-Pulvern bei 1.5 und 300 K durch Neutronen- und  Synchrotronstrahlenbeugung. <b>1990</b> , 123, 1629-1634	39
The solid phases of deuterium sulphide by powder neutron diffraction. <b>1990</b> , 193, 1-19	36
1414 Synthese und Kristallstruktur eines gemischtvalenten Lithium-Tantalnitrids Li2Ta3N5. <b>1991</b> , 176, 47-60	25
1413 A novel hydride phase in hydrogen charged Ti3Al. <b>1991</b> , 39, 2799-2803	35
1412 Magnetic properties of single-crystal Y-Ba-Cu-O containing Fe. <b>1991</b> , 69, 5388-5390	4
Topotactic lithium exchange in manganese(III)arsenate hydrate: a switchable JahnIIeller distorted framework. <b>1991</b> , 604-606	10
1410 GasBolid interactions studied by quantitative powder X-ray diffraction analysis. <b>1991</b> , 87, 3063-3066	
1409 Magnetic frustration, spirals and short-range order in CrxFe1 VO4Dsolid solutions. <b>1991</b> , 1, 867-873	5
$_{1408}$ Improved method for the determination of the oxygen content in YBa2Cu3O7 $\blacksquare$ <b>1991</b> , 1, 863-866	12

1407	Quantitative studies of gasBolid reactions by powder X-ray diffraction: stoichiometric and catalytic conversion of CO to CO2 over YBa2Cu3O6 +x. <b>1991</b> , 87, 3067-3075	15
1406	La2 \scrxCuO4 \textbf{L} structural, magnetic and transport measurements on antiferromagnets, insulators and superconductors. <b>1991</b> , 1, 597-610	10
1405	The mechanism of lithium ion mobility in solid electrolytes. <b>1991</b> , 64, 1113-1118	6
1404	Isomorphous substitution in non-linear optical KTiOPO4. Powder diffraction and magic angle spinning nuclear magnetic resonance study of (K[] Na[] )TiOPO4 and (Rb[] Na[] )TiOPO4. <b>1991</b> , 1, 113-119	12
1403	Crystallographic and magnetic structure of Pr2Fe17N2.8. <b>1991</b> , 12, 93-96	6
1402	Uniaxial antiferromagnetic ordering in TbNiSi2. <b>1991</b> , 171, 321-327	24
1401	Crystal and magnetic structure of the permanent magnet material Tb2Fe14C. <b>1991</b> , 169, 147-156	17
1400	Refinement of the crystal structure of Hf2Fe. <b>1991</b> , 171, 9-15	20
1399	Neutron diffraction studies of the Zr3P-D system. <b>1991</b> , 170, 263-270	4
1398	Structure of Y0.95Ni2 and its hydride. <b>1991</b> , 172-174, 198-205	16
1397	Neutron diffraction studies of deuterated Ti3P. <b>1991</b> , 172-174, 206-212	7
1396	Na3RhH6, Na3IrH6 und Li3IrH6, neue komplexe Hydride mit isolierten [RhH6]3 - und [IrH6]3Oktaedern. <b>1991</b> , 176, 255-262	32
1395	Magnetic structure of KMnPO4?H2O. <b>1991</b> , 69, 6016-6018	23
1394	Magnetic phase transition in cobalt iodine boracite. <b>1991</b> , 33, 149-157	19
1393	X-Ray Powder Diffraction Rietveld Characterization of Synthetic Aluminum-Substituted Goethite. <b>1991</b> , 39, 248-253	28
1392	Applications of Rietveld Analysis to Materials Characterization in Solid-State Chemistry, Physics and Mineralogy. <b>1991</b> , 35, 25-38	2
1391	New Features and Advanced Applications of Siroquant: A Personal Computer XRD Full Profile Quantitative Analysis Software Package. <b>1991</b> , 35, 49-55	7
1390	De Gruyter. <b>1991</b> , 196, 111-120	20

1389	The structure of solid dichlorodifluoromethane CF2Cl2 by powder neutron diffraction. <b>1991</b> , 197, 121-130	8
1388	Cation distribution studies of three (Ni, Mg) orthovanadates. <b>1991</b> , 194, 49-55	8
1387	Solving the Crystal Structure of Cd5(OH)8(NO3)2l2H2O from Powder Diffraction Data. A Comparison with Single Crystal Data. <b>1991</b> , 6, 10-15	9
1386	Quantitative X-Ray Structure Determination of Superlattices and Interfaces. <b>1991</b> , 229, 41	6
1385	Effect of Structure on the Anomalous Mechanical Properties of Metallic Superlattices. <b>1991</b> , 239, 499	5
1384	Preparation and Crystal Structure of a New Barium Niobium Sulfide, Ba9Nb4S21. <b>1991</b> , 64, 2923-2925	11
1383	Neutron diffraction study of the nitride YTiFe11Nx. <b>1991</b> , 78, 313-316	84
1382	Synchrotron X-ray powder diffraction study of the phase I' compound: SnLa3Rh4Sn12. <b>1991</b> , 78, 359-366	29
1381	The crystal and magnetic structure of tetragonal Pd3Mn. <b>1991</b> , 78, 767-772	16
1380	Neutron profile refinement study of the low-temperature structural phases of LiKSO4. <b>1991</b> , 174, 95-100	10
1379	Structural aspects of high-Tc superconductors from neutron profile refinement studies. <b>1991</b> , 174, 311-322	9
1378	Structure and superconducting properties of Tl1PpbyY1NCaxSr2Cu2O7. <b>1991</b> , 179, 183-190	16
1377	Thermal expansion of Y2Ba4Cu7O15 in the temperature range 10🛭90 K, and comparison with YBa2Cu3O7 and YBa2Cu4O8. <b>1991</b> , 172, 491-494	10
1376	Effect of hydrogen reduction on the structure and conductivity of YBa2Cu3Oy. <b>1991</b> , 174, 23-27	6
1375	Structural changes accompanying oxygen incorporation in (Pb0.65Cu0.35Sr2(Y0.7Ca0.3)Cu2O7+1 1991, 175, 393-400	65
1374	Neutron powder diffraction study of the Pb-based copper oxide containing thick fluorite blocks: (Pb,Cu)Sr2(Ho,Ce)3Cu2O11+z. <b>1991</b> , 179, 455-460	18
1373	Influence of gamma-irradiation on oxygen distribution and YBa2Cu3O7⊠ ceramics stability. <b>1991</b> , 38, 175-179	
1372	Automated structure factor refinement from convergent-beam patterns. <b>1991</b> , 35, 185-196	117

Successful use of a linear position-sensitive neutron detector in solid state physics and materials science. **1991**, 310, 416-417

1370	High-temperature diffraction study of LnCoO3 perovskites: A high-order electronic phase transition. <b>1991</b> , 52, 441-448	57
1369	Structure determination and refinement with synchrotron X-Ray powder diffraction data. <b>1991</b> , 52, 1199-1208	337
1368	The crystal structures of Ag4Ge7O16ြ6D2O and Na3(ND4)Ge7O16[6D2O refined from high resolution synchrotron radiation and neutron powder diffraction data. <b>1991</b> , 52, 1209-1218	23
1367	Resonant powder x-ray diffraction applied to mixed valence compounds and the possibility of site-resolved x-ray absorption spectroscopy illustrated for YBa2Cu3O6.27. <b>1991</b> , 52, 1243-1249	16
1366	The Ab initio crystal structure determination of CuPt3O6 from a combination of synchrotron X-ray and neutron powder diffraction data. <b>1991</b> , 52, 1273-1279	7
1365	Synthesis, crystal structure, and properties of metallic PrNiO3: Comparison with metallic NdNiO3 and semiconducting SmNiO3. <b>1991</b> , 91, 225-237	320
1364	X-ray and neutron diffraction studies of the diffuse phase transition in ceramics. <b>1991</b> , 91, 350-361	299
1363	The high temperature synthesis of CsAlSiO4-ANA, a new polymorph in the system Cs2O?Al2O3?SiO2. <b>1991</b> , 95, 335-345	18
1362	Structure and thermal expansion of LiGe2(PO4)3. <b>1991</b> , 90, 185-193	90
1361	The crystal and magnetic structures of Ca2NdRuO6, Ca2HoRuO6, and Sr2ErRuO6. 1991, 90, 302-312	70
1360	The crystal and magnetic structures of Ca2Cr0.5Fe1.5O5 at 2.1 K. <b>1991</b> , 90, 42-46	18
1359	Sr3U11O36: Crystal structure and thermal stability. <b>1991</b> , 94, 12-18	16
1358	Structure determinations of two new ternary oxides: Ti3PdO and Ti4Pd2O. <b>1991</b> , 92, 39-50	8
1357	Ordered magnetic frustration: XVI. Magnetic structure of CsCoF4 at 1.5 K. <b>1991</b> , 93, 37-45	6
1356	Crystal structure of ⊞-Li2.5Al0.5SiO4. <b>1991</b> , 93, 436-442	3
1355	Synthesis, crystal structure, and magnetic properties of Co3(HPO4)2(OH)2 related to the mineral lazulite. <b>1991</b> , 92, 273-285	17
1354	Preparation and crystal structures of new barium zirconium sulfides, Ba2ZrS4 and Ba3Zr2S7. <b>1991</b> , 92, 286-294	29

## (1991-1991)

1353	Ce-Er, Ce-Lu, U-La, and U-Ce. <b>1991</b> , 92, 301-311	15
1352	Preparation and thermal decomposition of yttrium hydroxide fluorides. <b>1991</b> , 92, 370-379	18
1351	BaBiO2.5, a new bismuth oxide with a layered structure. <b>1991</b> , 92, 473-479	22
1350	Neutron diffraction investigation of magnetic phase transitions to long-range antiferromagnetic ordering in the <b>fr</b> ee-electron[praseodymium halides Pr2X5 (X = Br, I). <b>1991</b> , 95, 1-13	13
1349	Ru-Ta (Ruthenium-Tantalum). <b>1991</b> , 12, 395-397	0
1348	Superconductivity in (Y1☑ Sr x ) (Ba1.5Sr0.5)Cu3O7ਰ compounds. <b>1991</b> , 14, 279-285	3
1347	Structural and physical properties of Tl1\(\text{\textit{B}}\)BixSr2CuO5 (0.20\(\text{\texictex{\text{\texictex{\text{\text{\text{\text{\text{\texitex{\text{\text{\tex{	4
1346	Crystal structure of Pd(NO3)2(H2O)2. <b>1991</b> , 26, 269-275	21
1345	Alkaline earth copper oxides. <b>1991</b> , 26, 323-331	33
1344	The structure of KUO2PO4.3D2O refined from neutron and synchrotron-radiation powder diffraction data. <b>1991</b> , 26, 407-414	34
1343	Novel defect pyrochlores M0.5Tl0.5(NbTe)O6: Preparation and structural characterization. <b>1991</b> , 26, 789-795	3
1342	Structure determination of #I3VO4 from synchrotron radiation powder diffraction data: Stereochemical role of the lone pair of thallium(I). <b>1991</b> , 26, 973-982	7
1341	Structure determination of SrBi2O4. <b>1991</b> , 26, 989-993	10
1340	Evolution of microstructure of nitrogen ion implanted iron at high temperatures. <b>1991</b> , 53, 35-45	7
1339	Polymorphism in isotactic polypropylene. <b>1991</b> , 16, 361-404	409
1338	The magnetic structure of Tb2.5Y0.5Fe5O12 and the magnetic form factor influence of the Fe3+ ions. <b>1991</b> , 94, 260-266	10
1337	Ordered magnetic frustration. <b>1991</b> , 94, 331-336	20
1336	Influence of phosphorus substitution on Mn0.63Cr0.37As. <b>1991</b> , 94, 347-354	1

1335	Magnetic structure of the new layered ferromagnetic chromium hexatellurosilicate Cr2Si2Te6. <b>1991</b> , 94, 127-133	38
1334	Neutron diffraction study of magnetic ordering in the system NdSix (1.67.似亿.00). <b>1991</b> , 97, 53-68	9
1333	Ordered magnetic frustration XII. The magnetic structures of Fe3F8(H2O)2 at 40 and 2 K. <b>1991</b> , 92, 359-365	8
1332	The magnetic properties of the frustrated bidimensional antiferromagnet CsBaFe3F12. <b>1991</b> , 92, 381-387	1
1331	Crystallographic and magnetic structures of highT c related (Bi/Pb)2Sr2FeO6.25 determined by neutron powder diffraction. <b>1991</b> , 83, 165-170	2
1330	Crystal structure of the ceramic superconductor BaPb0.75Bi0.25O3. <b>1991</b> , 82, 171-176	31
1329	Low temperature magnetic structure of erbium iron garnet. <b>1991</b> , 82, 283-294	9
1328	Structure of the two-dimensional medium-pore high-silica zeolite NU-87. <b>1991</b> , 353, 417-420	98
1327	Quantitative Analysis of High-Alumina Refractories Using X-ray Powder Diffraction Data and the Rietveld Method. <b>1991</b> , 74, 619-624	20
1326	The location of cations in Cs-exchanged ZSM-5 zeolite. <b>1991</b> , 11, 376-379	29
1325	In situ techniques for structural studies in heterogeneous catalysis. <b>1991</b> , 9, 161-173	4
1324	Thermal expansion measurements using neutron diffraction of Bi2CaSr2Cu2Ox. <b>1991</b> , 182, 73-78	33
1323	Synthesis and structural analysis of the superconducting lead cuprates, (Pb, Cu) (Sr, R)2 (R?, Ce)2Cu2Oz (R, R?: rare-earth element). <b>1991</b> , 177, 337-344	26
1322	High temperature transmission electron microscopy and X-ray diffraction studies of twinning and the phase transition at 145°C in LaGaO3. <b>1991</b> , 132, 13-21	34
1321	Locating the sites of sorbed chloroform and dichlorobenzene in a zeolite solid: A synchrotron-based diffraction study of zeolite Y at room temperature. <b>1991</b> , 52, 1219-1227	16
1320	Aniline in Yb,Na-Y: A neutron powder diffraction study. <b>1991</b> , 11, 832-836	63
1319	Second-Order Spin-Hamilton Parameters of Mn2+ in Zinc Oxalate Dihydrate. <b>1991</b> , 167, K107-K111	1
1318	The polymorphs of zirconia: phase abundance and crystal structure by Rietveld analysis of neutron and X-ray diffraction data. <b>1991</b> , 26, 127-134	57

1317 Structural analysis of a Ti-Al-silicate catalyst for propylene oligomerization. <b>1991</b> , 26, 1101-1105	2
1316 Li2MnBr4(o-rh.) Leine geordnete NaCl-Defektstruktur des SnMn2S4-Typs. <b>1991</b> , 592, 106-114	3
TernÆe intermetallische Phasen des Lithiums mit Elementen der 4. Neben- und 5. Hauptgruppe mit statistischer Metallverteilung im Kationen Teilgitter. <b>1991</b> , 597, 33-39	5
Ungewißnliche H-Brükenbindungen in Natriumhydroxidmonohydrat: Rißtgen- und Neutronenbeugung an NaOH []H2O bzw. NaOD []D2O. <b>1991</b> , 597, 97-106	10
Dynamik linearer Moleklanionen in den Hydrogensulfiden von Natrium, Kalium und Rubidium: Differential-Scanning-Kalorimetrie, R\(\text{ltgen-}\) und Neutronenbeugung. <b>1991</b> , 598, 175-192	13
Crystal and electronic band structure of IrTe2: Evidence of anionic bonds in a CdI2-like arrangement. <b>1991</b> , 598, 199-215	49
1311 A structural model for the relaxor PbMg1/3Nb2/3O3at 5 K. <b>1991</b> , 3, 8159-8171	296
1310 Nitrogen atom location in rhombohedral and hexagonal RE2Fe17Nxcompounds. <b>1991</b> , 3, 1219-1226	83
1309 Refinement of the Structure of MnSi by Powder Diffraction. <b>1991</b> , 6, 194-195	21
1308 The magnetic structure of DyMn2. <b>1991</b> , 3, 727-738	68
1307 On the magnetic structure of Bi2CuO4. <b>1991</b> , 3, 381-384	15
1306 Neutron crystallographic study of iron-substituted YBa2Cu3O7- delta. <b>1991</b> , 4, 55-56	2
1305 Magnetic structures of the Mn III weak ferromagnets AMnF4.H2O (A=Rb and K). <b>1991</b> , 3, 2379-2390	8
1304 Magnetic structures: neutron diffraction studies. <b>1991</b> , 44, 27-32	17
1303 Neutron diffraction study of ternary nitrides of the type R2Fe17Nx. <b>1991</b> , 70, 6018-6020	24
1302 Crystal-field splittings and magnetic properties of Pr3+ and Nd3+ in RBa2Cu3O7. <b>1991</b> , 43, 7923-7935	5 168
Effect of physical and chemical pressure on the superconductivity of high-temperature oxide superconductors. <b>1991</b> , 44, 7601-7606	56
1300 Perturbed magnetic ordering in the disordered spinel ZnxCo1-xFeCrO4. <b>1991</b> , 43, 6031-6036	41

1299	Composition dependence of topological and chemical orders in liquid Al1-x(Mny(FeCr)1-y)xalloys by neutron diffraction. <b>1991</b> , 3, 2801-2817	38
1298	Computer Programs for Standardless Quantitative Analysis of Minerals Using the Full Powder Diffraction Profile. <b>1991</b> , 6, 2-9	416
1297	Rietveld Refinement of the Crystal Structure of CuF2. <b>1991</b> , 6, 156-158	10
1296	Expanded Use of the Rietveld Method in Studies of Phase Abundance in Multiphase Mixtures*. <b>1991</b> , 6, 74-77	88
1295	Comparison of Intensities from Fixed and Variable Divergence X-Ray Diffraction Experiments. <b>1991</b> , 6, 78-81	11
1294	Crystal Structures of Pb2Sr2YCu3O8+⊡(⊡=0 and 1.67). <b>1991</b> , 60, 913-920	9
1293	Neutron scattering: progress and prospects. <b>1991</b> , 252, 795-802	5
1292	Study of the Crystal Structure of Titanylphthalocyanine by Rietveld Analysis and Intermolecular Energy Minimization Method. <b>1992</b> , 31, 2181-2184	64
1291	Simultaneous Use of Observed and Calculated Standard Profiles in Quantitative XRD Analysis of Minerals by the Multiphase Rietveld Method: The Determination of Pseudorutile in Mineral Sands Products. <b>1992</b> , 7, 152-161	33
1290	Quantitative X-Ray Diffraction From Superlattices. <b>1992</b> , 17, 33-38	33
1289	Structure of high-Tc superlattices. <b>1992</b> , 69, 2859-2862	59
1288	Structural refinement of superlattices from x-ray diffraction. <b>1992</b> , 45, 9292-9310	616
1288	Structural refinement of superlattices from x-ray diffraction. <b>1992</b> , 45, 9292-9310  Neutron-powder-diffraction study of the nuclear and magnetic structures of YBa2Fe3O8 at room temperature. <b>1992</b> , 45, 9611-9619	616 74
1287	Neutron-powder-diffraction study of the nuclear and magnetic structures of YBa2Fe3O8 at room	
1287	Neutron-powder-diffraction study of the nuclear and magnetic structures of YBa2Fe3O8 at room temperature. <b>1992</b> , 45, 9611-9619	74
1287 1286 1285	Neutron-powder-diffraction study of the nuclear and magnetic structures of YBa2Fe3O8 at room temperature. <b>1992</b> , 45, 9611-9619  The crystal structure of CBrF3 by high-resolution powder neutron diffraction. <b>1992</b> , 77, 45-50	74 9
1287 1286 1285	Neutron-powder-diffraction study of the nuclear and magnetic structures of YBa2Fe3O8 at room temperature. 1992, 45, 9611-9619  The crystal structure of CBrF3 by high-resolution powder neutron diffraction. 1992, 77, 45-50  Neutron diffraction studies of zirconia-toughened engineering ceramics. 1992, 3, 24-29	74 9 8

1281 Cation distribution studies of Mg, Co and Co	o, Ni orthovanadate solid solutions. <b>1992</b> , 198, 271-276	10
1280 Crystal chemistry of iron containing german	ium andalusites, FexAl8-xGe4O20. <b>1992</b> , 201, 19-36	Ο
Neutron powder diffraction study of the mi <b>1279 1992</b> , 202, 227-236	xed-valence vanadium pyrophosphate RbV3P4O17.	1
Neutron Diffraction, Structural Inorganic Ch 110, 408-416	nemistry, and High-Temperature Superconductors. <b>1992</b> ,	
Quantitative X-Ray Diffraction Analysis of T Ingrowth. <b>1992</b> , 294, 109	itanate Waste Forms and its Application to Damage	2
Powder Diffraction Data for Synthetic Pota Cobalt-Potassium-Richterite. <b>1992</b> , 7, 52-55	ssium-Richterite, Nickel-Potassium-Richterite and	2
Structure Determination of Tl4V2O7 from F Stereochemical Activity of Thallium(I) Lone	Powder Diffraction Data using an Inel X-Ray PSD: Pair. <b>1992</b> , 7, 206-211	11
X-ray and neutron diffraction investigation and cation H3N [H [NH3+ and D3N [D [ND3+. <b>199</b> ]	at 298 K of NH4I 🛮 NH3 and ND4I 🖺 ND3 containing the 12, 200, 225-235	5
1273 The structure of solid tribromofluorometha	ne CFBr3 by powder neutron diffraction. <b>1992</b> , 202, 243-250	1
The Background in X-Ray Powder Diffractor 1272 Phases Using Ni-Filtered and Graphite-Mono	grams: A Case Study of Rietveld Analysis of Minor ochromated Radiation. <b>1992</b> , 7, 63-70	4
		4
<sup>1272</sup> Phases Using Ni-Filtered and Graphite-Mond	ochromated Radiation. <b>1992</b> , 7, 63-70	4 74
Phases Using Ni-Filtered and Graphite-Mond 1271 De Gruyter. <b>1992</b> , 1, 277-284 1270 Neutron powder-diffraction study of Pr2Fe	ochromated Radiation. <b>1992</b> , 7, 63-70	
Phases Using Ni-Filtered and Graphite-Mono 1271 De Gruyter. <b>1992</b> , 1, 277-284  1270 Neutron powder-diffraction study of Pr2Fe	ochromated Radiation. <b>1992</b> , 7, 63-70	74
Phases Using Ni-Filtered and Graphite-Mond 1271 De Gruyter. 1992, 1, 277-284  1270 Neutron powder-diffraction study of Pr2Fe  1269 Crystal and magnetic structure of the permanent A neutron diffraction study of the anion-excess 1992, 183, 263-270	ochromated Radiation. <b>1992</b> , 7, 63-70 17 and Pr2Fe17N2.9. <b>1992</b> , 45, 2920-2926 anent magnetic material Ho2Fe14C. <b>1992</b> , 184, 161-173	74 5
Phases Using Ni-Filtered and Graphite-Mondon  1271 De Gruyter. 1992, 1, 277-284  1270 Neutron powder-diffraction study of Pr2Fer  1269 Crystal and magnetic structure of the permanent A neutron diffraction study of the anion-excess 1992, 183, 263-270  Ferromagnetic ordering of NdNiSi2 and PrN measurements. 1992, 185, 51-58	anent magnetic material Ho2Fe14C. <b>1992</b> , 184, 161-173 cess cubic ReO3-type derived phase Fe0.80Zr0.20F3.20. diSi2 studied by neutron diffraction and magnetic ructure of the perovskite system Sr2FeTiO6 \$\mathbb{I}\$ by	74 5 5
Phases Using Ni-Filtered and Graphite-Mond De Gruyter. 1992, 1, 277-284  Phases Using Ni-Filtered and Graphite-Mond De Gruyter. 1992, 1, 277-284  Phases Using Ni-Filtered and Graphite-Mond Temperature of the Gruyter. 1992, 1, 277-284  Phases Using Ni-Filtered and Graphite-Mond Temperature of the Property of Property of Property of Property of Property of Property of NdNiSi2 and Property of Property of NdNiSi2 and Property of Property	anent magnetic material Ho2Fe14C. <b>1992</b> , 184, 161-173 cess cubic ReO3-type derived phase Fe0.80Zr0.20F3.20. diSi2 studied by neutron diffraction and magnetic ructure of the perovskite system Sr2FeTiO6 \$\mathbb{I}\$ by	74 5 5

New 5H hexagonal perovskite-like oxides (the series ALa4Ti3RuO15, where A = Ca, Sr, Ba). **1992**, 27, 931-938 91262 The synthesis, structure and characterization of SrMoO2.615N0.4. 1992, 187, 145-156 37 1261 Crystal structure of LixNi2-xO2 and a lattice-gas model for the order-disorder transition. 1992, 46, 3236-3246 135 1260 Lithium intercalation into WO3 and the phase diagram of LixWO3. 1992, 46, 2554-2560 115 Determination of long range order and vacancy content in the NiAl 界phase alloys by x-ray 1259 57 diffractometry. 1992, 40, 1113-1120 1258 Crystal and magnetic structure of the permanent magnetic material Tm2Fe14C. 1992, 184, 175-185 Quantitative X-ray diffraction from thin films. 1992, 1, 387-395 5 1256 Structural study of hyperstoichiometric alloys ZrMn2+x and their hydrides. 1992, 186, 241-248 30 Darstellung und Struktur einiger Gemischtvalenter ternber Tantalnitride mit Lithium und 1255 34 Magnesium. 1992, 183, 325-344 Crystal structure of the compound DyGe3. 1992, 183, 181-186 32 Structural and magnetic behaviour of the series Th2Fe17Cx (x=0 to 1.25). 1992, 186, 135-145 1253 23 Magnetic ordering of TbNi0.4Ge2 and TbCu0.4Ge2 studied by neutron diffraction and magnetic 1252 17 measurements. 1992, 187, 73-80 1251 Structure and magnetic ordering of holmium carbide fluoride, Ho2CF2. 1992, 183, 241-251 5 1250 Quaternary selenodiphosphates(IV): MIMIII[P2Se6], (MI =Cu, Ag; MIII = Cr, Al, Ga, In). 1992, 186, 111-133 38 Microstructural characterization of Y-PSZ (4 mol%) polycrystals by means of X-ray diffraction 1249 15 experiments. 1992, 15, 39-44 1248 Structure refinements of LiCu2O2 and LiCu3O3 from neutron powder diffraction data. 1992, 184, 315-322 39 Low-temperature powder diffraction studies using synchrotron radiation. 1992, 39, 161-170 7 High pressure, high resolution synchrotron x-ray powder diffraction with a position-sensitive 1246 25 detector. 1992, 8, 667-676

1245	The crystal structure of russellite; a re-determination using neutron powder diffraction of synthetic Bi2WO6. <b>1992</b> , 56, 399-409	104
1244	Application of Rietveld Refinement Techniques to a Disordered IIb Mg-Chamosite. <b>1992</b> , 40, 319-322	12
1243	LnHal2Hn? Neue Phasen in den ternÆen Systemen Ln/Hal/H. I. Strukturen. <b>1992</b> , 607, 29-33	15
1242	Crystal structure of synthesized CuGaTe2 determined by X-ray powder diffraction using the Rietveld method. <b>1992</b> , 27, 4495-4500	15
1241	Structure and Atomic Position in Gd2Fe17 $\overline{M}$ Six (x = 0, 1, 2) Compounds. <b>1992</b> , 134, 77-85	9
1240	The location of mesitylene adsorbed in rare-earth-exchanged Y zeolite. <b>1992</b> , 12, 237-239	41
1239	X-ray powder diffraction and t.p.d. study of SO2 adsorption on type Y zeolite. <b>1992</b> , 12, 292-298	13
1238	Structural and electrical studies of mixed copper/ruthenium oxides and related compounds of zinc and antimony. <b>1992</b> , 96, 344-359	44
1237	Ba2PrPtO6: A novel double perovskite. <b>1992</b> , 96, 132-140	14
1236	The magnetic structure of Cr2F5. <b>1992</b> , 96, 227-236	2
1235	Thermal expansion measurements using neutron diffraction of (Bi, Pb)2Ca2Sr2Cu3Ox. <b>1992</b> , 194, 397-402	16
1234	Interactions of hydrogen with Tb3Ni6M2 (M= Al, Ga, or Si) alloys with structures of Ce3Ni6Si2 type. <b>1992</b> , 27, 350-353	
1233	Investigation of nonstoichiometric spinels by method of full-profile analysis. <b>1992</b> , 32, 325-331	2
1232	Neutron diffraction study of 152Sm, 154Sm and 63Cu isotopesubstituted SmBa2Cu3O7 from 1.5 K to 300 K. <b>1992</b> , 194, 415-424	11
1231	Lattice structure of the fullerene ferromagnet TDAE£160. <b>1992</b> , 355, 331-332	282
1230	Determination of complex structures by combined neutron and synchrotron X-ray powder diffraction. <b>1992</b> , 359, 519-522	49
1229	Phase Characterization of Lead Zirconate Titanate Obtained from Organic Solutions of Citrates. <b>1992</b> , 75, 2088-2093	25
1228	Quantitative Analysis of the Crystalline Phases in <b>8</b> -Alumina-Based Solid Electrolytes Using X-ray Powder Diffraction. <b>1992</b> , 75, 52-55	5

1227	Structure Refinement of Mullite by the Rietveld Method and a New Method for Estimation of Chemical Composition. <b>1992</b> , 75, 227-230	103
1226	Early diagenetic recrystallization of Holocene (. <b>1992</b> , 39, 143-160	105
1225	Structure determination and rietveld refinement of aluminophosphate molecular sieve AIPO4-8. <b>1992</b> , 12, 13-19	56
1224	Crystal structure of the new metallic copper oxide La2Sr6Cu8O18-II <b>1992</b> , 83, 59-62	6
1223	Kinetic of the atoms of a unit cell YBa2Cu3O6+x. <b>1992</b> , 82, 627-630	5
1222	Neutron powder diffraction study of R2Fe17Hx compounds with R = Pr and Nd. <b>1992</b> , 81, 13-19	48
1221	Neutron diffraction studies of interatomic distances in the Y1ŪxCaxThxBa2Cu3O7⊞ System. <b>1992</b> , 81, 425-429	11
1220	Neutron diffraction study of Y2Fe14BN1[I 1992, 83, 231-234	11
1219	Experimental study of Si?Ge tetrahedral solid solution in Ni?Co?Mg talcs. 1992, 222, 189-195	14
1218	Magnetic and crystal structures of iron borates. <b>1992</b> , 180-181, 581-584	64
1217	C2Br4: structure refinements using neutron powder diffraction data in the temperature range 100B00 K. <b>1992</b> , 180-181, 617-620	1
1216	YbNiSn, a ferromagnetic Kondo lattice. <b>1992</b> , 182, 105-117	51
1215	Magnetic structures of the orthorhombic GdNi1⊠Cux compounds. <b>1992</b> , 180-181, 100-104	7
1214	Synthesis and crystal structure of BaSrCuO2+x[CO3. <b>1992</b> , 195, 335-344	35
1213	The crystal structure of Pb2Sr2YCu3O8+□ with □=1.32, 1.46, 1.61, 1.71, by powder neutron diffraction. <b>1992</b> , 199, 365-374	16
1213		16 45
	diffraction. <b>1992</b> , 199, 365-374  The crystal structure of the superconducting copper oxide carbonate	

1209	Neutron powder diffraction study of the crystal structure of YSr2CoCu2O7 and Y1\(\mathbb{U}\)CaxSr2CoCu2O7. <b>1992</b> , 193, 196-206	58
1208	The defect structures of Mn1⊠O. <b>1992</b> , 53, 141-154	23
1207	Structures of C60 intercalation compounds. <b>1992</b> , 53, 1373-1390	143
1206	Determination of the structure of (VO)3(PO4)2 🛘 9H2O by powder X-ray diffraction analysis. <b>1992</b> , 97, 10-18	9
1205	Structure and properties of a new compound AgTaS3. <b>1992</b> , 97, 29-35	10
1204	Structure and phase transitions of low-dimensional thallium vanadium bronze TlxV2O5 (0.44 🕅 🗓 0.48). <b>1992</b> , 97, 186-198	15
1203	Synthesis, X-ray single crystal structure determination, and dehydration study of BaZr2F10 [2H2O by X-ray powder thermodiffractometry. <b>1992</b> , 98, 11-24	9
1202	Formation of Cu2+3 clusters: Structure, bonding, and topotactic reactivity of chalcogen spinels Cu1-yCr2Se3Br. <b>1992</b> , 98, 71-81	9
1201	Crystal structure and thermolysis of K2(H5O2)Al2F9. <b>1992</b> , 98, 151-158	12
1200	The fluorite-related anion-excess structure of CeN0.222O0.667F1.333: Ordering of defect clusters. 1992, 100, 246-254	3
1199	The crystal structure and magnetic properties of SrLaFeSnO6 and SrLaNiSbO6. <b>1992</b> , 100, 37-48	38
1198	Ordered magnetic frustration: XVII. Is BaMnFeF7 frustrated? M\(\beta\)sbauer spectroscopy, magnetic susceptibility, and magnetic structure at 2 K. <b>1992</b> , 101, 296-308	6
1197	Structure determination of ⊞TiOSO4 from powder X-ray diffraction data. <b>1992</b> , 101, 331-339	11
1196	Comparative study of defect structures in lithium niobate with different compositions. <b>1992</b> , 101, 340-352	349
1195	The crystal structure and electronic properties of Ba4Ru3MO12(M =Li, Na, Mg, Zn). <b>1992</b> , 101, 161-172	28
1194	Spin glass behavior in Sr3FeRuO7 and Sr4FeRuO8. <b>1992</b> , 99, 267-275	38
1193	Rietveld refinements of four (Zn,Mg)3(PO4)2 solid solutions. <b>1992</b> , 99, 290-296	4
1192	The polymorphic behaviour and the crystal structure of one modification of poly(dimethylphosphazene). <b>1992</b> , 33, 2364-2369	13

1191	A neutron polarization analysis study of Ce2Fe17 in its paramagnetic phase. <b>1992</b> , 38, 669-672	5
1190	Crystal and magnetic structure of TbNiGe and DyNiGe compounds. <b>1992</b> , 116, 375-385	13
1189	Magnetic structure of TbAgSn and HoAgSn. <b>1992</b> , 117, L1-L4	12
1188	Neutron powder diffraction study on the magnetic phase of FeCoAs <b>1992</b> , 104-107, 1989-1990	3
1187	Neutron diffraction study of the magnetic structure of ErSi. <b>1992</b> , 109, 197-208	13
1186	Crystal structure of the metallic layered barium lead oxide. <b>1992</b> , 27, 1371-1377	8
1185	Structure of La2Sr6Cu8O16 : An oxygen deficient perovskite containing twofold O-Cu-O linear bonds. <b>1992</b> , 27, 287-293	9
1184	The monoclinic perovskite La2LiSbO6. A rietveld refinement of neutron powder diffraction data. <b>1992</b> , 27, 647-654	27
1183	Modification of the nanostructure and dielectric properties of lead magnoniobate ceramics by doping. <b>1992</b> , 27, 867-876	23
1182	Hydrothermal synthesis of calcium - niobium and tantalum oxides with the pyrochlore structure. <b>1992</b> , 27, 981-988	39
1181	An x-ray crystallographic study of superconducting bismuth-lead cuprates without superlattice modulation. <b>1992</b> , 27, 1153-1159	
1180	Structure determination of calcium dibismuth tetraoxide. <b>1992</b> , 27, 1243-1248	7
1179	One-dimensional antiferromagnetic ordering for a novel nickel-antimony oxide. <b>1992</b> , 27, 1041-1047	9
1178	Structure and physical properties of bacterially synthesized polyesters. <b>1992</b> , 17, 571-610	180
1177	A Remarkable Change in Framework Cation Positions upon Lithium Exchange: the Crystal Structure of LiMnPO4(OH). <b>1992</b> , 31, 1090-1092	20
1176	ពីderung von Kationengitterp <b>k</b> tzen beim Austausch von Wasserstoff- gegen Lithium-Ionen: Kristallstruktur von LiMnPO4(OH). <b>1992</b> , 104, 1056-1058	4
1175	LBung der Struktur eines metallsubstituierten Alumophosphatkatalysators durch Elektronenmikroskopie, Computersimulation und Pulver-RBtgenbeugungsuntersuchung. <b>1992</b> , 104, 1526-1529	7
1174	Beugungsuntersuchungen mit Synchrotron-Rfltgen- und Neutronenstrahlen in der Festkfiperchemie. <b>1992</b> , 104, 1594-1608	23

1173	Die Struktur der Tiefsttemperaturphase des festen Benzol-Hexafluorbenzol-Addukts. <b>1992</b> , 104, 1666-1669	55
1172	Intercalation of AlCl3 into FeCl3-graphite intercalation compounds and occurrence of BI-intercalation. <b>1993</b> , 31, 777-781	9
1171	Ba44Cu48(CO3)6O87.9: The Structure of <b>B</b> aCuO2lfrom Simultaneous X-ray and Neutron Powder Diffraction. <b>1993</b> , 32, 1454-1456	38
1170	Ba44Cu48(CO3)6O87.9: Strukturbestimmung von <b>B</b> aCuO2IIdurch kombinierte Riltgen- und Neutronenbeugungsuntersuchungen an Pulvern. <b>1993</b> , 105, 1511-1513	9
1169	Crystal structures of oligothiophenes and their relevance to charge transport. <b>1993</b> , 5, 896-908	181
1168	Hydroabrasive wear behaviour of high velocity oxyfuel thermally sprayed WC-M coatings. <b>1993</b> , 62, 493-498	30
1167	Structural phase transitions and orientational ordering in C70. <b>1993</b> , 178, 599-613	78
1166	Structure refinement of large-pore aluminophosphate molecular sieve, H1, by Rietveld methods. <b>1993</b> , 13, 542-548	7
1165	Magnetic structure of UCo1.5Sn2. <b>1993</b> , 85, 485-489	5
1164	Magnetic structure of Fe3GaAs. <b>1993</b> , 87, 151-155	9
1163	Crystal structure of Bi2Sr2CuO6: A structure based on periodic crystallographic shear planes in the \textbf{\textit{I201}}\textbf{\textit{B}}\text{tructure}. <b>1993</b> , 86, 227-230	13
1162	Magnetic structures of Nd2Fe2Si2C and Tb2Fe2Si2C. <b>1993</b> , 86, 675-678	10
1161	The crystallization of highly perfect metal-free phthalocyanine powders for ab-initiolstructure solution by diffraction methods. <b>1993</b> , 128, 1257-1262	5
1160	Low temperature powder diffraction on vapour deposited disordered solids. <b>1993</b> , 297, 407-413	9
1159	The preferential site occupation and magnetic properties of GdxY2NO3. <b>1993</b> , 54, 967-972	35
1158	Structure of layered ⊞-zirconium phosphite and zirconium phosphatephosphites from X-ray powder diffraction data. <b>1993</b> , 2, 41-54	4
1157	Influence of the size of the alkali ion on the thermal expansion of alkali-doped cordierites: A powder neutron diffraction study. <b>1993</b> , 12, 257-265	2
1156	Recent advances in magnetic structure determination by neutron powder diffraction. <b>1993</b> , 192, 55-69	11006

1155	Neutron diffraction studies of Ca-Pr doped YBa2Cu3O7🛭 <b>1993</b> , 205, 105-110	18
1154	Synthese und Struktur von Zr4ON3F5, einer Verbindung mit fluorit-verwandter <b>B</b> erstruktur vom Vernier-Typ. <b>1993</b> , 619, 367-373	13
1153	V4+ doping into SiO2, ZrO2 and ZrSiO4 structures. An ab initio perturbed ion study. <b>1993</b> , 48, 175-186	3
1152	Neutron Diffraction Study of the Structural Phase Transition in Lithium and Vanadium Substituted Copper Ferrite. <b>1993</b> , 136, 57-65	2
1151	Localization of hydrogen atoms in rare earth metal trihydroxides R (OH)3. <b>1993</b> , 140, K59-K62	6
1150	Crystal structure of synthesized CuGa0.5In0.5Te2 determined by X-ray powder diffraction using the Rietveld method. <b>1993</b> , 28, 2466-2470	2
1149	Neutron diffraction of Ealuminium oxynitride. <b>1993</b> , 12, 1470-1472	32
1148	Infrared Reflection of Ba(Mg1/3Ta2/3)O3 Ceramics. <b>1993</b> , 76, 2433-2436	44
1147	Analysis of Local Cation Arrangement in Mullite Using 29Si Magic-Angle Spinning Nuclear Magnetic Resonance Spectra. <b>1993</b> , 76, 2491-2496	16
1146	Assessment of Residual Strain in Zirconia-Toughened Alumina Using Neutron Diffraction. <b>1993</b> , 76, 2133-213	5 9
1146 1145	Assessment of Residual Strain in Zirconia-Toughened Alumina Using Neutron Diffraction. 1993, 76, 2133-213  Structural study on new ordered potassium-nickel fluoride-type oxides, strontium lanthanum magnesium manganese oxide and strontium lanthanum zinc manganese oxide. 1993, 28, 597-603	5 9
1145	Structural study on new ordered potassium-nickel fluoride-type oxides, strontium lanthanum	
1145	Structural study on new ordered potassium-nickel fluoride-type oxides, strontium lanthanum magnesium manganese oxide and strontium lanthanum zinc manganese oxide. <b>1993</b> , 28, 597-603	3
1145	Structural study on new ordered potassium-nickel fluoride-type oxides, strontium lanthanum magnesium manganese oxide and strontium lanthanum zinc manganese oxide. <b>1993</b> , 28, 597-603  Structure determination of praseodymium hexaaluminate. <b>1993</b> , 28, 111-116  Synthesis and structure refinement of sodium titanogallate containing one-dimensional channels of large cross section. <b>1993</b> , 28, 173-178	3 7
1145 1144 1143	Structural study on new ordered potassium-nickel fluoride-type oxides, strontium lanthanum magnesium manganese oxide and strontium lanthanum zinc manganese oxide. 1993, 28, 597-603  Structure determination of praseodymium hexaaluminate. 1993, 28, 111-116  Synthesis and structure refinement of sodium titanogallate containing one-dimensional channels of large cross section. 1993, 28, 173-178	3 7 4
1145 1144 1143 1142	Structural study on new ordered potassium-nickel fluoride-type oxides, strontium lanthanum magnesium manganese oxide and strontium lanthanum zinc manganese oxide. 1993, 28, 597-603  Structure determination of praseodymium hexaaluminate. 1993, 28, 111-116  Synthesis and structure refinement of sodium titanogallate containing one-dimensional channels of large cross section. 1993, 28, 173-178  The structure of a calcium deficient hexagonal calcium iridium oxide compound. 1993, 28, 1145-1151  Structure and oxygen stoichiometry in complex neodymium strontium cobalt copper oxides:	<ul><li>3</li><li>7</li><li>4</li><li>18</li></ul>
1145 1144 1143 1142	Structural study on new ordered potassium-nickel fluoride-type oxides, strontium lanthanum magnesium manganese oxide and strontium lanthanum zinc manganese oxide. 1993, 28, 597-603  Structure determination of praseodymium hexaaluminate. 1993, 28, 111-116  Synthesis and structure refinement of sodium titanogallate containing one-dimensional channels of large cross section. 1993, 28, 173-178  The structure of a calcium deficient hexagonal calcium iridium oxide compound. 1993, 28, 1145-1151  Structure and oxygen stoichiometry in complex neodymium strontium cobalt copper oxides: [NdSrCo1NCuxO4N]. 1993, 28, 685-692	3 7 4 18

1137	Neutron diffraction and magnetic study of the HoNiGe and ErNiGe compounds. <b>1993</b> , 127, 83-92	9
1136	Magnetic phase diagram of ErGe1⊠Six (0. <b>1993</b> , 127, 93-102	4
1135	Thermal variation of incommensurate magnetic phases in TbSi as observed by neutron diffraction. <b>1993</b> , 127, 115-128	11
1134	Magnetic ordering of NdNiGe2 and CeNiGe2 studied by neutron diffraction and magnetic measurements. <b>1993</b> , 125, 151-156	17
1133	Powder diffraction for solid state reaction studies. <b>1993</b> , 82, 146-150	11
1132	Molecular motion and phase transitions of clathrate hydrates**. <b>1993</b> , 1, 221-233	19
1131	Thermal expansion and structural distortion of perovskite ldata for NaMgF3 perovskite. Part I. <b>1993</b> , 76, 1-16	140
1130	Critical phenomena and phase transition of perovskite Idata for NaMgF3 perovskite. Part II. <b>1993</b> , 76, 17-34	90
1129	Zinc chlorohydroxosulfates: Newly-discovered corrosion products on zinc. Structure determination of NaZn4Cl(OH)6SO4 []6H2O and x-ray study of Zn4Cl2(OH)4SO4 []5H2O. <b>1993</b> , 34, 1231-1242	36
1128	Static mean-square displacement as an indicator of the crystal-to-amorphous transformation. <b>1993</b> , 156-158, 506-509	8
1127	Structural Instability in R1⊠Ni2 Compounds and Their Hydrides (R = Y, Rare Earth)*. <b>1993</b> , 179, 261-268	54
1126	New high-pressure phase of Si. <b>1993</b> , 47, 8337-8340	202
1125	STRUCTURAL MINERALOGY AND PROPERTIES OF NATURAL PHOSPHATES. <b>1993</b> , 9,	9
1124	The crystal structure of a new boron selenide, B12Se2⊠Bx. <b>1993</b> , 202, 73-76	17
1123	Crystal structure of the Zr3Pd4 phase. <b>1993</b> , 201, 121-126	22
1122	Low-temperature structure of KUO2PO4BD2O determined from combined synchrotron radiation and neutron powder diffraction measurements. <b>1993</b> , 3, 519-522	8
1121	The High-Temperature Phase Transition in Perovskite. <b>1993</b> , 24, 281-285	31
1120	Magnetic structures and phase transitions of Nickel-Bromine boracite Ni3B7O13Br. a neutron powder diffraction study. <b>1993</b> , 146, 81-97	10

Structural aspects of oligothienyls from X-ray powder diffraction data. <b>1993</b> , 55, 408-413	39
1118 Neutron diffraction study of the structure of chalcogen spinels Cu1+yCr2X4 (X? Se, Te). <b>1993</b> , 191, 37	7-42 23
The magnetic properties of iridium in mixed-metal oxides. <b>1993</b> , 201, 73-84	78
1116 Crystal structure and magnetic properties of DuY2BaCuO5 (u = 0.00, 0.61, 1.31). <b>1993</b> , 194, 13-17	5
1115 Structural and magnetic properties of new rocksalt-related compounds of ruthenium. <b>1993</b> , 201, 85-9	98 2
1114 XRD characterization of highly dispersed metal catalysts on carbon support. <b>1993</b> , 8, 1829-1835	16
Crystal and magnetic structures of the permanent magnet material R2Fe14C0.95B0.05 (R?Ce, Pr). 1113 1993, 190, 229-235	1
1112 X-ray powder structure determination and magnetic behavior of CsNiPdF5. <b>1993</b> , 17, 287-291	1
1111 The defect structure of congruently melting lithium niobate. <b>1993</b> , 74, 3080-3083	67
1110 On the cationic distribution in zinc-cobalt oxide spinels. <b>1993</b> , 5, 9287-9294	18
1109 Crystal structure of chloroiodomethane. <b>1993</b> , 79, 869-874	7
1108 Polymorphism of Li3AsO4 and structure refinement of its low-temperature form. <b>1993</b> , 45, 281-288	6
Neutron Scattering Study of Sr Substitution for Ba in YBa 2 Cu 3 O 7-y. <b>1993</b> , 10, 486-488	
Crystal structure and magnetic ordering of the rare-earth and Cu moments in RBa2Cu2NbO8 (R=Nd,Pr). <b>1993</b> , 47, 15256-15264	40
1105 Phase transitions in InSb at pressures up to 5 GPa. <b>1993</b> , 47, 35-54	55
1104 Observation of a high-pressure cinnabar phase in CdTe. <b>1993</b> , 48, 1314-1317	44
1103 Neutron powder diffraction study of Tb2Fe14B. <b>1993</b> , 73, 5884-5886	7
1102 Phase transitions in CdTe to 5 GPa. <b>1993</b> , 48, 16246-16251	73

1101	Neutron diffraction studies of ices III and IX on under-pressure and recovered samples. <b>1993</b> , 98, 4878-4888	104
1100	Stability and crystal structure of BC8 germanium. <b>1993</b> , 48, 9883-9886	130
1099	Structure and properties of the LaCuO3- delta perovskites. <b>1993</b> , 47, 15269-15275	52
1098	Crystal structure of the cinnabar phase of HgTe. <b>1993</b> , 48, 13111-13114	49
1097	Incorporation of microabsorption corrections into Rietveid analysis. 1993, 8, 223-228	27
1096	The influence of surface roughness on diffracted X-ray intensities in BraggBrentano geometry and its effect on the structure determination by means of Rietveld analysis. <b>1993</b> , 8, 74-83	56
1095	Full-profile Rietveld quantitative XRD analysis of Portland cement: Standard XRD profiles for the major phase tricalcium silicate (C3S: 3CaO.SiO2). <b>1993</b> , 8, 138-144	51
1094	Synchrotron powder diffractometry at Hasylab/DORIS reviewed. <b>1993</b> , 204, 1-41	11
1093	Structural Change in Lithium Intercalation of Defect Perovskite LiCuM3O9(M = Ta, Nb). <b>1993</b> , 66, 2255-2259	О
1092	The structure of solid carbon tetrafluoride. <b>1993</b> , 203, 29-39	8
1091	The Crystal Structure of Pure and Deuterated Zr5Al3O0.5Dx ( $x = 0$ , $x = 2.7$ )*. <b>1993</b> , 179, 217-224	4
1090	Complete sets of factors for absorption correction and air scattering subtraction in X-ray powder diffraction of loosely packed samples. <b>1993</b> , 8, 149-154	13
1089	Quantitative phase analysis of $\Box$ -Fe impurity in Ce2Fe17 matrix from neutron powder diffraction data. <b>1993</b> , 8, 236-239	
1088	Structure refinement and calculated X-ray powder data for the pyrochlore Y2Sn2O7 derived from powder neutron data. <b>1993</b> , 8, 245-248	10
1087	The structure characteristics of the diluted magnetic semiconductor Y2⊠DyxO3. <b>1993</b> , 8, 216-220	27
1086	Powder diffraction data of two tricydic diazonia diiodide salts used in silver iodide solid electrolytes. <b>1993</b> , 8, 175-179	
1085	Rietveld Refinement and Fourier-Transform Infrared Spectroscopic Study of the Dickite Structure at Low Temperature. <b>1993</b> , 41, 297-304	49
1084	Characteristics and Verification of a Low Hydrogen Embrittling Zinc-Nickel Electroplate, Developed for Corrosion Protection of High Strength Steels. <b>1994</b> , 72, 130-133	4

KCr3(SO4)2(OH)6: Synthesis, characterization, powder diffraction data, and structure refinement by the Rietveld technique and a compilation of alunite-type compounds. <b>1994</b> , 9, 265-271	26
1082 A powder neutron diffraction study of land limanganese dioxide and of LiMn2O4. <b>1994</b> , 209, 941-945	46
A crystal structure determination of HgC2O4 from synchrotron X-ray and neutron powder diffraction data. <b>1994</b> , 209, 874-877	12
1080 Neutron Scattering Studies of Host-Guest Interaction in Zeolites. <b>1994</b> , 248, 5-11	1
The Crystal Structure of Triphendioxazine as Solved by a New Ab Initio Method Utilising High Resolution Powder Diffraction and Computational Chemistry Techniques. <b>1994</b> , 248, 277-289	3
Investigation of magnetic structure and phase transitions in Co3 11B7O13Br boracite by neutron diffraction. <b>1994</b> , 162, 93-101	4
1077 Pressure-Induced Orientational Order in C 60 at 300 K. <b>1994</b> , 25, 429-434	17
A new method for Rietveld clay analysis. Part I. Use of a universal measured standard profile for Rietveld quantification of montmorillonites. <b>1994</b> , 9, 119-123	40
1075 Influence of oxygen partial pressure on the kinetics of YBa2Cu3O7⊠ formation. <b>1994</b> , 9, 275-285	20
1074 Structural study of the series NdBa2-xSrxCu3Oy. <b>1994</b> , 50, 218-221	2
Neutron power diffraction study of Fe3Ga1.7As0.3and Fe3Ga1.15Sb0.85B82-type compounds. <b>1994</b> , 6, 10435-10444	0
1072 Optical vibrations of hydrogen in some rare-earth monohalide hydrides. <b>1994</b> , 6, 4053-4066	4
1071 Advances in Powder Diffraction Methods for Zeolite Structure Analysis. <b>1994</b> , 341-356	17
1070 The essential identity of the framework structures of ZSM-8 and ZSM-5. <b>1994</b> , 84, 551-558	1
1069 Properties of PZT ceramics prepared from aqueous solutions. <b>1994</b> , 3, 243-247	10
Structures and molecular dynamics of solution-grown and melt-grown samples of n-hexatriacontane. <b>1994</b> , 6, 7605-7616	12
An investigation of anharmonic atomic vibrations of gamma -CuCl and gamma -CuBr by powder neutron diffraction. <b>1994</b> , 6, 9949-9962	15
1066 . <b>1994</b> , 30, 1039-1041	5

1065	Synchrotron powder diffraction study of the low-temperature lattice distortion of PbMo6S8. <b>1994</b> , 75, 423-430	11
1064	Molecular dynamics simulation of crystalline poly(ethylene oxide). <b>1994</b> , 101, 10064-10073	97
1063	Crystal structure of ZnTe III at 16 GPa. <b>1994</b> , 73, 1805-1808	76
1062	Structure and growth of butane films adsorbed on graphite. <b>1994</b> , 50, 15287-15297	45
1061	Structure of GaSb to 35 GPa. <b>1994</b> , 50, 13047-13050	19
1060	Structure of D2 in zeolite. <b>1994</b> , 50, 12291-12296	7
1059	Neutron-powder-diffraction study of the nuclear and magnetic structures of the substitution compound (Y1-xCax)Ba2Fe3O8+ delta (x=0.05, 0.10, and 0.20). <b>1994</b> , 49, 3465-3472	18
1058	Phase transformation induced by gas phase reaction in RFe10SiCx alloys. <b>1994</b> , 75, 6000-6002	7
1057	Structure of LaFe9Si4 intermetallic compound. <b>1994</b> , 76, 4095-4098	38
1056	Rietveld refinement of several structural models for mordenite that account for differences in the X-ray powder pattern. <b>1994</b> , 14, 137-146	25
1055	Synthesis and crystal structures of aluminum and iron phosphites. <b>1994</b> , 24, 155-163	16
1054	Applications of temperature-resolved diffraction methods in thermal analysis. <b>1994</b> , 42, 559-593	21
1053	Cation substitution models of congruent LiNbO3 investigated by X-ray and neutron powder diffraction. <b>1994</b> , 55, 145-152	107
1052	Preparation and x-ray diffraction characterization of the kambaldaite-like sodium cobalt carbonate hydroxide hydrate, Na2Co8(CO3)6(OH)66H2O. <b>1994</b> , 13, 3269-3275	4
1051	Structure, stoichiometry and phase purity of strontium-doped lanthanum manganite powders. <b>1994</b> , 29, 4065-4069	22
1050	Kristallstrukturanalyse von Ammonium-catena-polyphosphat II mit Rfltgenpulvertechniken. <b>1994</b> , 620, 931-935	3
1049	Synthese und Kristallstruktur von Cu2PtIIPtS8. <b>1994</b> , 620, 1909-1914	1
1048	Crystal structures and cation distributions in simple spinels from powder XRD structural refinements: MgCr2O4, ZnCr2O4, Fe3O4 and the temperature dependence of the cation distribution in ZnAl2O4. <b>1994</b> , 20, 541-555	197

1047 Fracture properties of layered mullite/zirconia-toughened alumina composites. <b>1994</b> , 13, 1334-1336	17
1046 Induction of bidimensionality in mixed Cu?Ti perovskites. <b>1994</b> , 6, 54-57	17
Borophosphate Leine vernach Lesigte Verbindungsklasse: die Kristallstrukturen von MII[BPO5] (MII = Ca, Sr) und Ba3[BP3O12]. <b>1994</b> , 106, 791-793	34
Cation distribution in the superconducting Tl, Pb-1223 phase (IIl0.5Pb0.5Sr2Ca2Cu3O9)Ifrom resonant synchrotron powder X-ray diffraction. <b>1994</b> , 221, 304-310	23
Neutron powder diffraction study of the superconducting quaternary intermetallic compound YNi2B2C. <b>1994</b> , 227, 143-150	38
$_{1042}$ Neutron-diffraction study of reduced and reoxidized YBa2(Cu0.90Co0.10)3O7 $\blacksquare$ <b>1994</b> , 219, 315-326	13
1041 Structure of the Li1+xTi2⊠O4 superconducting system. <b>1994</b> , 221, 149-156	21
Cation distribution and composition of the Tl-2223 superconductor from combined powder neutron and resonant X-ray diffraction. <b>1994</b> , 225, 307-316	21
Studies of structural disorder in ReBa2Cu3O7II thin films (Re=rare earth) as a function of rare-earth ionic radius and film deposition conditions. <b>1994</b> , 232, 288-308	69
1038 The crystal structure of (Pb0.5Cd0.5)Sr2 (Y1⊠Cax)Cu2O7. <b>1994</b> , 230, 389-396	12
1037 Electron- and powder neutron-diffraction studies of YBa2(Cu1 Coy)3O6+x with 0.05. <b>1994</b> , 220, 143-15	9 46
1037 Electron- and powder neutron-diffraction studies of YBa2(Cu1)(Coy)3O6+x with 0.05. <b>1994</b> , 220, 143-15	8
	·
1036 The structure of new nickel(I) oxides: LnSr5Ni3O8 (Ln = Y, Dy, Ho, Er and Tm). <b>1994</b> , 235-240, 751-752	8
The structure of new nickel(I) oxides: LnSr5Ni3O8 (Ln = Y, Dy, Ho, Er and Tm). <b>1994</b> , 235-240, 751-752  The structure of Li0.43Na0.36CoO1.96 using neutron powder diffraction. <b>1994</b> , 69, 69-74	24
The structure of new nickel(I) oxides: LnSr5Ni3O8 (Ln = Y, Dy, Ho, Er and Tm). 1994, 235-240, 751-752  The structure of Li0.43Na0.36CoO1.96 using neutron powder diffraction. 1994, 69, 69-74  Crystal structure of BiPbSr2MnO6 by powder neutron diffraction. 1994, 92, 659-663	24
The structure of new nickel(I) oxides: LnSr5Ni3O8 (Ln = Y, Dy, Ho, Er and Tm). 1994, 235-240, 751-752  The structure of Li0.43Na0.36CoO1.96 using neutron powder diffraction. 1994, 69, 69-74  Crystal structure of BiPbSr2MnO6 by powder neutron diffraction. 1994, 92, 659-663  Structural and magnetic properties of the anion-deficient LaVO3II 1994, 92, 541-546	8 24 7 20

Location of meta-xylene in BaX zeolite and model for the filling of the supercages. <b>1994</b> , 27, 159-169	44
1028 Magnetic structure of U2(Ru0.65Rh0.35)3Si5 silicide. <b>1994</b> , 134, 88-94	9
1027 Magnetic properties of Ba2(UCu)O6. <b>1994</b> , 137, 139-144	9
Structural and magnetic properties of RCoC2 (R = Pr, Dy, Ho) compounds studied by neutron diffraction. <b>1994</b> , 132, 243-248	14
1025 Incommensurate magnetic structure of CeSi as observed by neutron diffraction. <b>1994</b> , 130, 242-246	15
1024 Determination structurale des fluorozirconates de thallium trivalent. <b>1994</b> , 29, 405-415	5
Crystal structure and phase stability of the new metallic lanthanum strontium copper oxide. <b>1994</b> , 29, 629-636	3
A package of dedicated PC software for neutron powder diffraction data processing and analysis. <b>1994</b> , 75, 233-237	
1021 Flat pearls from biofabrication of organized composites on inorganic substrates. <b>1994</b> , 371, 49-51	201
Recrystallization of dolomite: evidence from the Monterey Formation (Miocene), California. <b>1994</b> , 41, 1223-1239	46
At-Temperature Neutron Diffraction Investigation of the Aging Process in Magnesia-Partially-Stabilized Zirconia. <b>1994</b> , 77, 3073-3076	5
1018 Creep of Mg-PSZ at Room Temperature. <b>1994,</b> 77, 617-624	15
1017 Relationship between Fracture. Toughness and Phase Assemblage in Mg-PSZ. <b>1994</b> , 77, 571-579	55
1016 Structural study of barium titanate between 150 and 425 K. <b>1994</b> , 48, 217-236	20
1015 X-ray powder diffraction study of BiSbO4. <b>1994</b> , 9, 164-167	13
1014 Crystal and molecular structures of rhenium heptafluoride. <b>1994</b> , 263, 1265-7	40
Crystal structures and physical properties of some new ternary compounds U2T3X (T?Ru, Os; X? Si, Ge). <b>1994</b> , 209, 251-255	9
Method for the simultaneous determination of anisotropic residual stresses and texture by x-ray diffraction. <b>1994</b> , 76, 7246-7255	278

1011	P-V-T equation of state of (Mg,Fe)SiO3 perovskite: constraints on composition of the lower mantle. <b>1994</b> , 83, 13-40	172
1010	Use of Two-Phase Standards of Unknown Compositions to Determine Calibration Constants for Powder XRD by Linear Regression. <b>1994</b> , 77, 2226-2228	8
1009	Differenzthermoanalyse der Bildung des Pentastrontiumchloridphosphats und r\(\textit{B}\)tgenographische Untersuchung seiner Struktur. <b>1994</b> , 215, 281-288	15
1008	Crystal structure of hydride and deuteride of unial. <b>1994</b> , 213-214, 533-535	12
1007	Structural determination of a 1/1 rational approximant to the icosahedral phase in Ti-Cr-Si alloys. <b>1994</b> , 49, 11675-11681	25
1006	Structural and magnetic characterization of novel stoichiometric LnCaCrO4 oxides (Ln, rare earth). <b>1994</b> , 203, 143-148	4
1005	YSr5Ni3O8Ea new nickel(I) oxide with a defect Sr2CuO3 structure. <b>1994</b> , 1185-1186	6
1004	Neutron diffraction study of the doubled perovskitelphases Ba2M2⊠CuxO4+E(M = In, Sc). <b>1994</b> , 4, 921-929	5
1003	Pressure dependence of the Imma phase of silicon. <b>1994</b> , 50, 739-743	161
1002	Cation ordering in distorted perovskites (MLa)(MgTe)O6, M = Na, K. <b>1994</b> , 4, 547-550	20
1001	Structural study of potassium niobate between 200 and 823 K. <b>1994</b> , 52, 261-275	10
1000	Practical Aspects of Powder Diffraction Data Analysis. <b>1994</b> , 391-428	24
999	Prediction of Unknown Uranyl Oxide Hydrate Structure Types: Comparison of Calculated and Measured XRD Powder Patterns. <b>1994</b> , 353, 653	
998	Structural Chemistry of Some Phases in The YC-Ni-B System. <b>1994</b> , 376, 547	
997	Ionic Conductivities of Lithium Phosphorus Oxynitride Glasses, Polycrystals and Thin Films. <b>1994</b> , 369, 445	
996	Neutron Diffraction Study of Radiation Damage in U3Si at 30°C and 350°C. <b>1994</b> , 373, 227	
995	Neutron Powder Diffraction Studies of Portland Cement and Cement Compounds. <b>1994</b> , 376, 487	
994	An analysis of preferred orientation in YBa2Cu3O7\( superconducting films deposited by CVD on single-crystal and polycrystalline substratesa). <b>1994</b> , 9, 250-259	3

993	Refinement of unit-cell parameters by whole-powder-pattern fitting technique. <b>1994</b> , 9, 272-279	7
992	X-ray powder diffraction analysis of the incommensurate modulated structure of Bi2Sr2CaCu2O8. <b>1994</b> , 9, 28-37	6
991	Sm(OH)2NO3: Synthesis, characterization, powder diffraction data, and structure refinement by the Rietveld technique. <b>1994</b> , 9, 115-118	12
990	Oxidative Coupling of Methane over Ti-La-Na catalysts. <b>1994</b> , 82, 443-450	2
989	Cation Segregation in Simulated Radioactive-Waste Zeolite-A Mixtures. <b>1994</b> , 84, 741-747	
988	Crystal Structure Refinement of Gaivinoxyl Radical, C29H41O2, Based on Synchrotron X-ray Powder Diffraction and Rietveld Method. <b>1994</b> , 41, 797-802	3
987	Rietveld refinement of the solid-solution series: (Cu,Mg)SO4[H2O. <b>1995</b> , 10, 189-194	7
986	Powder X-ray characterisation of natrolite, Na2Al2Si3O10.2H2O. <b>1995</b> , 10, 243-247	8
985	Quantitative mineraiogical analyses of carbonate rich sediments by X-ray powder diffraction. <b>1995</b> , 10, 112-116	1
984	Preparation and structural characterization of the rare-earth oxides BaR2O4, R=Pr, Tb. <b>1995</b> , 10, 122-126	8
983	Structure of [Pd(NH3)4]Cr2O7. <b>1995</b> , 10, 159-164	4
982	Structure refinement and X-ray powder diffraction data for kalipyrochlore (K,Sr,Na,Ca,H2O)2 $\ln$ (Nb,Ti)2 $\ln$ O6 $\ln$ Y1 $\ln$ , with (0<m<0.8, x~0.2, W = 0 and 0.2<n<1). <b>1995</b> , 10, 180-184	7
981	A semi-empirical asymmetry function for X-ray diffraction peak profiles. <b>1995</b> , 10, 204-206	7
981	A semi-empirical asymmetry function for X-ray diffraction peak profiles. <b>1995</b> , 10, 204-206  Quantitative determination of chrysotile asbestos in bulk materials by combined Rietveld and RIR methods. <b>1995</b> , 10, 269-277	7
	Quantitative determination of chrysotile asbestos in bulk materials by combined Rietveld and RIR	
980	Quantitative determination of chrysotile asbestos in bulk materials by combined Rietveld and RIR methods. <b>1995</b> , 10, 269-277	42
980 979	Quantitative determination of chrysotile asbestos in bulk materials by combined Rietveld and RIR methods. <b>1995</b> , 10, 269-277  Powder diffraction data and Rietveid refinement of the compound Ba2Cl2Cu3O4. <b>1995</b> , 10, 282-287	42 10

Temperature dependence of intersite distribution of Zn and Mg in E(Zn, Mg)-orthophosphates. **1995**, 210, 260-264

974	Crystal structure of lead hydroxyapatite from powder X-ray diffraction data. <b>1995</b> , 236, 209-212	34
973	X-ray study and physico-chemical analyses of magnesium hexaaquabromate. <b>1995</b> , 30, 255-262	3
972	Crystal structure analysis of polycrystalline Bi3Fe5O12 thin film by using asymmetric and symmetric diffraction techniques. <b>1995</b> , 56, 1317-1322	21
971	Structural analysis of fullerene and fulleride solids from synchrotron X-ray powder diffraction. <b>1995</b> , 56, 1445-1457	49
970	Crystal structures and electrochemical properties of LiAlyNi1DO2 solid solution. <b>1995</b> , 54, 221-223	70
969	Neutron-diffraction studies of the crystal structure of CaNdAlO4. <b>1995</b> , 213-214, 417-419	5
968	Magnetic order in TbNiAl and TbCuAl intermetallic compounds. <b>1995</b> , 99, 145-150	57
967	The phase diagram of (NH4I)x(KI)1⊠. <b>1995</b> , 99, 333-338	18
966	The phase diagram of (NH4I)x(KI)1⊠. <b>1995</b> , 99, 333-338	
965	Profile function modeling for fitting powder diffraction peaks. <b>1995</b> , 36, 121-125	
964	Thermal expansion behaviour of M?Ti2P3O12 (M?=Li, Na, K, Cs) and M?Ti4P6O24 (M?=Mg, Ca, Sr, Ba) compounds. <b>1995</b> , 30, 3509-3514	19
963	Phase examination of 5 mol % Nd2O3-doped ZrO2 from a coprecipitation process. <b>1995</b> , 14, 796-798	4
962	Structural and Optical Properties of the System (Ca, Sr, Eu)5(PO4)3CI. <b>1995</b> , 191, 21-30	25
961	Effect of Stacking Faults on the X-ray Diffraction Profiles of 眡iC Powders. <b>1995</b> , 78, 774-782	124
960	Residual Stresses in Alumina/Ceria-Stabilized Zirconia Composites. <b>1995</b> , 78, 2213-2214	37
959	Confirmation by X-ray diffraction of the endohedral nature of the metallofullerene Y@C82. <b>1995</b> , 377, 46-49	436
958	Geological applications of synchrotron radiation. <b>1995</b> , 45, 459-481	54

957	Powder diffraction pattern fitting and structure refinement by means of the CPSR v.3.1 software package. <b>1995</b> , 354, 134-138	1
956	Use of finite element modeling to interpret diffraction peak broadening from elastic strain distributions. <b>1995</b> , 201, 134-142	25
955	Structural changes upon sorption and desorption of Xe from Cd-exchanged zeolite rho: a real-time synchrotron X-ray powder diffraction study. <b>1995</b> , 4, 99-110	12
954	Textural analysis of eggshells. <b>1995</b> , 3, 95-100	20
953	New ternary compounds in the phase diagram U?Ru?Si. 1995, 206-207, 522-524	1
952	Neutron-diffraction studies of the crystal and magnetic structure of BaSn2Fe4O11. <b>1995</b> , 213-214, 227-229	5
951	Neutron diffraction study of Y(TiFeC)12. <b>1995</b> , 213-214, 297-299	6
950	Neutron-diffraction study of CD3ND3SnBr3: SemiconductorIhsulator transition with orientational ordering. <b>1995</b> , 213-214, 411-413	12
949	Rietveld refinement of magnetic structures from pulsed-neutron-source powder-diffraction data. <b>1995</b> , 213-214, 985-989	10
948	Neutron powder diffraction study of the crystal structure of Na-doped Y-1-2-3 high-Tc superconductor. <b>1995</b> , 248, 71-77	4
947	Preparation at moderate pressures (PÆ0 kbar) of (Sr,Ca)CuO2 phases with infinite-layer structure Superconductivity at 34 K in (Sr0.75Ca0.25)0.85Nd0.15CuO2. <b>1995</b> , 250, 93-100	3
946	Electrochemical and X-ray photoelectron spectroscopic evidence for differences in the binding sites of alkanethiolate monolayers chemisorbed at gold. <b>1995</b> , 396, 103-114	236
945	X-ray and neutron diffraction studies of methylammonium tetrafluoroborate: Highly disordered orientations of CH3NH3+ and BF4IIons. <b>1995</b> , 56, 183-188	3
944	The structure of La4Ti9O24 from synchrotron X-ray powder diffraction. <b>1995</b> , 56, 1297-1303	9
943	Synthesis, crystal structure and magnetism of Sr3Sb2NiO9A ferrimagnetic perovskite. <b>1995</b> , 56, 1331-1337	11
942	A high resolution powder neutron diffraction study of the novel layered oxide BiMo2O7OD 🛮 2D2O. <b>1995</b> , 56, 1339-1343	1
941	The crystal structures of (NH4)3HGe7O16[hH2O and Li4NHxGe7O16[hH2O determined from powder diffraction data using synchrotron radiation. <b>1995</b> , 56, 1353-1358	19
940	Precision of a crystal structure derived from a synchrotron X-ray powder pattern. The structure of Barium oxalate hydrate, BaC2O4[2H2O. <b>1995</b> , 56, 1359-1362	12

939	Preparation and structure of BiCaRu2O7 J. 1995, 119, 254-259	11
938	Quantitative X-ray diffraction analysis of mineral and organic phases in organic-rich rocks. <b>1995</b> , 28, 51-69	43
937	A comparative study on the structure of APbO3 (A=Ba,Sr). <b>1995</b> , 95, 581-585	27
936	Residual stresses of types II and III and their estimation. <b>1995</b> , 20, 39-52	6
935	Structural and magnetic properties of Ni-Li oxides. <b>1995</b> , 1, 421-426	2
934	Cation distribution and magnetic structure of some substituted barium hexaferrites. <b>1995</b> , 140-144, 2101-210	0213
933	Incommensurate magnetic ordering in CePtSn and TbPtSn. <b>1995</b> , 145, 85-92	15
932	Structure properties and magnetic susceptibility of diluted magnetic semiconductor Y2\(\text{\text{M}}\)HoxO3. <b>1995</b> , 145, 349-356	36
931	Fluorocomplexes of niobium IV: the magnetic structure of VNbF6. <b>1995</b> , 146, 129-132	4
930	Neutron diffraction investigation of preferred site occupation in several CaCu5-type compounds of cerium. <b>1995</b> , 146, 111-116	37
929	Note on the crystal structure and the magnetic properties of the compound CeNi9In2. <b>1995</b> , 150, 345-348	13
928	X-ray and neutron diffraction studies of UPdSn. <b>1995</b> , 151, 102-110	10
927	Preparation, neutron structural study and characterization of BaNbo3: A Pauli-like metallic perovskite. <b>1995</b> , 30, 201-208	48
926	High pressure synthesis and structural characterization of the deficient perovskite Ba0.88NbO2.3. <b>1995</b> , 30, 251-256	3
925	Structural evolution of the Aurivillius framework in the solid solutions Bi2WO6-Sb2WO6. <b>1995</b> , 30, 871-882	39
924	High resolution powder diffraction studies of polycrystalline materials. <b>1995</b> , 97, 63-69	11
923	Ordering due to disorder in an antiferromagnet with continuously degenerate NBl ground state: A combined neutron diffraction and magnetization study of (FexGa1-x)2 Ca3Ge3O12. <b>1995</b> , 97, 391-401	5
922	Failure mechanisms of ceramic membrane reactors in partial oxidation of methane to synthesis gas. <b>1995</b> , 30, 201-212	229

921	Magnetic order in TbNiAl and TbCuAl intermetallic compounds. <b>1995</b> , 99, 145-150	1
920	Distribution of K ions in intermediate KC60. <b>1995</b> , 52, 3199-3205	22
919	Structure of helium and neon in zeolite. <b>1995</b> , 52, 12614-12617	7
918	Quadrupolar effects in the temperature dependence of the lattice parameters of HoP1-xVxO4. <b>1995</b> , 51, 5644-5648	25
917	Phase relation, crystal structure, and magnetic properties of La-Co-Si alloys. <b>1995</b> , 51, 60-66	9
916	Neutron-powder-diffraction study of the long-range order in the octahedral sublattice of LaD2.25. <b>1995</b> , 51, 12116-12126	30
915	Structural changes of ZrO2-CeO2 solid solutions around the monoclinic-tetragonal phase boundary. <b>1995</b> , 51, 8018-8025	111
914	Magnetic phase transitions and crystal-field splitting in K2UX5 (X=Cl,Br,I). <b>1995</b> , 51, 2881-2890	9
913	Preferential occupancy and composition-driven c-axis variation in (Pb0.5Cd0.5)(Sr,Y,Ca)3Cu2O7-delta. <b>1995</b> , 51, 9261-9270	1
912	Ion distribution and saturation magnetization of aluminum substituted lithium ferrites. <b>1995</b> , 31, 3979-3981	9
911	Structural, magnetic, and heat-capacity studies on Zn- and Ga-substituted PrBa2Cu3O7- delta. <b>1995</b> , 52, 13006-13012	14
910	Cation distributions and possible phase separation in Tl2Ba2CuO6+ delta from synchrotron powder x-ray diffraction. <b>1995</b> , 51, 12747-12753	21
909	Model-Free Search for Extra-Framework Cations in Zeolites Using Powder Diffraction. <b>1995</b> , 32, 337-342	20
908	Structure and Electronic Properties of TeBe Mixtures under High Pressure. <b>1995</b> , 64, 4766-4789	54
907	Nanometer size copper particles in copper chromite catalysts. <b>1995</b> , 91, 533-537	
906	Neutron diffraction study of the boride Y(Fe11.04Ti0.52B0.43)Ti0.39: a new phase of a ThMn12-type intermetallic interstitial compound. <b>1995</b> , 7, 2587-2592	7
905	Neutron powder diffraction study of the ferroelastic phase transition and lattice melting in sodium carbonate, Na2CO3. <b>1995</b> , 7, 4395-4417	33
904	Time-of-flight neutron diffraction and magnetization investigation of the crystal and magnetic structure of YCo11Ti and YCo10Mo2. <b>1995</b> , 7, 9255-9262	15

903	Effect of high-angle diffraction data on Rietveld structure refinement. <b>1995</b> , 4, 259-267	4
902	Powder X-ray diffraction and solid state NMR techniques forzeolite structure determination. <b>1995</b> , 94, 78-100	7
901	Studies on commercial carbon black by radial distribution function and rietveld refinement. <b>1995</b> , T57, 98-101	3
900	Characterization of a new Pb-based 1222 cuprate Pb(Sr1.2La0.8)Gd2Cu2O9.06. <b>1995</b> , 7, L405-L410	
899	Crystal structure and superconductivity of new Pb-based 1222 cuprate (Pb0.5Cd0.5)(Sr0.9Eu0.1)2(Eu0.7Ce0.3)2Cu2O9+ delta. <b>1995</b> , 7, 5975-5982	9
898	Synchrotron X-Ray Techniques in Soil, Plant, and Environmental Research. <b>1995</b> , 55, 1-66	52
897	Diffraction Methods and Crystal Structure Analysis. <b>1995</b> , 15-63	1
896	Precursors of amorphization in supersaturated Nb-Pd solid solutions. <b>1995</b> , 10, 280-291	13
895	Crystal structure of the three-dimensional magnetic network of type Mek[Fe(CN)6]l[mH2O, where Me=Cu, Ni, Co. <b>1995</b> , 10, 300-305	13
894	(Mn,Zn,Fe)1⊠O thin films showing ferrimagnetic property deposited by ion beam sputtering. <b>1995</b> , 10, 274-279	4
893	Commensurate-incommensurate magnetic phase transitions of CePtAl. <b>1995</b> , 7, 1663-1678	22
892	Crystallographic, magnetic and electronic structures of a new layered ferromagnetic compound Cr2Ge2Te6. <b>1995</b> , 7, 69-87	159
891	Crystal Structure and Phonon Density of States of High-Temperature Ceramic Silicon Nitride. <b>1995</b> , 31, 201-206	47
890	Magnetic ordering of TbCoSn and HoCoSn studied by neutron diffraction and magnetic measurements. <b>1995</b> , 221, 254-263	7
889	The site occupancies for the excess manganese atoms and the third element niobium in the intermetallic compound ZrMn2. <b>1995</b> , 224, 70-75	9
888	Comparative study of some rare earth sulfides: doped $\mathbb{E}[A]M2S3$ (M = La, Ce and Nd, A = Na, K and Ca) and undoped $\mathbb{E}M2S3$ (M = La, Ce and Nd). <b>1995</b> , 223, 130-138	61
887	Formation and crystal structure of UTi2Dx. <b>1995</b> , 224, 36-38	8
886	Characterization and magnetic properties of R2⊠CaxBaNiO5 oxides (R?Y and Sm). <b>1995</b> , 225, 208-211	1

## (1996-1995)

	Temperature-induced structural changes in Be2ZrD1.5 studied by powder neutron diffraction. <b>1995</b> , 224, 241-243	6
884	Magnetic structures of RNi2Ge2 (R = Dy, Ho and Er) and YbNi2Si2. <b>1995</b> , 224, 253-261	18
883	New intermetallic compounds RCo9Si4 (R = Pr, Nd) with a tetragonal NaZn13-derivative structure. <b>1995</b> , 226, 139-142	8
882	Characterization of the structure of TbD2.25 at 70 K by neutron powder diffraction. <b>1995</b> , 231, 95-98	17
881	Structure and properties of silicon XII: A complex tetrahedrally bonded phase. <b>1995</b> , 52, 4072-4085	207
880	Modelling the silica glass structure by the Rietveld method. <b>1995</b> , 183, 39-42	110
879	Crystal structure and physical properties of new ternary silicides R4T13X9 (R, rare earth or uranium; T, rhodium or iridium; X, silicon or germanium). <b>1995</b> , 218, 197-203	11
878	Lattice dynamics and related diffusion properties of intermetallics: I. Fe3Si. <b>1995</b> , 7, 5983-5999	29
877	Preparation and crystal structure of the deficient perovskite LaNiO2.5, solved from neutron powder diffraction data. <b>1995</b> , 2819-2824	22
876	Phase transitions in CdTe to 28 GPa. <b>1995</b> , 51, 15723-15731	56
875	Magnetic properties of La2CuTi1⊠RuxO6 and La2ZnRuO6. <b>1995</b> , 5, 1003-1006	
		13
874	Sr4 ☑CaxRhO6: a magnetically ordered RhIV compound. <b>1995</b> , 5, 1785-1789	36
8 <sub>74</sub>	Sr4 \( \text{NCaxRhO6}: a magnetically ordered RhIV compound. 1995, 5, 1785-1789\)  Non-stoichiometric tubular nickel(II) hydroxyarsenates of the dumortierite family: crystal structure and topochemical thermal reduction of Ni12+xH6\( \text{M}(AsO4)8(OH)6(x=1.16 and 1.33). 1995, 5, 917-925\)	
	Non-stoichiometric tubular nickel(II) hydroxyarsenates of the dumortierite family: crystal structure	36
873	Non-stoichiometric tubular nickel(II) hydroxyarsenates of the dumortierite family: crystal structure and topochemical thermal reduction of Ni12+xH6\(\text{M}(AsO4)8(OH)6(x= 1.16 and 1.33). \) <b>1995</b> , 5, 917-925  Solid\(\text{Solid}\) on	36 12
8 <sub>73</sub>	Non-stoichiometric tubular nickel(II) hydroxyarsenates of the dumortierite family: crystal structure and topochemical thermal reduction of Ni12+xH6\(\text{M}(AsO4)\(\text{8}(OH)\(\text{6}(x=1.16\) and 1.33). <b>1995</b> , 5, 917-925  Solid\(\text{Bolid}\) block of the dumortierite family: crystal structure and topochemical thermal reduction of Ni12+xH6\(\text{M}(AsO4)\(\text{8}(OH)\(\text{6}(x=1.16\) and 1.33). <b>1995</b> , 5, 917-925  Solid\(\text{Bolid}\) block of the dumortierite family: crystal structure and topochemical thermal reduction of Ni12+xH6\(\text{M}(AsO4)\(\text{8}(OH)\(\text{6}(x=1.16\) and 1.33). <b>1995</b> , 5, 917-925	36 12
8 <sub>73</sub> 8 <sub>72</sub> 8 <sub>71</sub>	Non-stoichiometric tubular nickel(II) hydroxyarsenates of the dumortierite family: crystal structure and topochemical thermal reduction of Ni12+xH6\(\text{M}(AsO4)\(\text{8}(OH)\(\text{6}(x=1.16\) and 1.33). <b>1995</b> , 5, 917-925  Solid\(\text{Bolid}\) phase transitions in n-alkanes C23H48 and C25H52: X-ray power diffraction study on new layer stacking in phase V. <b>1995</b> , 103, 5762-5766  REFERENCES. <b>1995</b> , 457-476  Synthesis of Crystalline Superlattices by Controlled Crystallization of Modulated Reactants. <b>1995</b> ,	36 12 49

867	Quantitative multiphase determination using the Rietveld method with high accuracy. <b>1996</b> , 26, 171-175	22
866	Control of Reaction Pathway and the Nanostructure of Final Products through the Design of Modulated Elemental Reactants. <b>1996</b> , 8, 1625-1635	44
865	Crystal Structure of the Isotactic Alternate Copolymer between Carbon Monoxide and Styrene. <b>1996</b> , 29, 1535-1539	31
864	Crystal structure of dichlorofluoromethane. <b>1996</b> , 87, 999-1005	2
863	Structural Investigations on(BaxSr1-x)(ZryTi1-(y+1)Ta1)O3Dielectric Resonator Compounds Used for Microwave Applications. <b>1996</b> , 35, 179-181	9
862	Syntheses and Crystal Structures of New Ternary Selenides: Rb3Yb7Se12 and CsEr3Se5. <b>1996</b> , 35, 5283-5289	27
861	Electrochemical and X-ray diffraction study of the redox cycling of nanocrystals of 7,7,8,8-tetracyanoquinodimethane. Observation of a solidBolid phase transformation controlled by nucleation and growth. <b>1996</b> , 92, 3925-3933	93
860	Unusual Metal <b>[</b> hsulator Transitions in the LaTi1-xVxO3 Perovskite Phases. <b>1996</b> , 8, 418-427	11
859	Unusual Chemical Behavior for Potassium under Pressure: PotassiumBilver Compounds. <b>1996</b> , 118, 12104-12108	30
858	Structure Determination of the One-Dimensional Compound Sr3ZnPtO6, Containing Zinc in a Highly Unusual Trigonal Prismatic Coordination Environment. <b>1996</b> , 35, 2155-2156	20
857	Nb(x)()Ru(6)(-)(x)()Te(8), New Chevrel-Type Clusters Containing Niobium and Ruthenium(,). <b>1996</b> , 35, 5622-5626	14
856	Neutron diffraction study of the S2 monolayer phase of ethane physisorbed on graphite. <b>1996</b> , 364, 273-278	7
855	Magnetic properties and neutron diffraction of TbMn4Al8. <b>1996</b> , 232, 154-159	12
854	Magnetic structure and preferred site occupation of Cr in the compound YFe10Cr2. <b>1996</b> , 233, 165-168	7
853	Ferromagnetic properties of U2M17ŪGey systems (M ? Fe, Co). <b>1996</b> , 233, 174-182	18
852	Ab initio crystal structure solution of the novel intermetallic compound Nd3(Fe,Ti)29. <b>1996</b> , 234, 62-66	16
851	Mechanical alloying of Fe and Zn: phase analysis and MBsbauer studies. <b>1996</b> , 234, 43-47	27
850	The crystal structure of Ti3PD2.4. <b>1996</b> , 236, 26-29	4

849	Structure determination of Fe2N by neutron and synchrotron powder diffraction. 1996, 235, 15-22	70
848	Note on the crystal structure and magnetic properties of the compounds Ce2Ni17Si9 and Ce2Co17Si9. <b>1996</b> , 235, 62-65	17
847	On the stoichiometry, space group and polymorphism of TlCu7S4. <b>1996</b> , 237, 33-38	13
846	Crystal structure and magnetic properties of CeNi11⊠Six compounds. <b>1996</b> , 241, 124-126	1
845	Crystal structure of Ce2Mn7Al10 determined by neutron diffraction. <b>1996</b> , 242, 45-48	1
844	New group V Ephases. <b>1996</b> , 241, 98-111	4
843	Mechanical milling of auriferous arsenopyrite and pyrite. <b>1996</b> , 242, 22-34	8
842	Crystal structures and magnetic properties of Ba4Ru3O10 and Ba5Ru3O12. <b>1996</b> , 233, 15-22	32
841	Crystallographic structures and phase transformations in ZrPd. <b>1996</b> , 236, 19-25	47
840	A new stroboscopic neutron diffraction method for monitoring materials subjected to cyclic loads: Thermal cycling of metal matrix composites. <b>1996</b> , 35, 717-720	28
839	Recrystallization of dolomite: An experimental study from. <b>1996</b> , 60, 2189-2207	60
838	X-ray diffraction analysis of the modulated structure of Bi2Sr2CaFe2O y. <b>1996</b> , 62, 275-279	
837	The symmetry of garnets on the pyrope (Mg3Al2Si3O12)-majorite (MgSiO3) join. <b>1996</b> , 23, 3799-3802	32
836	Crystal structure of CeCuAl3 and its influence on magnetic properties. <b>1996</b> , 245, 112-115	15
835	Cation disorder and size effects in magnetoresistive manganese oxide perovskites. <b>1996</b> , 54, R15622-R15625	802
834	Crystal and magnetic structures of the colossal magnetoresistance manganates Sr2-xNd1+xMn2O7 (x=0.0, 0.1). <b>1996</b> , 54, 15967-15977	94
833	Magnetic properties of ternary chromium sulfides, VxCr3 ⊠S4(0 ?x?1.0). <b>1996</b> , 6, 807-813	9
832	Constrained Rietveld refinement of [即H1]decadeuteriodopamine deuteriobromide using powder neutron diffraction data. <b>1996</b> , 92, 4555-4559	4

831	Crystal structures and magnetic properties of La2ZnxMg1 IrO6. <b>1996</b> , 6, 1375-1378	14
830	Synthesis, crystal structure and magnetic properties of Ln2⊠SrxNiO4 ∸⊡solid solutions (Ln = La, Nd, Sm and Gd; 1.0 ?x? 1.67). <b>1996</b> , 6, 57-62	23
829	Structural and magnetic properties of Sr4⊠MxIrO6(M = Ca, Zn, Cd, Li, Na). <b>1996</b> , 6, 395-401	44
828	Structure and phase formation in amorphous IrxSi/sub 1-x/ thin films at high temperatures. <b>1996</b> ,	O
827	Dark-clouded andesine from dolerite dikes at Lindfors, southern Sweden. <b>1996</b> , 118, 50-51	1
826	Structural chemistry of SrMn1 ☑FexO3 ቧ x匝.3. <b>1996</b> , 6, 1187-1190	15
825	Electronic properties of U2Pt2Sn. <b>1996</b> , 79, 6361	5
824	A neutron powder diffraction determination of the thermal expansion tensor of crocoite (PbCrO4) between 60 K and 290 K. <b>1996</b> , 60, 963-972	23
823	Examples of Hydrothermal Titration and Real Time X-Ray Diffraction in the Synthesis of Open Frameworks. <b>1996</b> , 453, 103	3
822	Synthesis, Structures and Magnetic Properties of a Family of One-Dimensional Oxides. <b>1996</b> , 453, 379	1
821	Salt-Occluded Zeolite Waste Forms: Crystal Structures and Transformability. <b>1996</b> , 465, 395	4
820	Synthesis and Structure of Two New Layered Ternary Nitrides, SrZrN2 and SrHfN2. <b>1996</b> , 35, 7608-7613	23
819	Crystal Structure Determination from Powder Diffraction Data. <b>1996</b> , 8, 2554-2570	170
818	Neutron diffraction study of austempered ductile iron. <b>1996</b> , 27, 923-928	3
817	Structural and magnetic properties of barium hexaferrite nanostructured particles prepared by the combustion method. <b>1996</b> , 152, 61-69	58
816	Crystal structure and the magnetic properties of the compound ThCo9Si2. <b>1996</b> , 152, 341-344	3
815	Saturation magnetizations and Curie temperatures of Co?Zn Y-type ferrites. 1996, 153, 279-284	34
814	A new magnetic intermetallic compound: UFe6Ga6. <b>1996</b> , 157-158, 692-693	5

813 Unit cell determination of sotalol hydrochloride by powder x-ray diffraction. 1996, 139, 9-14

812	Real-time observations of the oxidation of mild steel at high temperature by neutron diffraction. <b>1996</b> , 27, 993-997	9
811	On the crystal structure of the ¶201ြsuperconductors Hg0.5Bi0.5Sr2☐LaxCuO5☐ <b>1996</b> , 257, 195-209	11
810	Observation of superconductivity (Tc = 50 K) in a new tetragonal alkaline-earth cuprate Sr0.8Ba1.2CuO3+[], synthesised at ambient pressure. <b>1996</b> , 260, 249-256	13
809	Neutron diffraction structure determination of the superconducting copper oxychromate Tl3(CrO4)Sr8Cu4O16. <b>1996</b> , 262, 159-167	13
808	Growth of rhodium dispersions in zeolite NaX: Identification of a precursor state by Rietveld refinement. <b>1996</b> , 17, 244-249	11
807	Characterization of the structure of YD3 by neutron powder diffraction. <b>1996</b> , 57, 423-435	75
806	X-Ray Study of the Structure and Thermal Properties of Ba1⊠KxBiO3 at Different Temperatures. <b>1996</b> , 31, 107-117	2
805	Rietveld Refinement of the Crystal Structure of Nickel Hexaamina Perchlorate and -Tetrafluorborate. <b>1996</b> , 31, 435-440	2
804	Ein ferrimagnetisches Manganoxid mit einer Perowskit-Schichtstruktur: YBaMn2O5. <b>1996</b> , 108, 2634-2637	O
803	The crystal structure of perdeuterated pyrene II at 4.2 K. <b>1996</b> , 258, 490-494	10
802	Modeling of disorder and X-ray diffraction in coal-based graphitic carbons. <b>1996</b> , 34, 1259-1265	106
801	A new nickel(III) oxide family: MSr3NiO6 (M = Sc, In, Tm, Yb and Lu). <b>1996</b> , 2, 737-741	21
800	Quantitative mineralogical analysis of coals from the Callide Basin, Queensland, Australia using X-ray diffractometry and normative interpretation. <b>1996</b> , 30, 211-229	40
799	Thermally induced phase transformations of Ca-exchanged LTA and FAU zeolite frameworks: Rietveld refinement of the hexagonal CaAl2Si2O8 diphyllosilicate structure. <b>1996</b> , 16, 294-300	42
798	Materials science in the information age. <b>1996</b> , 18, 151-164	1
797	Neutron and magnetisation study of the low temperature magnetic phase of UCu2Ge2. <b>1996</b> , 223-224, 201-203	6
796	Magnetic ordering in UPtSi. <b>1996</b> , 225, 166-176	4

795	Structural analysis of superconducting NdBa1.5Sr0.5Cu3o7🛭 <b>1996</b> , 261, 97-104	6
794	Neutron-diffraction studies and interatomic distances in Ca?Pr doped NdBa2Cu3O7년 <b>1996</b> , 269, 231-241	24
793	Mapping of the residual stress distribution in a brazed zirconia-iron joint. <b>1996</b> , 211, 45-53	34
792	Thermal residual stress distribution in WC-Ni composites. <b>1996</b> , 209, 318-328	28
791	Residual stress in WC-Co measured by neutron diffraction. <b>1996</b> , 209, 197-205	58
790	Characterization of low temperature mullitization. <b>1996</b> , 16, 127-132	33
789	Adducts between silver nitrate and di-iodo compounds, and some analogues. <b>1996</b> , 15, 2409-2419	4
788	Empirical potential Monte Carlo simulation of fluid structure. <b>1996</b> , 202, 295-306	597
787	Ab initio prediction of polymorphs. <b>1996</b> , 166, 900-903	57
786	Amorphization of U3Si2 by ion or neutron irradiation. <b>1996</b> , 230, 158-163	56
7 <sup>8</sup> 5	Preparation and crystal structure of the ammonium cobalt carbonate hydroxide hydrate (NH4)2Co8(CO3)6(OH)6[4H2O. <b>1996</b> , 92, 303-308	4
784	Synthesis, thermal decomposition and vibrational spectra of the phases MICr(CrO4)2 (MI = Na, K, Rb). <b>1996</b> , 57, 1929-1935	13
783	Synthesis and structural characterization of solid solutions: Li3xLa(1☑)VO4 (0?x?0.3), monazite-type. <b>1996</b> , 31, 4689-4692	4
782	Die Pentatelluride M2Te5 (M = Al, Ga, In): Polymorphie, Strukturbeziehungen und HomogenitÆsbereiche. <b>1996</b> , 622, 985-993	16
781	Structure refinement of synthetic hureaulite: Mn5(H2O)4[PO3(OH)]2[PO4]2. 1996, 15, 1895-1897	9
780	Crystal Phase and Phonon Densities of States of 聞SiAION Ceramics, Si6-zAlzOzN8-z (0 <i>周</i> 四). <b>1996</b> , 79, 3250-3256	16
779	Synthesis and structure of a layered titanosilicate catalyst with five-coordinate titanium. <b>1996</b> , 381, 401-404	142
778	Crystal structure of Tl0.5Pb0.5Sr2Ca2Cu3O9 at 300 K and around Tc (118 K). <b>1996</b> , 270, 267-273	10

777	Low-temperature magnetic phase of UCu2Ge2: A macroscopic, mesoscopic, and microscopic study. <b>1996</b> , 53, 28-31	19
776	Phase transitions in triammonium hydrogen disulphate. Crystal structures at 🛭 10°c and +140°c. <b>1996</b> , 58, 263-271	11
775	Structure of solid fluoroform. <b>1996</b> , 87, 1007-1013	12
774	"Hidden" High-to-Low Cristobalite Type Transition in HgSe and HgTe at High Pressure. <b>1996</b> , 77, 1781-1784	31
773	Magnetism in URhSi. <b>1996</b> , 79, 5221	10
772	Cationic and magnetic order in LiNiO2- and NiO-type Li-Ni mixed oxides. <b>1996</b> , 53, 703-709	32
771	Magnetic structure and anisotropy of Ga- and Al-substituted LaCo5 and YCo5 intermetallics. <b>1996</b> , 53, 11550-11556	27
770	Oxygen-vacancy induced ferroelectricity in nitrogen-doped nickel oxide. <b>2022</b> , 131, 164304	
769	Assessment of the data repeatability of x-ray diffraction study for silicon nitride powders of different dispersion. <b>2022</b> , 88, 27-32	1
768	Structural Aspects of Memory EffectIfor MgGa LDHs: New Data Obtained by Simulation of XRD Patterns for 1D Disordered Crystals. <b>2022</b> , 12, 629	1
767	and X-ray Diffraction and Small-Angle X-ray Scattering Investigations of the Sol-Gel Synthesis of FeN and FeC <b>2022</b> ,	O
766	Apatite, Ca10(PO4)6(OH,F,Cl)2: Structural Variations, Natural Solid Solutions, Intergrowths, and Zoning. <b>2022</b> , 12, 527	O
765	Probing the Electrode-Electrolyte Interface of a Model K-Ion Battery Electrode-The Origin of Rate Capability Discrepancy between Aqueous and Non-Aqueous Electrolytes <b>2022</b> ,	O
764	Softening and Microstructure Evolution of Pure Copper Disks Processed by High Pressure Torsion. 1	О
763	Electrical conductivity of titanium dioxide ethylene glycol-based nanofluids: Impact of nanoparticles phase and concentration. <b>2022</b> , 404, 117423	1
762	Novel Multiferroic-Like Nanocomposite with High Pressure-Modulated Magnetic and Electric Properties. 2113022	O
761	Quantitative phase analysis of anhydrous clinker Portland using Rietveld method. 2022,	
760	Cobalt-Doped Chemically Deposited Lead-Sulfide Films. 1	

759	Effect of Cr Substitution on Magnetic and Magnetocaloric Properties for La0.62Nd0.05Ba0.33MnO3.	
75 <sup>8</sup>	Investigating the structural, vibrational, optical, and dielectric properties in Mg-substituted LaAlO3. 1	2
757	Room-Temperature Mixed Spin State of Co3+ in Sr2Co0.02Ga0.98NbO6 Double Perovskites: Combined NMR and EPR Studies in a Potential Inorganic Pigment.	О
756	Study of the radiation tolerance of MgFe2O4 by XRD, TEM, MBsbauer, and EPR spectroscopy. <b>2022</b> , 137, 1	
755	Phase-dependent electrocatalytic activities of Pt-anchored rutile, anatase and mixed anatase-rutile TiO2 nano-composites for methanol oxidation in alkali. <b>2022</b> , 106903	0
754	Unlocking the potential of hydraulic fracturing flowback and produced water for CO2 removal via mineral carbonation. <b>2022</b> , 105345	
753	Probing the effect of R-cation radii on structural, vibrational, optical, and dielectric properties of rare earth (R=La, Pr, Nd) aluminates. <b>2022</b> ,	2
75 <sup>2</sup>	Synthesis, structural, and ionic conductivity characterizations of new spinel material: LiCoNbO4. 1	
751	Impact of structure and magnetic parameters of nanocrystalline cores on surface properties of molecularly imprinted nanoconjugates for analysis of biomolecules a case of tyramine. <b>2022</b> , 107571	1
750	Laboratory measurements of ultrasonic wave velocities and anisotropy across a gold-hosting structure: a case study of the Thunderbox Gold Mine, Western Australia. <b>2022</b> , 104928	
749	Tracking perovskite crystallization via deep learning-based feature detection on 2D X-ray scattering data. <b>2022</b> , 8,	2
748	High Dielectric Permittivity of ⊞-NaFeO2-Type Layered Nitrides.	1
747	Interface matters: Design of an efficient CaCu3Ti4O12-rGO photocatalyst. <b>2022</b> , 117478	О
746	Novel corrosion-resistant tool steels with superior wear properties.	1
745	Direct determination of thermal expansion coefficients from the profile fitting of a diffractogram. <b>2022</b> ,	
744	Two La0.5Ag0.1Ca0.4MnO3 Manganite Nanoparticles Synthesized via Sol©el and Solid-State MethodsBtructural, Magnetic, and Magnetocaloric Properties.	O
743	X-ray powder diffraction data for the second and third polymorphs of 1-methylhydantoin. 1-7	
742	Multi-phase interaction accompanied with the phase transformation process in U-21 at%Nb alloy quantified by in-situ neutron diffraction during heating. <b>2022</b> , 153776	

741	Mesoporous carbon from SiO2-C nanocomposite prepared with industrial raw materials: Synthesis and characterization. <b>2022</b> , 126, 109047	0
740	Pore space of steatite ceramics triggered by the allowance of natural fibers: High-resolution X-ray microscopy analysis and related thermo-mechanical properties. <b>2022</b> , 218, 110704	Ο
739	Waste clay from bauxite beneficiation to produce calcium sulphoaluminate eco-cements. <b>2022</b> , 340, 127703	2
738	Late Holocene peat paleodust deposition in south-western Sweden - exploring geochemical properties, local mineral sources and regional aeolian activity. <b>2022</b> , 602, 120881	Ο
737	Microstructural evolutions, phase transformations and hard magnetic properties in polycrystalline Celloffellu alloys. <b>2022</b> , 286, 126179	
736	Tensile deformation behavior related with strain-induced martensitic transformation in a duplex Fe-Mn-Al-C low-density steel. <b>2022</b> , 189, 111954	Ο
735	Alternative flotation collectors for the environmental desulfurization of gersdorffite (NiAsS) bearing mine tailings: Surface chemistry. <b>2022</b> , 647, 128943	0
734	Formation of the intermetallic phases Al12Mg17 and Al3Mg2 during heating of elemental Al-Mg composites studied by high-energy X-ray diffraction. <b>2022</b> , 911, 165114	Ο
733	On the Co solubility in Ce0.9Zr0.1O2 nanoparticles studied by EXAFS. <b>2022</b> , 312, 123184	
73²	Novel Zn(II) and Cd(II) coordination polymers derived from 1,2,3-triazole-1,3-diketone ligand. Syntheses and structural, thermal, computational, and luminescent studies. <b>2022</b> , 312, 123156	1
731	Effect of heat treatment temperature and turning residual stresses on the plain and notch fatigue strength of Ti-6Al-4V additively manufactured via laser powder bed fusion. <b>2022</b> , 107009	0
730	Structural and phase evolution in U3Si2 during steam corrosion. <b>2022</b> , 110373	Ο
729	Revealing superstructure ordering in Co1+xMnSb Heusler alloys and its effect on structural, magnetic, and electronic properties. <b>2022</b> , 105,	
728	FTIR and Electrical Properties of Cr Substituted Li0.5Fe2.5-xO4 Synthesized Using Sol-Gel Auto Combustion.	О
727	From Powders to Single Crystals: A Crystallographer's Toolbox for Small-Molecule Structure Determination <b>2022</b> ,	
726	Structural, morphological, and electrical properties of silver-substituted ZnAl2O4 nanoparticles. <b>2022</b> , 12, 15848-15860	1
7 <sup>2</sup> 5	Anomalous luminescence properties and cytotoxicity assessment of Sr3(PO4)2 co-doped with Eu2+/3+ ions for luminescence temperature sensing.	О
724	Crystal structure and microwave dielectric properties of garnet-type Ca2YZr2-Ti Al3O12 ceramics for dual-band bandpass filters. <b>2022</b> ,	O

723 Mexican agricultural soil dust as a source of ice nucleating particles. **2022**, 22, 6435-6447

722	pdCIFplotter: visualizing powder diffraction data in pdCIF format. <i>Journal of Applied Crystallography</i> , <b>2022</b> , 55,	3.8	0
721	Synthesis and characterisation of yittrium doped cerium oxide nanoparticles and their efficient antibacterial application invitro against gram-positive and gram-negative pathogens. <b>2022</b> ,		
720	Powder X-Ray Diffraction Pattern Is All You Need for Machine-Learning-Based Symmetry Identification and Property Prediction. 2200042		O
719	Reduced Hysteresis and Enhanced Giant Magnetocaloric Effect in B-Doped all- d -Metal Ni - Co - Mn <b>2022</b> , 17,		1
718	Synthesis, Structure and Superconducting Properties of Ba1-xLax/4K3x/4(Bi0.25Pb0.75)O3-Perovskites. <b>2022</b> , 598, 1354075		
717	Development and stabilization of Co2.4Ni0.6O4 material for long-term thermochemical energy storage. <b>2022</b> , 52, 104876		1
716	Production of AB5 materials from spent Ni-MH batteries with further tests of hydrogen storage suitability. <b>2022</b> , 539, 231459		О
715	Optical absorption measurements and optoelectronic DFT calculations for ethanol solvated quercetin and anhydrous/hydrated quercetin crystals. <b>2022</b> , 312, 123242		O
714	Li4(OH)3Br/MgO shape stabilized composite as novel high temperature thermal energy storage material. <b>2022</b> , 52, 104921		
713	Mechanical performance and deformation mechanisms at cryogenic temperatures of 316L stainless steel processed by laser powder bed fusion: In situ neutron diffraction. <b>2022</b> , 218, 114806		O
712	Improving the thermoelectric performance of double half-Heusler compounds ZrNi(In,Sb).		1
711	Investigation of Adsorption-Desorption Characteristics of Co and H2 on Cu2+ Doped Sno2 for Identifying Gas Components by Temperature Modulation.		
710	The influence of iodide addition on the composition, morphology, crystal structure, and semiconductor and photoelectric properties of PbS films.		О
709	Microstructural and Optical Properties of Manufactured Zno Nanoparticles and Their Bioactivity Against Pathogenic Bacteria.		
708	Systemically study of optoelectronic and transport properties of chalcopyrite HgAl2X4 (X= S, Se) compounds for solar cell device applications. <b>2022</b> ,		Ο
707	Structural and Optical Characterization of Mechanochemically Synthesized CuSbS2 Compounds. <b>2022</b> , 15, 3842		O
706	Al-Doped SrMoO3 Perovskites as Promising Anode Materials in Solid Oxide Fuel Cells. <b>2022</b> , 15, 3819		

705	Effect of B Addition on Microstructure and Mechanical Properties of High-Strength 13Mn TRIP Steel with Different Annealing Temperatures. <b>2022</b> , 12, 776	
704	Dimensionality switching and superconductivity transition in dense 1T⊞fSe2. <b>2022</b> , 105,	O
703	Insights on the various structural, optical and dielectric characteristics of La1-xCaxFeO3 perovskite-type oxides synthesized through solution-combustion technique. <b>2022</b> , 128,	0
702	Crystal Structure and Twisted Aggregates of Oxcarbazepine Form III.	
701	Magnetic properties, critical behavior and magnetocaloric effect in the nanocrystalline Pr2Fe16Al. <b>2022</b> , 110752	0
700	New High-Pressure and High-Temperature CaCO3 Polymorph.	2
699	X-ray Diffraction and Piezoelectric Studies during Tensile Stress on Epoxy/SbSI Nanocomposite. <b>2022</b> , 22, 3886	
698	Oxygen crystallographic positions in thin films by non-destructive resonant elastic X-ray scattering. <i>Journal of Applied Crystallography</i> , <b>2022</b> , 55, 526-532	
697	Crystal structure, morphology and magnetic properties of nanocrystalline Zr\$\$_{6}\$\$Fe\$\$_{23}\$\$ thin films grown on Si(001) substrate. <b>2022</b> , 128,	0
696	Synthesis of new mixed metal oxide RuNi2O4 phase decorated on reduced graphene oxide for supercapacitor applications. <b>2022</b> , 140666	1
695	Fe3 $\square$ InSnxO6 (x = 0, 0.25, or 0.5): A Family of Corundum Derivatives with Sn-Induced Polarization and Above Room Temperature Antiferromagnetic Ordering.	
694	Dimethylaniline-Based Hybrid Compounds of Cadmium Diiodide: Synthesis, Crystal Structure, and Physical Properties.	
693	Powder X-ray structural analysis and bandgap measurements for (Ca $\times$ Sr2 $\square$ )MnWO6 (x = 0.25, 0.5, 0.75, 1.5, 1.75). 1-11	
692	Oxygen nonstoichiometry effects in spin Seebeck insulating Y3⊠PrxFe5O12+☐materials. <b>2022</b> , 12, 065103	
691	Stabilization of the Trigonal Langasite Structure in Ca3Ga2包xZnxGe4+xO14 (0.股間) with Partial Ordering of Three Isoelectronic Cations Characterized by a Multitechnique Approach.	О
690	Influence of order⊞isorder effects on the optical parameters of Ag7(Si1⊠Gex)S5I-mixed crystals.	O
689	Crystal Structure, Magnetic Properties and Thermal Behavior of BaFe 11.9 In 0.1 O 19 Ferrite. 2100655	
688	The tri-emitting phosphate phosphors SrIn 2 (P 2 O 7 ) 2 : Tm, Dy, Eu for ratiometric optical thermometer.	2

687	Low-sulfate autoclaved aerated concrete (AAC): A recyclable AAC with calcined clay. 2022, 342, 127984	О
686	Impact of F and S doping on (Mn,Fe)2(P,Si) giant magnetocaloric materials. 2022, 234, 118057	1
685	The triphylite NaFe1-yMnyPO4 solid solution (0 <i>四</i> 加): Kinetic strain accommodation in NaxFe0.8Mn0.2PO4. <b>2022</b> , 425, 140650	1
684	The quantitative estimation of amorphous content at the zirconium-containing chloraluminates by the XRD-background level. <b>2022</b> ,	
683	Investigation of structural, morphological, and transport properties of a multifunctional Li-ferrite compound. <b>2022</b> , 12, 18697-18708	1
682	Vacancy assisted growth of copper tantalum sulfide nanocrystals.	
681	Dual-emission luminescence thermometry using LaGaO3:Cr3+, Nd3+ phosphors.	3
680	Achieving ultrahigh energy storage density and efficiency in 0.90NaNbO3 <b>D</b> .10BaTiO3 ceramics via a composition modification strategy.	О
679	Photovoltaic properties and phase composition of CdPbS films. 2022,	
(-0		
678	Extensive characterization of choline chloride and its solid I quid equilibrium with water. <b>2022</b> , 24, 14886-1	48970
678	Extensive characterization of choline chloride and its solidliquid equilibrium with water. <b>2022</b> , 24, 14886-1 Electronic structure and low-temperature thermoelectric transport of TiCoSb single crystals.	4897 <sub>0</sub>
677	Electronic structure and low-temperature thermoelectric transport of TiCoSb single crystals.	
6 <sub>77</sub>	Electronic structure and low-temperature thermoelectric transport of TiCoSb single crystals.  Defects and disorder in apatite-type silicate oxide ion conductors: implications for conductivity.  Tuning magnetic properties with crystal engineering in a family of coordination polymers based on	O
6 <sub>77</sub> 6 <sub>76</sub>	Electronic structure and low-temperature thermoelectric transport of TiCoSb single crystals.  Defects and disorder in apatite-type silicate oxide ion conductors: implications for conductivity.  Tuning magnetic properties with crystal engineering in a family of coordination polymers based on Ni(II) sulphates.	O
6 <sub>77</sub> 6 <sub>76</sub> 6 <sub>75</sub>	Electronic structure and low-temperature thermoelectric transport of TiCoSb single crystals.  Defects and disorder in apatite-type silicate oxide ion conductors: implications for conductivity.  Tuning magnetic properties with crystal engineering in a family of coordination polymers based on Ni(II) sulphates.  Magnetic and Structural Properties of the Fe5si1-Xgexb2 System.  Thermally stable mesoporous tetragonal zirconia through surfactant-controlled synthesis and	O
677 676 675 674	Electronic structure and low-temperature thermoelectric transport of TiCoSb single crystals.  Defects and disorder in apatite-type silicate oxide ion conductors: implications for conductivity.  Tuning magnetic properties with crystal engineering in a family of coordination polymers based on Ni(II) sulphates.  Magnetic and Structural Properties of the Fe5si1-Xgexb2 System.  Thermally stable mesoporous tetragonal zirconia through surfactant-controlled synthesis and Si-stabilization. 2022, 12, 16875-16885	O

669	A comprehensive study on crystal structure, magnetic, and electrical properties of Ni-doped FeIId spinel nano-ferrites.	1
668	On the influence of hydrothermal treatment pH on the performance of Bi2WO6 as photocatalyst in the glycerol photoreforming.	Ο
667	Synthesis and Properties of La1-x Sr x NiO3 and La1-x Sr x NiO2.	Ο
666	Fabrication of BaZr0.80Y0.20O3 II Sputtering Target for Thin-Film Proton Conducting Oxides.	
665	Mineralogical and geochemical study of industrial clinker: material behavior in the burning zone. <b>2022</b> , 15,	
664	Aging Enhanced Super-Elasticity and Ductility of a Cold NiTiTa Alloy.	
663	Effect of Magnesium Powder Application on the Microstructure and Properties of Rods Extruded by the Forward-Backward Rotating Die Extrusion Method. <b>2022</b> , 15, 4094	
662	Paper of RILEM TC 282-CCL: mineralogical characterization methods for clay resources intended for use as supplementary cementitious material. <b>2022</b> , 55,	
661	Study of Thermal, Microstructural, Optical, Dielectric, and Magnetic Characterizations of Ni <b>E</b> e Spinel Cobaltite for Various Applications.	
660	Formation of ceramics from K-activated FeOx-(Al2O3)-SiO2 inorganic polymers: effect of Al/K and Si/K molar ratio. <b>2022</b> ,	
659	Stable stoichiometric copper nitride thin films via reactive sputtering. <b>2022</b> , 128,	1
658	Abrupt change from moderate positive to colossal negative thermal expansion caused by imidazolate composite formation.	O
657	Bentonite Powder XRD Quantitative Analysis Using Rietveld Refinement: Revisiting and Updating Bulk Semiquantitative Mineralogical Compositions. <b>2022</b> , 12, 772	1
656	Efficient Screening of Coformers for Active Pharmaceutical Ingredient Cocrystallization.	1
655	Enhanced bending strength and microwave dielectric properties of Li2MgTi3O8 ceramics by adding Si3N4 reinforcing phase. <b>2022</b> ,	0
654	Revealing dynamic processes in laser powder bed fusion with in situ X-ray diffraction at PETRA III. <b>2022</b> , 93, 065104	1
653	Quantitative ion exchange reactions to form from Li2Vac2-2La2Ti3O9+ defect layered perovskites from H2La2Ti3O10 via solid acid/base reaction. <b>2022</b> , 123354	
652	Structural, optical and magnetic properties of CoFe2O4 nanoparticle synthesized by ultrasonication-assisted solgel technique. <b>2022</b> , 128,	O

651	Magnetoelectric multiferroicity in a newly derived nanocomposite system of (Y0.97Al0.03FeO3)x((Bi0.5Na0.5)0.94Ba0.06TiO3)(1-x) [x=0.3, 0.5]. <b>2022</b> , 169553	1
650	How Brine Composition Affects Fly Ash Reactions: The Influence of (Cat-, An-)ion Type. <b>2022</b> , 11, 20210155	
649	Formation of vacancies and metallic-like domains in photochromic rare-earth oxyhydride thin films studied by in-situ illumination positron annihilation spectroscopy. <b>2022</b> , 6,	2
648	Phase evolution and valence state change in Gd-Ce co-doped zirconolite glass-ceramics. <b>2022</b> , 153879	O
647	Structural and optical properties of newly synthesized Fe2WO6 compound. 2022,	1
646	Studying the structural, optical spectroscopic ellipsometry and electrical properties of variable-CdS thickness/CdTe for solar cell applications. <b>2022</b> , 19, 389-408	
645	Metal-ligand lability and ligand mobility enables framework transformation via ligand release in a family of crystalline 2D coordination polymers.	
644	Petrographic and geochemical characteristics of selected coal seams from the Late Cretaceous-Paleocene Guaduas Formation, Eastern Cordillera Basin, Colombia. <b>2022</b> , 259, 104042	О
643	Additively manufactured AlSi10Mg lattices iPotential and limits of modelling as-designed structures. <b>2022</b> , 220, 110796	О
642	In situ micromechanical analysis of a nano-crystalline W-Cu composite. <b>2022</b> , 220, 110848	О
641	Synthesis, physico-chemical, and structural properties of silicate apatites: Effect of synthetic methods on apatite structure and dye removal. <b>2022</b> , 142, 109628	
640	Modulating Na vacancies of Na4FeV(PO4)3 via Zr-substitution: Toward a superior rate and ultrastable cathode for sodium-ion batteries. <b>2022</b> , 541, 231727	1
639	Clay mineralogy and texture of deep-sea hydrothermal mudstone associated with the Cerro Matoso peridotite in accreted oceanic crust from Colombia. <b>2022</b> , 117, 103886	0
638	Pore system evolution in arenaceous regoliths - Case study from the Sila Massif (southern Italy). <b>2022</b> , 143, 105781	
637	Crystal growth and electrical conductivity of Ag7PS6 and Ag8GeS6 argyrodites. 2022, 168, 110828	О
636	Effect of alumina content on the crystal structure, lattice thermal expansion and thermal conductivity of aluminium-rich spinel solid solutions. <b>2022</b> , 288, 126366	1
635	Solubility and characterization of synthesized 11 TAl-tobermorite. 2022, 159, 106871	0
634	Liquid phase assisted synthesis of (Ti,V,Nb,Ta,W)C-Ni high entropy carbide cermets by conventional pressureless sintering. <b>2022</b> , 107, 105914	O

633	Is freeze-drying an alternative to solvent exchange for the hydration stop of cementitious suspensions?. <b>2022</b> , 159, 106841	О
632	An effective activation method for industrially produced TiFeMn powder for hydrogen storage. <b>2022</b> , 919, 165847	O
631	Magnetic and transport properties of chiral magnet Co7Zn8Mn5. <b>2022</b> , 560, 169631	О
630	Deformation behavior of high-entropy oxide (Mg,Co,Ni,Cu,Zn)O under extreme compression. <b>2022</b> , 219, 114879	O
629	Highly functional bio-based micro- and nano-structured materials for neodymium recovery. <b>2022</b> , 447, 137418	0
628	Thermoelectric properties and low thermal conductivity of Zintl compound Yb10MnSb9.	O
627	Magnetic and Structural Properties of the Fe5si1-Xgexb2 System.	
626	Oxygen deficiency in Sr2FeO4ष्ट: electrochemical control and impact on magnetic properties.	
625	Synthesis and evaluation of a ZnAl layered double hydroxide for the removal of ochratoxin A. Greenness assessment.	О
624	In-Situ Dehydration Study of the Sr-, Cd-And Pb-Exchanged Natrolite.	
623	The kesteriteBtannite structural transition as a way to avoid Cu/Zn disorder in kesterites: the exemplary case of the Cu2(Zn,Mn)SnSe4.	0
622	Acidic medium synthesis of zeolites han avenue to control the structure-directing power of organic templates.	O
621	Phase Compositions and Crystal Structure of Sn-Deficient Ca2sn2al2o9 Microwave Dielectric Ceramics with High QE Values.	
620	Spray Cooling Investigation of Very-Hot Aisi 304 Steel Plate with Mono and Mixed Sio2, Cuo Nanofluid.	
619	Synchrotron PXRD deconvolutes nickel particle and support changes in Ni/ZrO2 methanation catalysts.	
618	Material Design Towards Theory-Experiment Congruence: A Thermodynamically Stable Co-Cr-Fe-Al Heusler Phase.	
617	Structural Characterization and Influence of Defects on the Optical Properties of the Oxygen-Deficient Perovskite Ba3LiNb2O8.5?0.5. <b>2022</b> , 61, 10272-10282	
616	Coexisting magnetic structures and spin reorientation in Er0.5Dy0.5FeO3: Bulk magnetization, neutron scattering, specific heat, and density functional theory studies. <b>2022</b> , 105,	O

615	Optical and thermoelectric properties of NaNbO3 thin film deposed by spray pyrolysis: experimental and DFT study. <b>2022</b> , 137,	0
614	Describing the Influence of Ball-milling on the Amorphization of Flubendazole Using the PDF and RMC Methods with X-ray Powder Diffraction Data. <b>2022</b> ,	1
613	Study of the structural properties and temperature-dependent hopping conductivity mechanism to the analysis of nonlinearity exponent in Nd0.7\( \text{MCexSr0.3MnO3 manganites.} \)	
612	Effect of Cobalt Doping on Magnetocaloric Properties of La0.8Na0.2Mn1-xCoxO3 Manganite.	
611	Structural and electric properties of strontium fluorbritholites containing gadolinium and neodymium. <b>2022</b> , 128,	
610	Hexavalent chromium mobility in a high amorphous phase Chromite Ore Processing Residue (COPR) in the perspective of a chromium remediation treatment.	
609	Multi-Scale Pore Structure Characterization of Silurian Marine Shale and Its Coupling Relationship With Material Composition: A Case Study in the Northern Guizhou Area. 10,	
608	Charge Transfer between Fe and Ti Induced by Ln Substitution and Temperature in the B-Site-Disordered Perovskites Ln2(FeTi)O6 (Ln = La, Pr, and Nd). <b>2022</b> , 95, 1011-1015	
607	Conjunctive use of synchrotron X-ray diffraction and Rietveld refinement in Fe-oxide clays for forensic applications.	
606	Chemical Composition, Optical Properties and Sources of PM2.5 From a Highly Urbanized Region in Northeastern Mexico. 10,	o
605	An experimental analysis of the correlation between electronic structure and room temperature magnetism in Cu-doped CoFe2O4 spinel ferrite. <b>2022</b> , 128,	0
604	Enhancement of intrinsic green emission in phase pure ZnO. <b>2022</b> , 414155	o
603	BaFe0.875Re0.125O3🛘 and BaFe0.75Ta0.25O3🔻 as potential cathodes for solid-oxide fuel-cells: a structural study from neutron diffraction data. <b>2022</b> ,	
602	Microstructure, optical and electrical characterizations of Bi-incorporated Sb2Te3 thermoelectric compound synthesized by mechanical alloying: A comparative study with undoped Sb2Te3. <b>2022</b> ,	o
601	Structure and Electronic Structure Evolution of P2-NaxCoO2 Phases from X-ray Diffraction and 23Na Magic Angle Spinning Nuclear Magnetic Resonance.	1
600	Ultrastable Asymmetric Supercapacitor Device with Chemically Derived and Mechanically Activated NiCo2O4.	3
599	Microstructure, Exchange Interaction and Magnetic Properties of Nanocrystalline Zr\$\$_{6}\$\$Co\$\$_{23}\$\$/MgO(001) Films.	
598	Enhanced photocatalytic performance of cauliflower-like CeO2-TiO2 nanocomposite for the RhB dye degradation under visible light. <b>2022</b> ,	2

597	Investigation of adsorption-desorption characteristics of CO and H2 on Cu2+ doped SnO2 for identifying gas components by temperature modulation. <b>2022</b> , 132375		О
596	Feasibility and Limitations of High-Voltage Lithium-Iron-Manganese Spinels. <b>2022</b> , 169, 070518		
595	Mineralogical analysis of Brazilian Portland cements by the Rietveld method with emphasis on polymorphs M1 and M3 of alite. <b>2022</b> ,		
594	TSFZ Growth of Eu-Substituted Large-Size LSCO Crystals. <b>2022</b> , 12, 998		1
593	Historical ferrous slag induces modern environmental problems in the Moravian Karst (Czech Republic). <b>2022</b> , 157433		
592	Tuning the Magnetization of Manganese (II) Carbonate by Intracrystalline Amino Acids. 2201652		1
591	Wide-Band-Gap p-Type GaCrO3:Ni Semiconductor: A Hole Transport Material.		
590	Mechanically stimulated reactions in metalBxide (carbide) systems. <b>2022</b> , 66, 365-376		
589	Multivariate versus traditional quantitative phase analysis of X-ray powder diffraction and fluorescence data of mixtures showing preferred orientation and microabsorption. <i>Journal of Applied Crystallography</i> , <b>2022</b> , 55,	3.8	1
588	Observation of Griffith like phase and large magnetocaloric effect in nanocrystalline La0.7Ag0.2Bi0.1MnO3. <b>2022</b> , 132, 023901		
587	Evaluation of the impact of pH of the reaction mixture, type of the stirring, and the reagents' concentration in the wet precipitation method on physicochemical properties of hydroxyapatite so as to enhance its biomedical application potential.		
586	Synergistic Effects of Ni2+ and Mn3+ on the Electrochemical Activation of Li2MnO3 in Co-Free and Ni-Poor Li-Rich Layered Cathodes.		
585	Influence of the addition of CaTiO3 on the microwave dielectric properties of the BaMoO4 matrix. <b>2022</b> , 289, 126478		1
584	Designing a simple semi-automated system for preconcentration and determination of nickel in some food samples using dispersive liquid I quid microextraction based upon orange peel oil as extraction solvent. <b>2022</b> , 15, 104094		O
583	Assessing the dislocation density in CdSe nanocrystals from XRD peak profile analysis (XDPPA) assisted by first principles method. <b>2022</b> , 144, 115376		
582	Annealing effect on microstructure and magnetic properties of nanocrystalline Zr6Fe23 compound. <b>2022</b> , 560, 169650		
581	Structure and properties of the Sr2In1-Sn SbO6 double perovskite. <b>2022</b> , 314, 123355		
580	The contribution of hydrothermal mineral alteration analysis and gas geothermometry for understanding high-temperature geothermal fields The case of Ribeira Grande geothermal field, Azores. <b>2022</b> , 105, 102519		1

579	Structural elucidation of phenoxybenzaldehyde derivatives from laboratory powder X-ray diffraction: A combined experimental and theoretical quantum mechanical study. <b>2022</b> , 1268, 133697	1
578	Effect of Holmium substitution on magnetic, dielectric, and magnetodielectric properties of polycrystalline KBiFe2O5. <b>2022</b> , 155, 111947	O
577	High resistance and giant permittivity study of Ni0.4Zn0.6Fe2O4 spinel ferrite as a function of frequency and temperature.	O
576	TL and OSL study of Li2B4O7:Cu,Ag synthesized by combustion and solid-state reactions. <b>2022</b> , 10,	
575	Structural evolution and microwave dielectric properties of CaTiO 3 -La(Mg 2/3 Nb 1/3 )O 3 ceramics.	0
574	Structural and Morphological Characterization of the Chromium-doped 断podumene to Ceramic Pigment. <b>2022</b> , 10,	
573	Real-Time Monitoring of the Dehydrogenation Behavior of a Mg 2 FeH 6 MgH 2 Composite by In Situ Transmission Electron Microscopy. 2204147	1
57 <sup>2</sup>	Short- and Long-Range Cation Disorder in (AgxCu1☑)2ZnSnSe4 Kesterites.	O
571	Effect of Higher Carrier Mobility of the Reduced Graphene OxideZinc Telluride Nanocomposite on Efficient Charge Transfer Facility and the Photodecomposition of Rhodamine B.	1
570	Practical insights into the recycling of green mussel shells (Perna Viridis) for the production of precipitated calcium carbonate. 1-11	1
569	Melting behaviour of simulated radioactive waste as functions of different redox iron-bearing raw materials. <b>2022</b> , 153946	O
568	Magneto-elastic coupling in a sinusoidal modulated magnet Cr2GaN.	
567	Photocatalytic NOx abatement: The effect of high air flow velocity. 2022, 102820	
566	Two-fold improvement in chemical adsorption ability to achieve effective carbon dioxide electrolysis. <b>2022</b> , 317, 121754	O
565	Investigations on phase coexistence and functional properties of BCZT lead-free piezoceramic. <b>2021</b> , 31, 20-26	
564	Ion transport mechanism in anhydrous lithium thiocyanate LiSCN Part I: ionic conductivity and defect chemistry.	1
563	The Effect of Ion Irradiation (⊞, E = 1500 keV) on the Microstructure of the Deformed Ni 13.9 wt.% W Alloy. <b>2022</b> , 65, 123-130	
562	Physiochemical and thermal characterisation of faba bean starch.	O

561	Large Electrocaloric Responsivity and Energy Storage Response in the Lead-Free Ba(GexTi1☑)O3 Ceramics. <b>2022</b> , 15, 5227	О
560	Effects of doping, hydrostatic pressure, and thermal quenching on the phase transitions and magnetocaloric properties in Mn1⊠CoxNiGe. <b>2022</b> , 132, 045107	1
559	Hydroxyapatite nanoparticles synthesized with a wide range of Ca/P molar ratios and their structural, optical, and dielectric characterization.	O
558	Ge-Containing Oxide-Ion Conductors with CaEu2Ge3O10-Type Structure Discovered by the Bond-Valence Method and Experiments. <b>2022</b> , 61, 12327-12336	
557	Correlated negative magnetization, exchange bias, and electrical properties in La1 $\mbox{\ensuremath{\mathbb{N}}}$ PrxCrO3. <b>2022</b> , 6,	O
556	Valence bond glass state in the 4d1 fcc antiferromagnet Ba2LuMoO6. <b>2022</b> , 7,	Ο
555	Individual diametral compression behavior of a ceramic proppant. 2022,	
554	A semi-supervised deep-learning approach for automatic crystal structure classification. <b>2022</b> , 55, 882-889	O
553	Time-Dependant Microstructural Evolution and Tribological Behaviour of a 26 wt% Cr White Cast Iron Subjected to a Destabilization Heat Treatment.	O
552	In Situ Study of Temperature Stability and Precipitation Kinetics of \$\$delta \$\$ and \$\$eta \$\$ Phases in Nickel Base Superalloys.	Ο
551	Effect of atomic substitution on the sodium manganese ferrite thermochemical cycle for hydrogen production. <b>2022</b> , 101094	
550	The effect of antisite disorder on magnetic and exchange bias properties of Gd-substituted Y2CoMnO6 double perovskite. <b>2022</b> , 34, 435801	O
549	Characterization Methodology and Activity Evaluation of Solar-Driven Catalysts for Environmental Remediation. <b>2022</b> , 380,	O
548	Temperature-Dependent Delocalization of Oxygen Vacancies in La-Substituted CeO2. <b>2022</b> , 5, 9759-9769	3
547	Green diesel rich product (C-15) from the hydro-deoxygenation of refined palm oil over activated NH4+-Indonesian natural zeolite. <b>2022</b> , 44, 7483-7498	O
546	Detection of Weyl fermions and the metal to Weyl-semimetal phase transition in WTe2 via broadband high resolution NMR. <b>2022</b> , 4,	
545	Role of manganite in enhancing dielectric cum magnetic properties of BTFO-LSMO composites. <b>2022</b> , 128,	
544	Unified understanding of the first-order nature of the transition in TbCo2. <b>2022</b> , 106,	O

543	Selective Chemical Substitution of Cu in the Structure of TiAl3 Type InPd3: Experimental and Theoretical Studies.	1
542	Crystal structure and specific heat of calcium lanthanide oxyborates Ca4 LnO(BO3)3. <b>2022</b> ,	
541	Strontium Nitridoborate Hydride Sr2BN2H Verified by Single-Crystal X-ray and Neutron Powder Diffraction. <b>2022</b> , 61, 12685-12691	
540	Digitization of imaging plates from Guinier powder X-ray diffraction cameras. <b>2022</b> , 55,	O
539	The apparent difference in microwave dielectric properties of $Ca3MZnGe3O12$ (M = $Zr$ , $Sn$ ) garnets originating from compression and rattling effects.	0
538	Thermoelectric properties of high-entropy rare-earth cobaltates. 2022,	O
537	Charge Transport in Twisted Organic Semiconductor Crystals of Modulated Pitch. 2203842	4
536	Structural, Magnetic and Electrical Properties of New Perovskite Pr0.67Sr0.16Ca0.17Mn0.75Fe0.25O3 Material.	O
535	Evolution of Structural Properties in Fe Intercalated 2H-NbSe2: Phase Transformation Induced by Strong Host <b>©</b> uest Interaction. <b>2022</b> , 126, 13762-13773	O
534	Extended investigation of LiOHLiBr binary system for high-temperature thermal energy storage applications.	O
533	Tuning skyrmions in B20 compounds by 4d and 5d doping. <b>2022</b> , 6,	
532	Peculiarity of topological Hall effect in Mn2Sb0.9Bi0.1 ferrimagnet. <b>2022</b> , 121, 082401	
531	Solid-State Nuclear Magnetic Resonance Spectroscopy-Assisted Structure Determination of Coordination Polymers.	
530	Parametrics XRD Rietveld refinements of mechanically activated solid-state reactions in iron-brass alloy. <b>2022</b> , 32, 104150	O
529	Thermo analytical characterization of tantalum oxide in the process for the development of tantalum nitride photoelectrodes. <b>2022</b> , 32, 104122	
528	Defect mediated structural, optical, electrical and mechanical properties of mechano-synthesized PbTe nanostructure as a superior thermoelectric material: correlation among electrical, mechanical and optical properties. <b>2022</b> , 166833	1
527	Crystalline Assembly and Solvent-induced Solid-state Transformation of 1D Zigzag Chains Based on Sulfonylcalix[4]arene Trinuclear Co (II) and Zn (II) Clusters.	
526	Effect of different synthesis routes on the morphology, optical, colorimetric, and photocatalytic properties of 料g2MoO4 microcrystals.	

525	ITO: n-ZnO: p-NiO and ITO: n-ZnO: p-NZO thin films: Study of crystalline structures, surface statistical metrics, and optical properties.	0
524	Appraisal of Ni Species Supported on Porous MgO during Ethanol Steam Reforming by XAS.	
523	The Development of Clathrate Hydrate Science.	2
522	Effect of Mediator on the Auto Combustion Synthesis, Magnetic Properties, and Electron Density Distribution of Spinel Ferrite Mn0.05Zn0.95Fe2O4. <b>2022</b> , 52,	
521	Physico-chemical properties and antimicrobial activity of silver nanoparticles fabricated by green synthesis. <b>2022</b> , 133960	2
520	Influence of crystal structure disordering on ionic conductivity of Ag7+x(P1-xGex)S6 single crystals. <b>2022</b> , 166873	
519	Impedance spectroscopic analysis and electrical proprieties in SrAgNiMnO6 double perovskite ceramic.	
518	Deconvolution of main hydration kinetic peaks in properly sulfated Portland cements with boundary nucleation and growth models and relation to early-age concrete strength development. <b>2022</b> , 348, 128602	
517	Study of cobalt-iron mixed oxides and catalytic behavior for decomposition of hydrogen peroxide. <b>2022</b> , 530, 112639	0
516	Structural and optical investigations on LaGaO3 synthesis by solgel method along with a blue luminescence property. <b>2022</b> , 143, 109807	
515	Potential, premises, and pitfalls of interpreting illite argon dates - A case study from the German Variscides. <b>2022</b> , 232, 104133	O
514	Effect of heat treatment on microstructure evolution and magnetocaloric properties of droplet melted MnHePBi alloys. <b>2022</b> , 20, 1593-1602	1
513	Impact of structural and optical properties tunability of SnSe2 thin films on its optoelectronic properties. <b>2022</b> , 33, 102251	
512	Microstructure and aqueous corrosion in carbon steel: An emerging correlation. <b>2022</b> , 290, 126623	O
511	Gadolinium oxyorthogermanate Gd2GeO5: An efficient solid refrigerant material for magnetic cryocoolers. <b>2022</b> , 27, 100810	2
510	Influence of alumina addition on steam corrosion behaviour of ytterbium disilicates for environmental barrier coating applications. <b>2022</b> , 207, 110555	o
509	In-situ high-temperature EBSD characterization during a solution heat treatment of hot-rolled Ti-6Al-4V. <b>2022</b> , 192, 112207	О
508	A single-phase white emitting nanophosphor with refined crystal structure and extremely luminescent characteristics for WLEDs and latent fingerprint detection. <b>2022</b> , 290, 126619	0

507	Photoluminescence and magnetic properties of SrMoO4 phosphors submitted to thermal treatment and electron irradiation. <b>2022</b> , 562, 169761	О
506	Structure-based magnetic, electrical and transport properties of Nillnto ferrite by V5+ substitution. <b>2022</b> , 43, 36-49	
505	Structural and magnetic properties evolution of Cu2Cr2Zr2-2Se4 for 0.500 🕸 🕮 0.650. <b>2022</b> , 645, 414249	
504	Spectroscopic and magnetic investigations of the dilute magnetically doped semiconductors BaSn1-Mn O3 (0.02 私心.1). <b>2022</b> , 170, 110942	
503	Nature-inspired construction of iridescent CNC/Nano-lignin films for UV resistance and ultra-fast humidity response. <b>2022</b> , 296, 119920	1
502	Solving inorganic crystal structures from X-ray powder diffraction using a generative first-principles framework. <b>2022</b> , 214, 111687	
501	Influence of hydrotalcite/rosasite precursors over Cu/Zn/Al mixed oxides on ethanol dehydrogenation. <b>2022</b> , 291, 126659	
500	Evolution of deformation microstructure in a coarse-grained Fe-Mn-Al-C steel under bending fatigue. <b>2022</b> , 327, 133006	
499	Use of Taguchi method to evaluate the unconfined compressive strength of quicklime stabilized silty clayey subgrade. <b>2022</b> , 17, e01417	
498	Te(IV) immobilization by siderite: Reaction kinetics, mechanism, and Te isotopic fractionation. <b>2022</b> , 121123	O
497	NMR Crystallography as a Vital Tool in Assisting Crystal Structure Determination from Powder XRD Data. <b>2022</b> , 12, 1277	1
496	Mechanisms for the Deactivation of the Electronic Excited States of ∃-(2-Hydroxyphenyl)-N-phenylnitrone: From Intramolecular Proton and Charge Transfer to Structure Twisting and Aggregation.	1
495	X-Ray Diffraction and M\(\text{S}\)sbauer Studies of Nanostructured Ni40Fe60 Powder: Structure Defects and Hyperfine Structure.	0
494	Band gap engineered Sn-doped bismuth ferrite nanoparticles for visible light induced ultrafast methyl blue degradation. <b>2022</b> ,	O
493	Automated Data Analysis for Powder X-Ray Diffraction Using Machine Learning. 1-7	0
492	Critical element (Nb-Ta-Zr-Hf-REE-Ga-Th-U) mineralization in Late Triassic coals from the Gaosheng Mine, Sichuan Basin, southwestern China: Coupled effects of products of sediment-source-region erosion and acidic water infiltration. <b>2022</b> , 262, 104101	1
491	A multi-methodological approach for mineral exploration and predictive metallurgy: the case of the Pilar gold deposit at the Quadrillero Ferrero, Brazil. <b>2022</b> , 149, 105113	0
490	High entropy steel processed through mechanical alloying and spark plasma sintering: Alloying behaviour, thermal stability and mechanical properties. <b>2022</b> , 856, 144029	O

489	Influence of calcium substitution on structural, morphological and electrical conductivity properties of La1- xCaxNi0.5Ti0.5O3 ( $x = 0.0$ , $x = 0.2$ ) compounds for energy storage devices. <b>2022</b> , 144, 109925	0
488	Paleoclimatic reconstruction during the North China Craton drifting: Evidence from hydrogen and oxygen isotope composition of kaolinite in coal-bearing strata claystone. <b>2022</b> , 605, 111241	Ο
487	Influence of suspended solid particles on calcium carbonate fouling in dripper labyrinths. <b>2022</b> , 273, 107890	2
486	High performance asymmetric supercapacitor device based on lanthanum doped nickel-tin oxide/reduced graphene oxide composite. <b>2022</b> , 55, 105526	4
485	Thermal expansivity and Raman spectra of natural cordierite: A potential cordierite-garnet elastic thermometer. <b>2022</b> , 332, 106939	О
484	Mechanochemical synthesis of strontium oxybritholites (Sr10-xLax(PO4)6⊠(SiO4)xO): Characterization, structural refinement, and adsorption characteristics toward Basic Blue 41. <b>2022</b> , 145, 109957	Ο
483	Significant enhancement in photosensitivity, responsivity, detectivity and quantum efficiency of Co3O4 nanostructured thin film-based photodetectors through Mo doping developed by spray pyrolysis method. <b>2022</b> , 34, 102366	0
482	Characterization of ashes produced from different biomass fuels used in combustion systems in a pulp and paper industry towards its recycling. <b>2022</b> , 166, 106598	Ο
481	Muskeg Soil Stabilization Using the Microbially Induced Calcite Precipitation Technique by the Urease Active Bioslurry Approach. <b>2022</b> , 148,	0
480	Magnetic and structural properties of the Fe5Si1-xGexB2 system. <b>2022</b> , 316, 123576	O
479	Monitoring the precipitation of the hardening phase in the new VDMI Alloy 780 by in-situ high-temperature small-angle neutron scattering, neutron diffraction and complementary microscopy techniques. <b>2022</b> , 928, 167203	0
478	Hard-core/zeolitized-shell beads obtained by surface zeolitization of activated clay particles. <b>2022</b> , 16, 100624	Ο
477	Molten salt-assisted synthesis of carbo-nitride TiC0.5N0.5 and MAX phases Ti2AlC0.5N0.5 and Ti3AlCN at low temperature under different atmospheres. <b>2022</b> , 26, 101160	0
476	Photocatalytic abatement of air pollutants: Focus on their interference in mixtures. <b>2023</b> , 434, 114235	1
475	Bimetallic ordered carbonaceous frameworks from Co- and Cu-porphyrin bimolecular crystals. <b>2023</b> , 201, 338-346	0
474	Biogenic synthesis of Cerium oxide nanoparticles using Justicia Adathoda leaves extract: Size-strain study by X-ray peak profile analysis and luminescence characteristics. <b>2023</b> , 1272, 134144	1
473	Catalyst supports based on ZnOIInAl2O4 nanocomposites with enhanced selectivity and coking resistance in isobutane dehydrogenation. <b>2022</b> , 51, 12213-12224	0
472	Energy landscapes in inorganic chemistry. 2022,	O

471	Polymorphs and solid solutions: materials with new luminescent properties obtained through mechanochemical transformation of dicyanoaurate(I) salts.	0
470	Combined characterization approaches to investigate magnetostructural effects in exchange-spring ferrite nanocomposite magnets. <b>2022</b> , 6, 2422-2437	O
469	New Alkali Lanthanide-free Polyoxometalates with Remarkable Water-Responsive Turn-Off-On Luminescence Properties.	0
468	Failure Analysis of Hydrothermal Synthesis for Spinel Manganese-Cobalt Oxide.	1
467	Synthesis of flexible Co nanowires from bulk precursors. <b>2022</b> , 12, 21153-21159	О
466	AC conductivity and phase transition of the BST <b>B</b> FO ceramic doped with Yb. <b>2022</b> , 12, 27154-27161	Ο
465	Effect of the Heat Treatment on the Microstructure, Magnetism and Magnetocaloric Effect in Fe-Rich (Mn,Fe)Y(P,Si) Melt-Spun Ribbons.	Ο
464	Expansion of the multifunctionality in off-stoichiometric manganites using post-annealing and high pressure: physical and electrochemical studies. <b>2022</b> , 24, 21872-21885	1
463	Vibrational, Electronic and Structural Study of Sprayed ZnO Thin Film Based on the IR-Raman Spectra and DFT Calculations. <b>2022</b> , 11, 23-38	Ο
462	Crystal Structure, Microstructure, and Ultra-High Energy Storage Properties of Lead-Free (x)Bi(Mg0.5Ti0.5O3-(1-x)[0.50Ba(Zr0.2Ti0.8)O3-0.50(Ba0.7Ca0.3)TiO3] Ternary Ceramics.	Ο
461	Extraordinary intense blue Tl+ lone-pair photoluminescence from thallium(i) chloride hydroborate Tl3Cl[B12H12]. <b>2022</b> , 51, 13331-13341	О
460	Ambient-pressure ozone treatment enables tuning of oxygen vacancy concentration in the La1 $\!$ BSrxFeO3 $\!$ B(0 $\!$ BL $\!$ D) perovskite oxides.	Ο
459	Raman mapping of piezoelectric poly(l-lactic acid) films for force sensors. 2022, 12, 27687-27697	0
458	Thermal Instability Originating from the Interface between Organic-Inorganic Hybrid Perovskite and Oxide Electron Transport layers.	2
457	High Entropy Steel Processed Through Mechanical Alloying and Spark Plasma Sintering: Alloying Behaviour, Thermal Stability, and Mechanical Properties.	О
456	Eldfellite NaV(SO4)2 as a versatile cathode insertion host for Li-ion and Na-ion batteries.	1
455	Upgrading a Brahmaputra River sand from northern Bangladesh by flotation to produce a high-grade silica glass sand concentrate. 1-15	1
454	Ultra-low hysteresis in giant magnetocaloric Mn1-V Fe0.95(P,Si,B) compounds. <b>2023</b> , 930, 167336	2

453	Effect of Post-thermal Annealing on the Structural, Morphological, and Optical Properties of RF-sputtered In2S3 Thin Films.	0
452	Phase Transformations of Zirconium Dioxide and Crystal Growth During Heat Treatment of the ZrO2(CeO2,Y2O3)[a0.85Y0.15Al11O18Al2O3 System. <b>2022</b> , 92, 1488-1497	O
451	Effect of milling time on the structural, microstructure, and magnetic properties of nanocrystalline Fe90Sb10 powders obtained by high-energy ball milling. <b>2022</b> , 122, 2043-2058	О
450	Reuse of Acid Bioleachate in Bacterial Oxidation of a Refractory Gold Sulfide Concentrate. <b>2022</b> , 12, 1087	O
449	Influence of Al Variation on the Mechanical Properties and Critical Shear Stress of Twinning in Fe-Mn-Al-C Steels.	0
448	Multiple strongly coupled antiferromagnetic spin $S'=1/2$ dimers in liroconite Cu2Al(As,P)O4(OH)4[4H2O. <b>2022</b> ,	O
447	Mn5+-activated Ca6Ba(PO4)4O near-infrared phosphor and its application in luminescence thermometry. <b>2022</b> , 11,	3
446	Low thermal conductivity in A-site high entropy perovskite relaxor ferroelectric. <b>2022</b> , 121, 112901	2
445	Synthesis and Characterization of Mechanically Alloyed Nanostructured (Ti,Cr)C Carbide for Cutting Tools Application. <b>2022</b> , 12, 1280	О
444	Communication Breakdown: Into the Molecular Mechanism of Biofilm Inhibition by CeO2 Nanocrystal Enzyme Mimics and How It Can Be Exploited.	О
443	Structure and Surface Relaxation of CeO2 Nanoparticles Unveiled by Combining Real and Reciprocal Space Total Scattering Analysis. <b>2022</b> , 12, 3385	О
442	Structural and magnetic properties of Ca1-xLaxFe0.5Mn0.5O3- $\square$ (0.05 $\rlap/\!\!\!L$ $\rlap/\!\!\!L$ 0.15) perovskites. <b>2022</b> , 128,	O
441	Computation-informed optimization of Ni(PyC)2 functionalization for noble gas separations. <b>2022</b> , 3, 101025	О
440	Study of structural, dielectric, and optical properties of Ni0.4Cu0.4Co0.2Fe2O4 spinel ferrite for electrical and optical applications.	O
439	Inverse exchange bias effects and magnetoelectric coupling of the half-doped perovskite-type chromites Gd0.5Sr0.5CrO3 and Gd. <b>2022</b> , 106,	О
438	Effects of the Parent Alloy Microstructure on the Thermal Stability of Nanoporous Au. <b>2022</b> , 15, 6621	O
437	Mechanochemical synthesis and crystal structure evaluation of Na 2 ZnSnS 4.	О
436	Thermal, Physical, and Optical Properties of the Solution and Melt Synthesized Single Crystal CsPbBr3 Halide Perovskite. <b>2022</b> , 10, 369	1

435	Feasibility of reprocessing gold tailings: Integrated management approach for the control of contaminated neutral mine drainage. <b>2022</b> , 187, 107821	0
434	Comparison of degradation behavior and osseointegration of 3D powder-printed calcium magnesium phosphate cement scaffolds with alkaline or acid post-treatment. 10,	Ο
433	Structural investigation and sonophotocatalytic properties of the solid solutions Sr(Mo1\( \text{Mwx}\)O4 crystals synthesized by the sonochemical method. <b>2022</b> , 33, 22127-22152	0
432	Similar and Dissimilar Properties of Polymorphic Phases of NdIr3. <b>2022</b> , 126, 16514-16521	Ο
431	Phase compositions and crystal structure of Sn-deficient Ca2Sn2Al2O9 microwave dielectric ceramics with high Qflvalues. <b>2022</b> ,	0
430	Tuning of microwave dielectric properties of garnets Ca3Mg2CV2O12 (C = Si, Ti) through compression and expansion effects. <b>2022</b> ,	0
429	Effect of configurational entropy on phase formation, structure, and magnetic properties of deeply substituted strontium hexaferrites. <b>2022</b> ,	0
428	Study of Structural and Optical Properties of Cullr Substituted Mgllo Spinel Ferrites for Optoelectronic Applications.	Ο
427	Microstructure Analysis, Optical, and Electrical Transport Properties of NiAl 2 O 4 /Al 2 O 3 Nanocomposite Powder. 2200386	0
426	Bromine Pentafluoride BrF5, the Formation of [BrF6] (Salts, and the Sterical (In) Activity of the Br Lone Pairs.	0
425	Pyrophosphate Na2CoP2O7 Polymorphs as Efficient Bifunctional Oxygen Electrocatalysts for ZincAir Batteries. <b>2022</b> , 14, 40761-40770	0
424	Sodium sulphate resistance of geopolymer mortar produced using ground ferronickel slag with fly ash. <b>2022</b> ,	0
423	Effect of processing parameters on texture and variant selection of as-built 300 maraging steel processed by laser powder bed fusion. <b>2022</b> , 12,	0
422	Crystallographic and shape preferred orientation producing anisotropy in slates from Northern Spain. <b>2022</b> , 104730	O
421	Corrosion Performance and Mechanical Strength in Aluminum 6061 Joints by Pulsed Gas Metal Arc Welding. <b>2022</b> , 15, 6226	0
420	Real space study of local bonding for zinc structure based on temperature-dependent x-ray pair distribution function analysis. <b>2022</b> , 12, 095313	0
419	Controlling Mechanical Behavior of TWIP Steels by Tuning Texture and Stacking Faults. <b>2022</b> , 53, 3986-4003	0
418	Recycling detoxified cement asbestos slates in the production of ceramic sanitary wares. 2022,	1

417	Role of nickel substitution in the structural, magnetic properties, and magnetocaloric effect in La0.67Ba0.22Sr0.11Mn0.95Ni0.05O3 sample.	O
416	The Stacking Faulted Nature of the Narrow Gap Semiconductor Sc2Si2Te6.	Ο
415	Colloidal stability improvement of cobalt ferrite encapsulated in carboxymethylated cashew gum. <b>2022</b> , 130307	O
414	Electronic structure and magnetic properties of 3daf double perovskite material. 2022, 6,	O
413	Crystal structure and spectral characterization of La 2 (CO 3 ) 3 $$ ? 5H 2 O $\Box$ an industrially relevant lanthanide carbonate.	0
412	High yield solvothermal synthesis of Ni nanoparticles: structural, microstructural, and magnetic properties. <b>2022</b> , 24,	O
411	Water driven phase transitions in Prussian White cathode materials.	O
410	Compositional effects on the hydrogen storage properties in a series of refractory high entropy alloys. 10,	1
409	Electrical conductivity through latacking in a two-dimensional porous gallium catecholate metalBrganic framework.	O
408	Ag nanoparticles synthesized by Datura metel L. Leaf extract and their charge density distribution, electrochemical and biological performance. <b>2022</b> , 807, 140083	О
407	Photoelectrochemical activity of Cu2O electrochemically deposited at different temperatures. <b>2022</b> , 115, 561-569	1
406	Cementation processes of Roman pozzolanic binders from Caesarea Maritima (Israel). <b>2022</b> , 355, 129128	2
405	Characterization of super duplex stainless steel SAF2507 deposited by directed energy deposition. <b>2022</b> , 857, 144084	О
404	Mineralogy, geochemistry, and K-Ar dating of feldspars and clays from an exceptional Cretaceous fossil locality (Tlaya, Puebla, Mexico): Insights into the depositional and diagenetic ages and processes. <b>2022</b> , 612, 121134	O
403	Origin of the crossover from ferroelectric to relaxor in tetragonal tungsten bronzes. <b>2022</b> , 929, 167314	1
402	To grind or not to grind? The influence of mechanical and thermal treatments on the Cu/Zn disorder in Cu2ZnSn(SxSe1-x)4 monograins. <b>2022</b> , 248, 112009	O
401	Novel antibacterial efficacy of ZnO nanocrystals/Ag nanoparticles loaded with extract of Ximenia americana L. (stem bark) for wound healing. <b>2022</b> , 151, 18-32	1
400	Densification, microwave dielectric properties and rattling effect of LiYbO2 ceramics with low $\mu$ and anomalous positive $\Pi$ <b>2022</b> , 42, 7455-7460	O

399	Contrasting microwave dielectric properties of zircon-structured AEuV2O8 (A = Bi, La) ceramics. <b>2022</b> , 42, 7461-7467	О
398	Reactive spark plasma assisted synthesis of metastable rare-earth ferrites with widely tunable charge ordering transfer properties.	o
397	Investigating the hydration of C3A in the presence of the potentially toxic element chromium route to remediation?. <b>2022</b> , 12, 29329-29337	О
396	Thermodynamic Simulation and Experimental Investigation of the Calciothermic Reduction of Metals from Manganese and Iron Niobates. <b>2022</b> , 2022, 909-918	o
395	Mechanism of long-term strength retrogression of silica-enriched Portland cement assessed by quantitative X-ray diffraction analysis. 9,	О
394	Incorporation of Silica Particles Attached to Nylon 66 Electrospun Nanofibers with Cement. <b>2022</b> , 15, 7011	O
393	Co(NCS)2 Chain Compound with Alternating 5- and 6-Fold Coordination: Influence of Metal Coordination on the Magnetic Properties. <b>2022</b> , 61, 16841-16855	0
392	Enhancement of magnetic entropy change in La0.57Nd0.1Sr0.33-xCaxMnO3 manganites.	О
391	Crystal structure, electric and microwave dielectric properties of La2Mg(Mg1/3Sb2/3)O6 novel double-perovskite with non-stoichiometric 1:1 cationic ordering. <b>2022</b> ,	0
390	Mineralogical Factors Affecting the Dense Medium Separation of Nickel Sulfide Ores. <b>2022</b> , 12, 1311	О
389	Revealing the Magnetic Structure and Properties of Mn(Co,Ge)2.	0
388	Obtaining a fused PLA-calcium phosphate-tobramycin-based filament for 3D printing with potential antimicrobial application.	O
387	Neutron scattering studies on ionic diffusion behaviors of superionic ⊞- Cu2⊡Se. <b>2022</b> , 121, 151901	0
386	Synthesis of Three-Dimensional Carbon Nanosheets and Its Flux Pinning Mechanisms in C-Doped MgB2 Superconductors. <b>2022</b> , 15, 7530	О
385	Li-Rich and Halide-Deficient Argyrodite Fast Ion Conductors.	0
384	Fundamental Behaviors, and Contributions of Hopping and Tunneling Mechanisms to the Transport Characteristics of the La0.5Ca0.5MnO3 Phase Separated Perovskite. <b>2022</b> , 4, 4893-4902	O
383	Approach to Estimate the Phase Formation and the Mechanical Properties of Alloys Processed by Laser Powder Bed Fusion via Casting. <b>2022</b> , 15, 7266	О
382	Spectral interpretation of late-stage mare basalt mineralogy unveiled by Chang <b>E</b> -5 samples. <b>2022</b> , 13,	1

381	Electrochemical Performance of Tunnelled and Layered MnO2 Electrodes in Aluminium-Ion Batteries: A Matter of Dimensionality. <b>2022</b> , 169, 100538	0
<b>3</b> 80	Multi-Method Characterization of the High-Entropy Spinel Oxide Mn 0.2 Co 0.2 Ni 0.2 Cu 0.2 Zn 0.2 Fe 2 O 4: Entropy Evidence, Microstructure, and Magnetic Properties.	O
379	Solgel method and reactive SPS for novel aluminagraphene ceramic composites. 2022,	3
378	Air plasma-sprayed high-entropy (Y0.2Yb0.2Lu0.2Eu0.2Er0.2)3Al5O12 coating with high thermal protection performance. <b>2022</b> , 11, 1571-1582	O
377	Influence of Graphene Sheets on Compaction and Sintering Properties of Nano-Zirconia Ceramics. <b>2022</b> , 15, 7342	О
376	Magnetization reversal tuning in honeycomb ferrimagnet Ni4Nb2O9. <b>2022</b> , 132, 153901	1
375	Thermokinetic evaluation of zircon oxide green synthesis mediated by plant extract of Abelmoschus esculentus L. Moench.	О
374	Nanocomposites of GaBr3 and BiBr3 Nanocrystals on BiOBr for the Photocatalytic Degradation of Dyes and Tetracycline. <b>2022</b> , 5, 15676-15691	O
373	Piezoelectric properties of mechanochemically processed 0.67BiFeO3-0.33BaTiO3 ceramics. 2022,	0
372	Room-temperature structure, magnetic, and magnetocaloric properties of (La0.8-xNdx)Sr0.2MnO3(0 $\/R$ $\/R$ 0.2). <b>2022</b> ,	O
371	Investigating porous catalysts with synchrotron X-rays and neutrons. 2022,	О
370	Reassigning the Pressure-Induced Phase Transitions of Methylammonium Lead Bromide Perovskite. <b>2022</b> , 144, 20099-20108	1
369	Synthesis and Crystal-Structure Analysis of the K 2 NiF 4 -Type Hydride Oxides Li Ln EuH 2lk O 2 (Ln =La, Ce, Pr, Nd, Sm) and LiEu 2 H 3 O by Neutron and X-Ray Diffraction. <b>2022</b> , 648,	О
368	Antisite disorder driven cluster glass state and colossal magnetoresistance in MnSb2Se4. <b>2022</b> , 106,	O
367	Solvent-Free Synthesis of Nickel Nanoparticles as Catalysts for CO2 Hydrogenation to Methane. <b>2022</b> , 12, 1274	1
366	Comparative Study of the Mineralogy and Chemistry Properties of Elephant Bones: Implications during Diagenesis Processes. <b>2022</b> , 12, 1384	O
365	Reticulated open-cellular aluminum nitride ceramic foams: Effect of sintering aids on microstructural, thermal, and mechanical properties.	О
364	Redox Dynamics of Pt and Cu Nanoparticles on TiO2 during the Photocatalytic Oxidation of Methanol under Aerobic and Anaerobic Conditions Studied by In Situ Modulated Excitation X-ray Absorption Spectroscopy. <b>2022</b> , 12, 12879-12889	O

363	Investigation of Magnetocaloric Effect and Critical Properties of Pr0.7Ca0.1Sr0.2Mn1-xSnxO3 ( $x = 0, 0.04$ and 0.08) Samples.	O
362	Effects of non-magnetic Ti4+ ion substitution at Mn site on structural, magnetic, and optical properties for La0.57Pr0.1Sr0.33Mn1⊠TixO3 manganites. <b>2022</b> , 128,	O
361	Highly Active and Stable Ni/La-Doped Ceria Material for Catalytic CO2 Reduction by Reverse Water-Gas Shift Reaction.	1
<b>3</b> 60	Effect of La Doping on Kinetic and Thermodynamic Performances of Ti1.2CrMn Alloy upon De/Hydrogenation.	O
359	A free and open-source solution for Rietveld refinement of XRD data from the CheMin instrument onboard the Mars rover Curiosity. <b>2022</b> , 105596	O
358	Facile synthesis of crack-free single-crystalline Al doped Co-free Ni-rich cathode material for lithium-ion batteries. <b>2022</b> , 141473	O
357	Doping nanoarchitectonics through exchange of Ag+ with Na+ in La0.7Ca0.1Sr0.1X0.1MnO3 (X = Ag+ or Na+) manganite ceramics for enhancement and levelling tendency of magneto resistivity. <b>2022</b> , 128,	O
356	Large magnetocaloric and magnetoresistance effects during martensitic transformation in Heusler-type Ni44Co6Mn37In13 alloy. <b>2022</b> , 563, 170034	O
355	Cole-Cole analysis and optoelectronic properties, using VEELS, of KNNS ferroelectric ceramics. <b>2022</b> , 33, 104781	0
354	Synthesis of a novel visible-light active Gd2O3/GdVO4/V2O5 photocatalyst for rapid purification of industrial wastewater containing organic dyes and bacteria. <b>2022</b> , 368, 120512	O
353	In-situ dehydration study of the Sr-, Cd- and Pb-exchanged natrolite. 2022, 346, 112277	0
352	Mn-doped NiWO4 quantum dots with superior electrochemical and conductivity performance for energy storage application. <b>2022</b> , 56, 105946	O
351	Multiwalled carbon nanotubes as an additive to Mg-Mg2Si in situ composite obtained by powder sintering. <b>2023</b> , 931, 167548	O
350	Random magnetic anisotropy in a new compound Sm2AgSi3. <b>2023</b> , 45, 1-5	O
349	New complexes of Zn(II) and Cd(II) halides with 1,8-diaminonaphthalene: Synthesis, structure, and thermal stability. <b>2023</b> , 1273, 134263	O
348	Effect of the heat treatment on the microstructure, magnetism and magnetocaloric effect in Fe-rich (Mn,Fe) (P,Si) melt-spun ribbons. <b>2023</b> , 932, 167635	O
347	Mn(II)-doped CdS/ZnS core/shell quantum dot film photocatalyzes reductive organic transformations with a boost in efficiency from enhanced Auger processes.	O
346	Effects of basicity and Al<sub>2</sub>O<sub>3</sub> content on the crystal structure of silico-ferrite of calcium and aluminum. <b>2022</b> ,	O

345	Lo que ganamos con el fuego. Estudio arqueomErico de las temperaturas de cocciB en alfarerB prehispBica del Delta Superior del rB Paran[[Argentina]. <b>2022</b> , 17,	O
344	Variability in X-ray induced effects in [Rh(COD)Cl]2 with changing experimental parameters.	O
343	New insights into the structural transition from UO2+x to U3O7 by Quantitative Raman Spectroscopy.	O
342	Quantum yield and energy transfer in up-conversion SrGd2O4:Yb, Er nanoparticles obtained via sol-gel assisted combustion. <b>2023</b> , 253, 119491	O
341	Mechanical property regulation of transformation induced plasticity (TRIP) multi-principal element alloys through multi-phase microstructural design. <b>2023</b> , 152, 107754	O
340	Na0.67Mn0.33Ni0.33Co0.33O2: Effect of synthesis technique on competing P3 and P2 phases. <b>2023</b> , 287, 116106	O
339	Impact of W doping on Fe-rich (Mn,Fe)2(P,Si) based giant magnetocaloric materials. 2023, 933, 167802	O
338	Vanadium oxide by radio frequency magnetron sputtering and spray pyrolysis technique: structural and optical properties. <b>2022</b> ,	O
337	CRYSTALS GROWTH AND REFINEMENT OF THE Cu3SbSe3 CRYSTAL STRUCTURE. <b>2022</b> , 88, 25-33	O
336	Continuous flow photoreactor undergoing variable simulated irradiation conditions: Experimentations and modeling. <b>2022</b> , 12, 100422	O
335	Study of structural features and thermal properties of barium hexaferrite upon indium doping.	6
334	Ultralow Loss and High Tunability in a Non-perovskite Relaxor Ferroelectric. 2210709	1
333	Structural and magnetic properties of LaVO3 - Absence of anomalous diamagnetism. 2022,	O
332	Insight into the negative magnetization and anomalous exchange-bias in DyFe5Al7 through neutron depolarization and neutron diffraction studies.	O
331	Mineralogy, geochemistry, and genesis of stones of arhat statuettes unearthed in Naju, Korea: geoarchaeological implications. <b>2022</b> , 14,	O
330	Automatic Rietveld refinement by robotic process automation with RIETAN-FP.	O
329	Rare Earth Ion-Doped Y2.95R0.05MgAl3SiO12 (R = Yb, Y, Dy, Eu, Sm) Garnet-Type Microwave Ceramics for 5G Application. <b>2022</b> , 12, 1608	O
328	Vacancy-Driven Disorder and Elevated Dielectric Response in the Pyrochlore Pb1.5Nb2O6.5.	O

327	Ferromagnetic Ni1🛮 VxO1 🖟 Nano-Clusters for NO Detection at Room Temperature: A Case of Magnetic Field-Induced Chemiresistive Sensing.	0
326	Magnetocaloric Effect in La0.7Pb0.3-xBaxMnO3 (x = $0.05$ , $0.10$ , and $0.15$ ): Direct and Indirect Measurements.	О
325	Effect of citric-acid-modified chitosan (CAMC) on hydration kinetics of tricalcium silicate (C3S). <b>2022</b> , 21, 3604-3616	0
324	The Effects of Surfactants and Essential Oils on MicrowaveAssisted Hydrothermal Synthesis of Iron Oxides. <b>2022</b> , 12, 1567	О
323	Mineral Changes to the Tufa Columns of Ikka Fjord, SW Greenland. <b>2022</b> , 12, 1430	0
322	Solvothermal Synthesis, Temperature-Dependent Structural Study, and Magnetic Characterization of a Multipolydentate Oxamate-Based 2D Coordination Network.	О
321	Broadening Phosphor-Converted Light-Emitting Diode Emission: Controlling Disorder.	0
<b>32</b> 0	BaTiO3 induced modification on the dielectric, ferroelectric and electrical conductivity properties of Pb(Fe0.5Nb0.5)O3-BaTiO3 solid solution. 1-14	O
319	The Control of Shale Composition on the Pore Structure Characteristics of Lacustrine Shales: A Case Study of the Chang 7 Member of the Triassic Yanchang Formation, Ordos Basin, North China. <b>2022</b> , 15, 8353	0
318	Pressure-induced first-order antiferromagnetic to ferromagnetic transition in MnN. <b>2022</b> , 168120	O
317	Structural phase transition and charge carrier dynamics in Dy containing La6MoO12 ionic conductor. <b>2022</b> , 107061	0
316	Charge transfer effects and O2- vacancies in pure CuO nanofibers and enriched with 3.0% Mn. <b>2022</b> , 126989	o
315	Kinetics and Rietveld XRD structural study of Cs+ sorption on natural and synthetic mordenites in the first $12\text{h}$ .	0
314	Crystal structure thermal evolution and novel orthorhombic phase of methylammonium lead bromide, CH3NH3PbBr3. <b>2022</b> , 12,	o
313	Effect of the partial substitution of K on the structural, magnetic and magnetocaloric properties of brownmillerite oxides La1 $\!$ MKxSrMn2O5+ $\!$ 1 (0.1 $\!$ M $\!$ 10.3).	О
312	Halogen (F, Cl, Br, and I) concentrations of the upper continental crust through time as recorded in ancient glacial diamictite composites. <b>2022</b> ,	O
311	Study of structural, dielectric, and electrical properties of the LaBaFe1.2Mn0.8O6 double perovskite.	0
310	Pressure Induced Reduction in SrUO4 la Topotactic Pathway to Accessing Extreme Incompressibility. <b>2022</b> , 118508	О

309	Defect-characterized phase transition kinetics. <b>2022</b> , 9, 041311	О
308	Assessment of deep cryogenic heat-treatment impact on the microstructure and surface chemistry of austenitic stainless steel. <b>2022</b> , 35, 102456	1
307	Insight into the intrinsic magnetic properties of dual-main-phase Ce magnets through Ce chemical state. <b>2022</b> , 564, 170180	О
306	Electrospun Sn-doped TiO2: Synthesis, structural, optical and catalytic performance as a function of Sn loading and calcination temperatures. <b>2022</b> ,	O
305	Effect of dopant oxidation states on enhanced low ppm CO sensing by copper doped zinc oxide. <b>2022</b> , 127047	О
304	Insights into stability, transport, and thermoelectric properties of transparent p-type copper iodide thin films.	O
303	Deciphering the peculiar hysteresis loops of 0.05Pb(Mn1/3Sb2/3)O3 <b>0</b> .95Pb(Zr0.52Ti0.48)O3 piezoelectric ceramics. <b>2023</b> , 244, 118563	O
302	Storm chasing: Tracking Holocene storminess in southern Sweden using mineral proxies from inland and coastal peat bogs. <b>2023</b> , 299, 107854	1
301	A compact-rigid multi-analyser for energy and angle filtering of high-resolution X-ray experiments. Part 1. Principles and implementation. <b>2023</b> , 30, 111-125	O
300	A compact-rigid multi-analyser for energy and angle filtering of high-resolution X-ray experiments. Part 2. Efficiency of a single-crystal-comb. <b>2023</b> , 30, 126-136	O
299	On the magnetic-structure origin of giant magnetostrictive effect in MnCoSi-based metallic helimagnets. <b>2023</b> , 30, 100930	О
298	Search for Lithium Ion Conducting Oxides Using the Predicted Ionic Conductivity by Machine Learning. <b>2023</b> , 64, 287-295	O
297	Hydrogen storage in Mo substituted low-V alloys treated by melt-spin process. <b>2023</b> , 455, 140970	О
296	Electron density and thermal motion of diamond at elevated temperatures. 2023, 79, 41-50	O
295	Transport properties of LaYbO3-based electrolytes doped with alkaline earth elements. <b>2023</b> , 439, 141702	O
294	Pair distribution function analysis driven by atomistic simulations: Application to microwave radiation synthesized TiO2 and ZrO2. <b>2023</b> , 218, 111964	O
293	Defects and oxygen vacancies modified properties of transition metal doped Ce0.95X0.05O2 (X´=´Fe, Co, Ni) nanoparticles. <b>2023</b> , 288, 116154	О
292	Synthesis, crystal structure, and superconductivity of Ba(Bi0.25Pb0.75)1Mg O3□2023, 360, 115051	O

291	Effect of an inner-transition metal (Dy) intercalation on the structure and magnetic properties of 1TTiSe2. <b>2023</b> , 318, 123782	O
290	X-ray line profile analysis on the deformation microstructure of Al-bearing high-Mn steels. <b>2023</b> , 196, 112567	O
289	Mixed ferro to diamagnetic transition in Hf doped CaSnO3 perovskite system. <b>2023</b> , 360, 115033	O
288	Long-lifespan layered Strontium vanadate for high-performance zinc-ion battery: Ultralow migration barrier of Zn2+ on the surface and the effect of pH value. <b>2023</b> , 318, 123788	O
287	Sintering behaviour and structure-thermal stability relationships of alkali-doped ternesite. <b>2023</b> , 164, 107043	0
286	Crystal structure, microstructure, and ultra-high energy storage properties of lead-free (x)Bi(Mg0.5Ti0.5O3-(1-x)[0.50Ba(Zr0.2Ti0.8)O3-0.50(Ba0.7Ca0.3)TiO3] ternary ceramics. <b>2023</b> , 288, 116194	O
285	Quantification of amorphous Si, Al, and Fe in palagonitic Mars analogs by chemical extraction and X-ray spectroscopy. <b>2023</b> , 392, 115362	O
284	Magnetic, magnetodielectric, and magnetoimpedance correlations in co-substituted (Co, Ho) KBiFe2O5 at room temperature. <b>2023</b> , 938, 168432	O
283	Synthesis, crystal structure and 19F NMR parameters modelling of CaTiF6(H2O)2 yielding to a revision of the bond-valence parameters for the Ti4+/Filon pair. <b>2023</b> , 319, 123793	O
282	Experimental determination of the HHf phase diagram using in situ neutron diffraction. <b>2023</b> , 937, 168353	O
281	Structure and properties of ZnO/ZnMn2O4 composite obtained by thermal decomposition of terephthalate precursor. <b>2022</b> , 90-90	O
280	Photocatalytic degradation of methylene blue and dye mixture using indium-doped CaWO4 synthesized by sonochemical and microwave-assisted hydrothermal methods. <b>2022</b> , 51, 18234-18247	O
279	Synthesis of LnCrO3 perovskites and their color properties. <b>2022</b> , 27,	O
278	Effect Cooling Conditions on the Structure and Properties of Alloy VTI-4. <b>2022</b> , 64, 451-457	O
277	Rietveld Refinement, Structural Characterization, and Methylene Blue Adsorption of the New Compound Ba0.54Na0.46Nb1.29W0.37O5. <b>2022</b> , 12, 1695	1
276	Comparison of the Structure and Properties of a Tube from Titanium Alloy Ti B% Al D.5% V with Results of Digitalization of the Process of its Pressing. <b>2022</b> , 64, 458-464	O
275	Correlation between local structure variations and critical temperature of (Bi1.6Pb0.4Sr2Ca2Cu3O10+E)1-x(TiO2)x superconductor. <b>2022</b> ,	O
274	Heterovalent Tin Alloying in Layered MA3Sb2I9 Thin Films: Assessing the Origin of Enhanced Absorption and Self-Stabilizing Charge States. <b>2022</b> , 126, 21040-21049	1

273	Tin Oxide (SnO2)-Decorated Reduced Graphene Oxide (rGO)-Based Hydroelectric Cells to Generate Large Current. <b>2022</b> , 7, 43647-43656	0
272	Experimental and Theoretical Correlation of Modulated Architectures of Ag2MoO4 Microcrystals: Effect of Different Synthesis Routes on the Morphology, Optical, Colorimetric, and Photocatalytic Properties.	O
271	Low-temperature crystallization and microwave dielectric properties of forsterite generated in MgOBiO2 system following LiF addition. <b>2022</b> ,	О
270	Probing the Signature of Disordering and Delocalization of Oxygen Vacancies and Anti-site Defects in Doped LaAlO3 Solid Electrolytes. <b>2022</b> , 126, 20251-20262	1
269	X-ray Diffractometry in Forensic Science. <b>2023</b> , 37-59	О
268	Silicon-Doped Nanostructured Fe <sub>80</sub> Ni <sub>20</sub> Alloys: The Role of Si on the Microstructure, Morphology and Magnetic Properties. 76, 1-14	О
267	Influence of microstructure on hydrogen trapping and diffusion in a pre-deformed TRIP steel. 2022,	О
266	Hydrogen-Induced Order <b>D</b> isorder Effects in FePd3. <b>2022</b> , 12, 1704	О
265	Preparation of pyrite concentrate powder from the Thackaringa mine for quantitative phase analysis using X-ray diffraction. <b>2022</b> , 55, 1572-1582	o
264	Implications changing of the CdS window layer thickness on photovoltaic characteristics of n-CdS/i-AgSe/p-CdTe solar cells. <b>2022</b> , 19, 825-839	o
263	Investigation of Structural, Morphological, Thermal, and Thermoelectric Properties of Zn1-xCuxAl2O4 (0.0個0.1).	0
262	Phase transition hysteresis at the antiferroelectric-ferroelectric boundary in PbZr1NTixO3. <b>2022</b> , 106,	О
261	Mineral carbonation of New Caledonian ultramafic mine slag: Effect of glass and secondary silicates on the carbonation yield. <b>2022</b> , 121282	O
260	Creating superconductivity in WB2 through pressure-induced metastable planar defects. <b>2022</b> , 13,	О
259	Boosting energy-storage efficiency and thermal stability via defect dipoles in BaTiO3-based lead-free ceramics. <b>2022</b> ,	O
258	The Influence of a Binder in a Composite Electrode: The Case Study of Vanadyl Phosphate in Aqueous Electrolyte. <b>2022</b> , 15, 9041	o
257	Growth and characterization of a new superconductor GaBa2Ca3Cu4O11+□.	0
256	Green and blue materials for the ceramic industry from pink MgCoxNi1-xSiO4 (0 $R L 1$ ) solid solutions. <b>2022</b> ,	O

255	A novel crystallographic location of rattling atoms in filled Eu x Co4Sb12 skutterudites prepared under high-pressure conditions. <b>2022</b> ,	O
254	Influence of fabrication conditions on the structural characteristics and the magnetic properties of FeAl 2 O 4.	O
253	High temperature effects on the properties of limestones: post-fire diagnostics and material durability. <b>2022</b> , 55,	O
252	Structural change-conductivity relationship in Na4\Zr2\NbxSi3O12 solid electrolytes over a wide temperature range.	O
251	Superconductivity arising from pressure-induced emergence of a Fermi surface in the kagome-lattice chalcogenide Rb2Pd3Se4. <b>2022</b> , 106,	O
250	Recognizing the Importance of an Urban Soil in an Open-Air City Museum: An Opportunity in the City of Madrid, Spain. <b>2022</b> , 11, 2310	O
249	Spin reorientation, negative magnetization and magnetocaloric effect in Nd0.5Dy0.5CrO3. <b>2022</b> , 170231	0
248	An Anomalous Electron Configuration Among 3d Transition Metal Atoms.	О
247	Structural, împedance Spectroscopy, and Electrical Properties in BiBaNiMnO6 Double Perovskite for some Device Applications.	О
246	Crystal Structures of Ce(IV) Nitrates with Bis(2-pyrrolidone) Linker Molecules Deposited from Aqueous Solutions with Different HNO3 Concentrations.	O
245	Deep-Level Emission Tailoring in ZnO Nanostructures Grown via Hydrothermal Synthesis. 2023, 13, 58	О
244	Effects of Mixed Phases on Electrical Conductivities for (CeF3)1th(CaF2)m Fast-Fluoride-Ion-Conducting Solid Electrolytes.	O
243	Feature Space of XRD Patterns Constructed by an Autoencoder. 2200613	О
242	Fabrication of NiO/YSZ-Based Anodes for Solid Oxide Fuel Cells by Hybrid 3D Inkjet Printing and Laser Treatment. <b>2022</b> , 5, 1115-1127	O
241	Structural and Superconducting Proximity Effect of SnPb Bimetallic Nanoalloys. 2022, 12, 4323	0
240	Highly active and stable OER electrocatalysts derived from Sr2MIrO6 for proton exchange membrane water electrolyzers. <b>2022</b> , 13,	O
239	Enhancement of Photocatalytic Activity of Electrodeposited Cu2O by Reducing Oxygen Vacancy Density. <b>2022</b> , 5, 15326-15332	0
238	Unravelling the convoluted and dynamic interphasial mechanisms on Li metal anodes.	1

237	AC Conductivity and Dielectric Behavior of a New Double Perovskite PrNaMnMoO6 System.	0
236	An Amine-Functionalized Ultramicroporous Metal®rganic Framework for Postcombustion CO2 Capture.	0
235	Relationship between Microstructure, Mechanical Properties and Creep Behavior of a Cr-Rich Ferritic Stainless Steel Produced by Laser Powder Bed Fusion. <b>2022</b> , 1, 263-276	O
234	Characterizing the ZrBe2Hx Phase Diagram via Neutron Scattering Methods. 2023, 11, 1	О
233	An Anomalous Electron Configuration Among 3d Transition Metal Atoms.	O
232	Atypical performance of CoO-accelerated interface tweaking in hierarchical cobalt phosphide/oxide@P-doped rGO heterostructures for hybrid supercapacitors. <b>2022</b> ,	O
231	Structure, evolutionary context and chronological data of the Monforte de Moyuela Roman dam (Ebro Basin, NE of Spain).	O
230	High-Pressure Synthesized Perovskite CdMnO3 with C-Type Antiferromagnetic Spin Configuration. <b>2022</b> , 61, 21011-21015	О
229	Properties of Thermochemical Remanent Magnetization on Basalt Samples Containing Titanomagnetites with Increased Thermal Stability. <b>2022</b> , 58, 842-858	О
228	Structural Features and Thermal Behavior of Ion-Exchanged Clinoptilolite from Beli Plast Deposit (Bulgaria). <b>2022</b> , 12, 1576	O
227	Structural, electrical, magnetic and magnetotransport properties of La0.7Ca0.18Ba0.12Mn0.95Sn0.05O3 manganite prepared with different quenching processes. <b>2023</b> , 129,	0
226	Facile and highly efficient wet synthesis of nanocrystalline BiFeO3particles by reverse co-precipitation method. <b>2022</b> ,	О
225	Thermochromic properties of pure NiTiO3 and its Cu- or Co-doped derivatives. 2022,	O
224	Polymorphism and intergrowth structures in the nanostructured Pr co system: Pr2Co7 and Pr5Co19. <b>2022</b> , 112621	O
223	Giant baroresistance effect in lanthanum-strontium manganite nanopowder compacts. 2022, 168591	O
222	Covalent organic frameworks. <b>2023</b> , 3,	O
221	Structural Characterization of Low-Sr-Doped Hydroxyapatite Obtained by Solid-State Synthesis. <b>2023</b> , 13, 117	0
220	The pressure and temperature evolution of the Ca3V2O8 crystal structure using powder X-ray diffraction.	О

219	Characterization data of reference materials used for phase II of the priority program DFG SPP 2005 Dpus Fluidum Futurum IRheology of reactive, multiscale, multiphase construction materials I 2023, 108902	O
218	Research progress of two-dimensional magnetic materials.	O
217	Topotactic synthesis of DyVO3; an investigation of magnetocaloric effect. 2023, 566, 170221	О
216	Tunable luminescence thermal stability in YVxAs1\( \text{IO}\)04:Eu3+ through the introduction of As5+ ions for remote temperature sensing applications.	O
215	Deformation Behavior, Recrystallization Kinetics, Strengthening Mechanisms and Residual Stress in Al-Mg-Si-Ag Alloy Processed by Equal-Channel Angular Pressing.	0
214	New Series of Red-Light Phosphor Ca9⊠ZnxGd0.9(PO4)7:0.1Eu3+ (x = 011). <b>2023</b> , 28, 352	1
213	Structural and magnetic analysis of Cd-Zn spinel ferrite nanoparticles.	0
212	Synthesis and hydrogenation properties of Nitto bimetallic nanoparticles.	O
211	Formation and Microstructural Evolution of Ferritic ODS Steel Powders during Mechanical Alloying. <b>2023</b> , 16, 765	0
210	Structural, Magnetic, and Magnetocaloric Features of La0.8Na0.2Mn0.97M0.03O3 (M = Ni, Fe) Manganite.	O
209	Evidence for vortex state in Fe2CoGe thin films using FORC and magnetic imaging. 2023, 566, 170318	O
208	Damage analysis of retrieved Biolox(R)delta components used in hard and soft bearings. 2023,	O
207	Importance of amorphous content, surface energy, and preferred orientation on the accurate quantification of cement minerals in clinkers. <b>2023</b> , 105887	O
206	Phase-structural transformation of erbium trihydride studied by thermal desorption spectroscopy. <b>2023</b> ,	O
205	Synthesis, structural and electrical properties of two congruent isotypic diphosphates: Li2Na2P2O7 and Li3NaP2O7. <b>2023</b> , 129,	0
204	Assessing the spatial variability of the $\sim$ 3 th OH / H 2 O absorption feature in CM2 carbonaceous chondrites.	O
203	A new high voltage alluaudite sodium battery insertion material. 2023, 27, 101316	0
202	A 3D oxalate-bridged [Cu II Fe II ] coordination polymer as molecular precursor for CuFe 2 O 4 spinelphotocatalytic features.	O

201	The planar anodic Al2O3-ZrO2 nanocomposite capacitor dielectrics for advanced passive device integration.	O
<b>2</b> 00	Reducing the Cobalt Content in SrCo0.95Ti0.05O3-I-Based Perovskites to Produce Cleaner Cathodes for IT-SOFCs.	O
199	Co-precipitation of Mg-doped Ni0.8Co0.1Mn0.1(OH)2: effect of magnesium doping and washing on the battery cell performance.	1
198	Geochronology, mineralogy, and geochemistry of tonsteins from the Pennsylvanian Taiyuan Formation of the Jungar Coalfield, Ordos Basin, North China. <b>2023</b> , 267, 104183	O
197	Optimized phase compositions and microwave dielectric properties of low loss Ca 2 Sn 2 Al 2 O 9 -based ceramics by M 4+ substitution.	O
196	Structural, mechanical, and tribological properties of CrCN coatings obtained by cathodic arc physical vapour deposition technology at different CH4/N2 gas ratio. <b>2023</b> , 766, 139669	O
195	Specimen-displacement correction for powder X-ray diffraction in DebyeBcherrer geometry with a flat area detector. <b>2023</b> , 56,	O
194	Effect of off-stoichiometry and Ta doping on Fe-rich (Mn,Fe)2(P,Si) based giant magnetocaloric materials. <b>2023</b> , 226, 115253	O
193	Active species identification in Zn and Mn-based materials for application in alcohol oxidation reactions. <b>2023</b> , 289, 116251	0
192	Eu3+-activated SrY2O4:Ce4+/3+ red-phosphor for WLEDs: Structural and luminescent insights from experimental and theoretical approaches. <b>2023</b> , 938, 168595	O
191	Uptake and incorporation of Al, Cr, V, Zn and Mo in hematite: Competition, synergies and influence on structural properties. <b>2023</b> , 445, 130630	O
190	Structural, morphological, magnetic and optical properties of Jeanbandyite prepared by the co-precipitation method. <b>2023</b> , 34, 105358	O
189	The quaternary fluoride LiNaCa2Al2F12 in aluminum electrolytes: synthesis, structure, thermal stability. <b>2023</b> , 319, 123825	O
188	Novel Bi La1-Mn Co1-O3 nanocrystalline perovskite based MIS Schottky UV photodetector device. <b>2023</b> , 161, 112154	O
187	Pressure-induced valence fluctuation in CsEuF3: From divalent Eu valence to trivalent Eu valence state. <b>2023</b> , 175, 111202	О
186	Highly Resistant LaCo1⊠FexO3 Perovskites Used in Chlorobenzene Catalytic Combustion. <b>2023</b> , 13, 42	O
185	The Influence of Zn Substitution on Physical Properties of CoFe2O4 Nanoparticles. <b>2023</b> , 13, 189	О
184	Phase Stability and Kinetics of Topotactic Dual Ca2+Na+ Ion Electrochemistry in NaSICON NaV2(PO4)3.	O

183	Development of high-performance Low-V BCC alloy for hydrogen storage by suction casting. 2022,	O
182	Use of Biomass Ash in Reinforced Clayey Soil: A Multiscale Analysis of Solid-State Reactions. <b>2023</b> , 8, 5	O
181	Structural Evolution from Neutron Powder Diffraction of Nanostructured SnTe Obtained by Arc Melting. <b>2023</b> , 13, 49	О
180	Elucidating Catalytic Sites Governing the Performance toward the Hydrogen Evolution Reaction in Ternary Nitride Electrocatalysts.	О
179	Photoluminescence and quantum yield behaviour of vanadium doped Zn2SiO4 phosphors facilely synthesized by sol-gel method.	О
178	Evaluation of phase and domain switching in Sn-doped BCZT piezoceramics with coexisting ferroelectric phases. <b>2023</b> ,	О
177	A review of small angle scattering, neutron reflection, and neutron diffraction techniques for microstructural characterization of polymer-bonded explosives. <b>2023</b> ,	1
176	Monitoring of Suspended Sediment Mineralogy in Puerto-Rican Rivers: Effects of Flowrate and Lithology. <b>2023</b> , 13, 208	O
175	Flame-Retardant Foamed Material Based on Modified Corn Straw Using Two Nitrogenous Layers. <b>2023</b> , 16, 952	О
174	Mixed Valence of Bismuth in Hexagonal Chalcohalide Nanocrystals.	O
173	Geochemical and mineralogical characterization of phosphogypsum and leaching tests for the prediction of the mobility of trace elements.	О
172	Oxide Ion Mobility in V- and P-doped Bi2O3-Based Solid Electrolytes: Combining Quasielastic Neutron Scattering with Ab Initio Molecular Dynamics.	O
171	Deformation, dislocation evolution and the non-Schmid effect in body-centered-cubic single- and polycrystal tantalum. <b>2023</b> , 103529	O
171 170		0
	polycrystal tantalum. <b>2023</b> , 103529	
170	polycrystal tantalum. <b>2023</b> , 103529  Experimental study on the methane adsorption behaviour in shale gas reservoir. <b>2023</b> ,	O
170 169	polycrystal tantalum. 2023, 103529  Experimental study on the methane adsorption behaviour in shale gas reservoir. 2023,  Nanoalloys and catalytic applications. 2023, 401-436  Synthesis, characterization and application of SiO2 and CuO nanofluid in spray cooling of hot steel	0

165	Thermal Properties of Pressure Core Samples Recovered from Nankai Trough Wells Before and After Methane Hydrate Dissociation.	O
164	Phase stability and tensorial thermal expansion properties of single to high-entropy rare-earth disilicates.	O
163	Temperature- and frequency-dependent dielectric and impedance spectroscopy of double perovskite oxide BiBa0.5Ag0.5Ni2O6 electronic material. <b>2023</b> , 34,	0
162	Effect of Microstructure and Dislocation Density on Material Removal and Surface Finish of Laser Powder Bed Fusion 316L Stainless Steel Subject to a Self-Terminating Etching Process.	O
161	Effect of Class C and Class F Fly Ash on Early-Age and Mature-Age Properties of Calcium Sulfoaluminate Cement Paste. <b>2023</b> , 15, 2501	0
160	Structural stability, optical and thermoelectric properties of the layered RbSn2Br5 halide synthesized using mechanochemistry.	Ο
159	Magnetoelectric coupling at room temperature in LaTiO3/SrTiO3 heterojunctions. <b>2023</b> , 162, 112169	Ο
158	Crystal structures for flexible photovoltaic application. <b>2023</b> , 493-525	O
157	Evolution of the valence state of Ru metal ions in correlation with the structural and electronic properties of double perovskite ruthenates; A2SmRuO6 (where $A = Ba \& amp; Sr$ ). <b>2023</b> , 11, 4081-4093	0
156	Effect of incorporation of alkali earth metal oxide on structural, optical and DC conduction mechanism in tellurium-phosphate glassy systems. <b>2023</b> , 34,	Ο
155	Influence of the Nature of Aminoalcohol on ZnO Films Formed by Sol-Gel Methods. 2023, 13, 1057	0
154	Environmental and Mineralogical Controls on Biosignature Preservation in Magnesium Carbonate Systems Analogous to Jezero Crater, Mars.	Ο
153	Synthesis, crystal structure, thermal and spectroscopic properties of ZnX2-2-methylpyrazine (X´=´Cl, Br, I) coordination compounds. <b>2023</b> , 78, 113-120	0
152	Active and durable R2MnRuO7 pyrochlores with low Ru content for acidic oxygen evolution. <b>2023</b> , 14,	Ο
151	White-light emission from yttrium iron garnet (YIG). <b>2023</b> , 11, 041116	Ο
150	Stabilization of the cubic perovskite La0.8Pr0.2BaCo2-yO6-□by introducing Co deficiency and its effect on thermal expansion, electrical conductivity and electrochemical properties. <b>2023</b> , 446, 142102	Ο
149	Temperature and magnetic field controlled dielectric relaxation and magnetodielectric response in KBiFe1.9Co0.1O5 polycrystalline. <b>2023</b> ,	0
148	Strikingly reduced critical field in Ti-doped KagomlYMn6Sn5.6Ti0.4 single crystal with large topological Hall effect. <b>2023</b> , 944, 169182	O

147	Incorporation of rare earth elements into (Ba,Ca)2(CO3. 2023, 139, 107129	O
146	Synthesis, structural characterization and magnetic behavior of a novel phosphate: K4(Co0.25Fe0.75)4(PO4)5. <b>2023</b> , 139, 107170	O
145	Undoped CdSiO3 for contactless thermometer in the cryogenic range: pH-dependent intrinsic defects and emitting colour. <b>2023</b> , 321, 123908	O
144	Excellent thermostability and emission properties of Sr2CaTeO6:Sm3+ red emitting phosphor for high color-rendering white LEDs. <b>2023</b> , 139, 107168	O
143	Procedures for microstructurally conditioning an Fe-22Mn-0.6C-1.5Al TWIP steel for optimal mechanical behaviour. <b>2023</b> , 199, 112790	O
142	Phase equilibria and non-transformable tetragonal zirconia in ZrO2-RETaO4 systems and their stabilization mechanism: Experiments and calculations. <b>2023</b> , 49, 15969-15978	O
141	Synchrotron X-ray diffraction of pyrolusite (MnO2) and rutile (TiO2) during heating to ~1000 °C. <b>2023</b> , 177, 111284	0
140	Photocatalytic properties insight of Sm-doped LiNbO3 in ferroelectric Li1িkNbSm1/3xO3 system. <b>2023</b> , 11, 109732	O
139	Multi-scale geophysical characterization of microporous carbonate reservoirs utilizing machine learning techniques: An analog case study from an upper Jubaila formation outcrop, Saudi Arabia. <b>2023</b> , 152, 106234	0
138	Structure and in vitro antimicrobial activity of sulfamethoxazole and sulfadiazine polyiodide salts. <b>2023</b> , 1282, 135199	O
137	Reactivity of waterglass in cementitious systems. <b>2023</b> , 12, 100067	0
136	Characterisation of residual stresses and oxides in titanium, nickel, and aluminium alloy additive manufacturing powders via synchrotron X-ray diffraction. <b>2023</b> , 35, 105900	O
135	Effects of Nd- and Zr- substitution for Sm on magnetic and structural properties in SmFe11V 1:12 compound. <b>2023</b> , 946, 169267	0
134	Influence of Process Variables on Shrinkage in Low-Calcium Fly-Ash Geopolymers. <b>2023</b> , 35,	O
133	Densification and microstructure features of lithium hydride fabrication. <b>2023</b> , 185, 109709	0
132	Effect of transition metal and alkali oxides on structural, optical and dielectric properties in Zinc-Phosphate amorphous glassy systems. <b>2023</b> , 609, 122235	O
131	Electron density distribution and microstructural spherical harmonic calculation of BaTiO3 powders and ceramics. <b>2023</b> , 322, 123988	0
130	The leaching behaviors of lead, zinc, and sulfate in pyrite ash contaminated soil: mineralogical assessments and environmental implications. <b>2023</b> , 11, 109687	O

129	Coupling microbial and abiotic amendments accelerates in situ remediation of bauxite residue at field scale. <b>2023</b> , 877, 162699	О
128	New insight into the effect of oxygen vacancies on electrochemical performance of nickel-tin oxide/reduced graphene oxide composite for asymmetric supercapacitor. <b>2023</b> , 62, 106922	О
127	A new method for determination of lignocellulose crystallinity from XRD data using NMR calibration. <b>2023</b> , 5, 100305	O
126	The reduction of molybdenum-VI-oxide to molybdenum: Kinetics versus thermodynamics and the associated structural aspects. <b>2023</b> , 113, 106210	О
125	Effects of ionic polarizability and crystal structure on microwave dielectric properties of RE2O3 (RE = La, Eu) ceramics with opposite and high Q. <b>2023</b> , 43, 4066-4072	0
124	Experimental investigation on phase equilibria in Mg-Y-Ag system at 400 and 500?. 2023, 945, 169312	О
123	Achieving exceptional wear resistance in a crack-free high-carbon tool steel fabricated by laser powder bed fusion without pre-heating. <b>2023</b> , 156, 1-19	0
122	Electric field-induced two-step phase transformation and its contribution to the electromechanical strain in lead-free relaxor-based ceramics. <b>2023</b> , 43, 3289-3296	О
121	Synthesis and characterization of a novel oxovanadium complex and stability of azo groups in the presence of laccase. <b>2023</b> , 1285, 135465	0
120	Magneto-electric effect in Y1-xRxFeO3 (R´=´Sm and Er) ceramics. <b>2023</b> , 293, 116419	О
119	High-stress abrasive wear performance of medium-carbon direct-quenched and partitioned, carbide-free bainitic, and martensitic steels. <b>2023</b> , 204925	0
118	Low temperature atmospheric synthesis of WAlB and Mn2AlB2 MAB phases by modified molten salt shielded synthesis method. <b>2023</b> , 34, 103983	О
117	Swelling of sulfate-bearing soil: a case study of A1 highway pavement failure. 2023, e02081	O
116	Effect of prior ⊞2 phase on precipitation kinetics of O-phase in advanced Ti2AlNb alloy. <b>2023</b> , 118930	О
115	Alternative reductants for foam control during vitrification of high-iron High Level Waste (HLW) feeds. <b>2023</b> , 608, 122240	O
114	The impact of granulation on the mineralogy of a modified-BOF slag and the effect on kinetics and compressive strength after alkali activation. <b>2023</b> , 140, 105038	О
113	Blending bauxite residues with multiple byproducts improves capping materials for tailings storage facilities. <b>2023</b> , 338, 117852	O
112	In situ high-temperature Raman scattering study of monoclinic Ag2Mo2O7 microrods. <b>2023</b> , 295, 122632	O

111	Pr2CrMnO6 double perovskite as new electrode material for electrochemical energy storage. <b>2023</b> , 302, 127726	O
110	Bauchemie. <b>2022</b> , 175-230	O
109	Evaluation of the potential use of granite waste in products of the red ceramic industry in the state of Amazonas. <b>2022</b> , 27,	0
108	Pampa La Cruz: un estudio diacrīlico de sus vasijas de cerīlica y fuentes de materia prima mediante tēnicas de rayos X. <b>2022</b> , 27,	O
107	Zeolitized volcanic ashes as supports for Anderson heteropolycompound catalysts. Application in the oxidation of diphenyl sulfide. <b>2023</b> , 34, 105459	O
106	Enhancing the thermal stability of alkali-activated Fe-rich fayalite slag-based mortars by incorporating ladle and blast furnace slags: Physical, mechanical and structural changes. <b>2023</b> , 166, 107098	1
105	Magnetoelectric coupling study of lead-free BaTiO3/NiFe2O4 mixed and coreBhell multiferroic composites. <b>2023</b> , 34,	0
104	Photocatalytic performance evaluation of flame - sprayed and polymeric suspension coatings from TiO 2 nanoparticles .	O
103	Microstructural evolution during post heat treatment of the TiBAlBV alloy manufactured by laser powder bed fusion. <b>2023</b> , 23, 1980-1994	0
102	Cavitation Wear of T91 Ferritic-Martensitic Steel. <b>2022</b> , 58, 364-368	O
101	Frustrated microstructures composite PbS material size perspective from XRD by variant models of Williamson Hall plot method. <b>2023</b> , 46,	0
100	In-depth knowledge of the low-temperature hydrothermal synthesis of nanocrystalline hydroxyapatite from waste green mussel shell (Perna Viridis). 1-13	O
99	A new procedure for separating a multi-component powder diffraction pattern into individual component patterns without utilizing the pattern model for one of the components. <b>2023</b> , 56, 263-274	O
98	Effect of tempering temperature and grain refinement induced by severe shot peening on the corrosion behavior of a low alloy steel. <b>2023</b> , 932, 117207	O
97	Structural features, dissolution performance and anthelmintic efficacy of multicomponent solid forms of fenbendazole with maleic and oxalic acids. <b>2023</b> , 25, 1301-1312	O
96	Single-Crystal Terbium Silicate Chloride CoreBhell Nanowires and Nanotubes for Monolithically Integrated Optoelectronics. <b>2023</b> , 6, 2963-2971	O
95	Mineralogy and geochemistry of pattern formation in zebra rock from the East Kimberley, Australia. <b>2023</b> , 622, 121336	О
94	Boosting Xe/Kr separation by a Mixed-linker strategy in Radiation-Resistant Aluminum-Based Metal TDrganic frameworks. <b>2023</b> , 311, 123335	O

93	Evaluation of the Sr2TiSi2O8 ceramic matrix for radiofrequency and microwave applications. <b>2023</b> , 34,	О
92	Effects of Ho doping on the structural, dielectric, and magnetic properties of GdMnO3 ceramics. <b>2023</b> , 34,	О
91	The 8-Hydroxyquinolinium Cation as a Lead Structure for Efficient Color-Tunable Ionic Small Molecule Emitting Materials. <b>2023</b> , 4, 2200279	О
90	Improving the Accuracy of Small-Molecule Crystal Structures Solved from Powder X-Ray Diffraction Data by Using External Sources. <b>2023</b> , 106,	О
89	Annealing Temperature Effects on Structural, Magnetic, and Optoelectronic Properties of Mixed Ni0.6Mg0.2Co0.2FeCrO4 Ferrites. <b>2023</b> , 52, 2878-2893	O
88	Enhanced magnetocaloric effects in metastable phases of Mn1\(\mathbb{R}\)CoxNiGe generated through thermal quenching and high-pressure annealing. <b>2023</b> , 133, 065104	О
87	Abnormal Eu3+ -Æu2+ Reduction in Ca9MmxEu(PO4)7 Phosphors: Structure and Luminescent Properties. <b>2023</b> , 16, 1383	O
86	Computational evaluation of halogen-bonded cocrystals enables prediction of their mechanochemical interconversion reactions. <b>2023</b> , 14, 3140-3146	О
85	Mineralizing CO2 and producing polymorphic calcium carbonates from bitumen-rock asphalt manufacturing solid residues. <b>2023</b> , 12, 100602	O
84	Autogenous deformation induced- stress evolution in high-volume GGBFS concrete: Macro-scale behavior and micro-scale origin. <b>2023</b> , 370, 130663	О
83	Evaluation of bimodal microstructures in selective-laser-melted and heat-treated Ti-6Al-4V. <b>2023</b> , 227, 111700	O
82	Cold Compaction Behavior of Unsaturated Titanium Hydride Powders: Validation of Two Compaction Equations. <b>2023</b> , 13, 360	О
81	Synthesis and Nanostructure Investigation of Hybrid ∰a 2 O 3 /ZnGa 2 O 4 Nanocomposite Networks with Narrow-Band Green Luminescence and High Initial Electrochemical Capacity. 2207492	0
80	Non-destructive structural studies of coins from the Uzundara Fortress using X-ray diffraction and neutron tomography. <b>2022</b> , 6, 256-265	О
79	Hot Corrosion Behavior of TWAS and HVOF NiCr-Based Coatings in Molten Salt. 2023, 16, 1712	1
78	Mechanochemical Modification of Nickel Aluminide with Aluminum Oxide. <b>2022</b> , 95, 1125-1128	О
77	CobaltBamarium Oxide Composite as a Novel High-Performance Catalyst for Partial Oxidation and Dry Reforming of Methane into Synthesis Gas.	0
76	Thickness determination of multiphase layer via combined Rietveld and Grazing Incidence X-ray diffraction approach. <b>2023</b> , 770, 139756	О

75	Quantifying structural disorder in spinels by X-ray diffractometry through constrained Rietveld refinements. <b>2023</b> , 49, 18264-18271	0
74	Exploring rare earth mineral recovery through characterization of riebeckite type ore in Bayan Obo. <b>2023</b> , 9, e14060	О
73	A Newly Designed High-Strength Tool Steel with High Wear and Corrosion Resistance. 2023, 16, 1941	O
<del>72</del>	CrystalMELA: a new crystallographic machine learning platform for crystal system determination. <b>2023</b> , 56, 409-419	О
71	Magnetic and electrical properties of high-entropy rare-earth manganites. 2023, 32, 101026	0
70	Straightforward synthesis of monodisperse Co/Zn-based nanoparticles and their antifungal activities on Botrytis cinerea. <b>2023</b> , 13, 035001	О
69	The Relationship between Photoluminescence Emissions and Photocatalytic Activity of CeO2 Nanocrystals. <b>2023</b> , 62, 4291-4303	0
68	Application of a new method for accurate determination of $\oplus$ and $\oplus$ texture in Ti-6Al-4V from synchrotron diffraction intensities. <b>2023</b> , 199, 112769	О
67	Synthesis, structural and optical characterization of LiNbO3 material for optical applications.	0
66	Refinement of the Crystal Structure of Low-Carbon Polycrystalline AISI 420 Martensitic Steel (C = 0.15%). <b>2023</b> , 53,	О
65	Zn-doped Mono- and Biphasic Calcium Phosphate Materials Derived from Agriculture Waste and Their Potential Biomedical Applications: Part I. <b>2023</b> , 16, 1971	0
64	Antiferromagnetism and Structure of Sr1\(\mathbb{B}\)axFeO2F Oxyfluoride Perovskites. <b>2023</b> , 9, 78	O
63	Effect of Double-Step and Strain-Assisted Tempering on Properties of Medium-Carbon Steel. <b>2023</b> , 16, 2121	0
62	Non-invasive evidence of mercury soaps in painted miniatures on ivory. <b>2023</b> , 138,	O
61	Mapping Brazilian soil mineralogy using proximal and remote sensing data. <b>2023</b> , 432, 116413	1
60	Insights into the Fe3+ Doping Effects on the Structure and Electron Distribution of Cr2O3 Nanoparticles. <b>2023</b> , 13, 980	O
59	Hydrothermal Synthesis of Ni3TeO6 and Cu3TeO6 Nanostructures for Magnetic and Photoconductivity Applications. <b>2023</b> , 6, 4887-4897	0
58	Mechanochemical synthesis and structural evaluation of a metastable polymorph of Ti3Sn. <b>2023</b> , 78, 209-214	O

57	Moisture expansion of tuff stones and sandstones. <b>2023</b> , 82,	O
56	Ni-Mg/Al Mixed Oxides Prepared from Layered Double Hydroxides as Catalysts for the Conversion of Furfural to Tetrahydrofurfuryl Alcohol. <b>2023</b> , 5, 571-588	O
55	Effect of Raw Material Particle Size on the Synthesis of La2Zr2O7 by the Molten Salt Method. <b>2023</b> , 62, 4558-4569	0
54	Effects of MgO and Fe2O3 additives on the microstructure and fracture properties of aluminium titanate flexible ceramics. <b>2023</b> ,	Ο
53	Synthesis and Characterization of High-Entropy Dawsonite-Type Structures. <b>2023</b> , 62, 4999-5007	О
52	Monoclinic symmetry of the hcp-type ordered areas in bulk cobalt. <b>2023</b> , 107,	O
51	Dielectric properties of Zn1⊠CuxO0.997N0.003 nanopowders synthesised via solgel method.	O
50	The Effect of Heating Temperature on $\oplus$ - $\oplus$ ? Miscibility and Separation in Fe-25Cr-5Al-RE Alloy. <b>2023</b> , 13, 597	O
49	A new ternary molybdenum phospho-silicide Mo3Si2P: Phase equilibria, structural, electronic, transport and thermal properties. <b>2023</b> , 111328	0
48	Structural forms of hormone auxins in Madeira vines.	Ο
47	Strong Magnetocaloric Coupling in Oxyorthosilicate with Dense Gd3+ Spins. <b>2023</b> , 62, 5282-5291	O
46	Mercury Clathration-Driven Phase Transition in a Luminescent Bipyrazolate Metal <b>©</b> rganic Framework: A Multitechnique Investigation. <b>2023</b> , 35, 2892-2903	O
45	Synthesis of the cerium doped Gd3Al3Ga2O12-based glass nanoceramics: Luminescence and optical absorption properties. <b>2023</b> , 163, 106932	O
44	HIDSAG: Hyperspectral Image Database for Supervised Analysis in Geometallurgy. 2023, 10,	Ο
43	Roman Well-cisterns[INavigational Routes, and Landscape Modifications in the Venice Lagoon and Northeastern Adriatic. 1-25	О
42	The influence of spin state of the Cr ions on the structural and magnetic behavior of orthorhombic LaFe1\( \text{MCrxO3}\) Perovskites (0.0<x<0.5). <b>2023</b> , 34,	O
41	Effect of annealing temperature on the photocatalytic activity of La0.8Nd0.1Sr0.1MnO3 manganite for methyl orange degradation and study of its thermoelectric properties using DFT calculations. <b>2023</b> , 34,	0
40	Polarization induced ferroelectric and magnetic ordering in double-perovskite-based flexible 0B composite. <b>2023</b> , 34,	Ο

39	CO2 Methanation: Solvent-Free Synthesis of Nickel-Containing Catalysts from Complexes with Ethylenediamine. <b>2023</b> , 16, 2616	0
38	Nanofluorapatite Hydrogels in the Treatment of Dentin Hypersensitivity: A Study of Physiochemical Properties and Fluoride Release. <b>2023</b> , 9, 271	О
37	Influence of surfactant on the structural, morphological and optical properties of SrWO4: Insights through electron density distribution analysis. <b>2023</b> , 46,	О
36	Alloyed triple half-Heuslers: a route toward high-performance thermoelectrics with intrinsically low lattice thermal conductivity.	Ο
35	Experimental and Theoretical Investigations of Out-of-Plane Ordered Nanolaminate Transition Metal Borides: M4CrSiB2 (M = Mo, W, Nb). <b>2023</b> , 62, 5341-5347	О
34	Neutron and muon characterisation techniques for battery materials.	О
33	Polarizable Anionic Sublattices Can Screen Molecular Dipoles in Noncentrosymmetric Inorganic Drganic Hybrids. <b>2023</b> , 15, 18006-18011	О
32	Oxygen-Redox Activity in Non-Lithium-Excess Tungsten-Doped LiNiO2 Cathode. <b>2023</b> , 2,	O
31	Electrochemical properties of the CaNi 4 . 8 M 0.2 (M?Mg, Zn, and Mn) mechanical milling alloys used as anode materials in nickel-metal hydride batteries.	О
30	Reactive spark plasma sintering of the hexacelcian barium aluminosilicate phase 2023,	O
29	Oxygen Vacancy Migration in Ca2Ga2+xGe1🛭O7D.5x Melilite. <b>2023</b> , 6, 3986-3995	О
28	Enhanced Thermoelectric Performance of Tin(II) Sulfide Thin Films Prepared by Aerosol Assisted Chemical Vapor Deposition.	О
27	Crystal packing driven comparable thermal expansion of a biimidazole-based energetic material.	О
26	Effect of Lithium Substitution on the Structural, Magnetic, and Magnetocaloric Properties of La0.7Sr0.3-xLixMnO3 (0 $\/R$ $\/L$ 0.15).	О
25	A NEW APPROACH TO THE ANALYSIS OF CLAY MINERALS IN ROCKS USING THE X-RAY SCATTERING METHOD: DIFFERENT RATIO OF CLAY MINERALS. <b>2023</b> , 9	О
24	Bulk Synthesis and Transport Properties of Rocksalt-Type Ti1MgxN Solid Solution. <b>2023</b> , 62, 5951-5960	O
23	Soil Minerals. <b>2023</b> , 39-104	0
22	New Zintl Phase Yb 10 MgSb 9 with High Thermoelectric Performance.	O

21	Influence of the hierarchical architecture of multi-core iron oxide nanoflowers on their magnetic properties. <b>2023</b> , 13,	O
20	Effect of rare earth Nd substitutions on the structural, dielectric, ferroelectric, and electrical characteristics of Pb1 IkNdx(Fe0.5Nb0.5)1 Ik/4O3 ceramics. <b>2023</b> , 129,	O
19	Performance of Sm-doped TiO2 in photocatalytic antibiotic degradation and photocatalytic CO2 reduction.	O
18	Synthesis, Crystal Structures, Thermal and Magnetic Properties of Mn(NCS)2 Coordination Compounds with 3-Cyanopyridine. <b>2023</b> , 121495	O
17	ZnWO4 nanocrystals prepared by thermal plasma processing.	0
16	Resulting Effect of the p-Type of ZnTe: Cu Thin Films of the Intermediate Layer in Heterojunction Solar Cells: Structural, Optical, and Electrical Characteristics. <b>2023</b> , 16, 3082	O
15	Geochronology, Mineralogy, and Geochemistry of the Tonsteins from the Permo-Carboniferous Benxi Formation, Ordos Basin, North China Craton.	0
14	Effects of the substitution by copper on structural, optical and dielectric properties of the spinel LiFe2O4. <b>2023</b> , 127753	O
13	Gowanus Canal Superfund Site. V: Evaluation of ISS Cylinder Sample Crusts Formed During EPA 1315M Testing. <b>2023</b> , 27,	0
12	Comparison of Quantitative X-ray Diffraction Mineral Analysis Methods. <b>2023</b> , 13, 566	О
11	Unveiling the secret of ancient Maya masons: Biomimetic lime plasters with plant extracts. <b>2023</b> , 9,	0
10	Fabrication and optical properties of transparent fine-grained Zn1.1Ga1.8Ge0.1O4 and Ni2+ (or Cr3+)-doped Zn1.1Ga1.8Ge0.1O4 spinel ceramics. <b>2023</b> ,	O
9	Halogenation of IAA by touch stimulus for rapid and differential growths of the Madeira vine.	О
8	Metamorphic reactions and their implication for the fluid budget in metapelites at seismogenic depths in subduction zones. <b>2023</b> , 229844	O
7	Structure, Oxygen Mobility, and Electrochemical Characteristics of La1.7Ca0.3Ni1 - xCuxO4 + ① Materials. <b>2023</b> , 59, 37-48	0
6	Structural and magnetic properties of Fe-Ti-O solid solution prepared by ball-milling and post annealing. <b>2023</b> ,	O
5	Rapid determination of solid-state diffusion coefficients in Li-based batteries via intermittent current interruption method. <b>2023</b> , 14,	O
4	All bio-based chiral nematic cellulose nanocrystals films under supramolecular tuning by chitosan/deacetylated chitin nanofibers for reversible multi-response and sensor application. <b>2023</b> , 143148	O

The Role of Protective Surface Coatings on the Thermal Stability of Delithiated Ni-Rich Layered Oxide Cathode Materials. 2023, 9, 245

Observation of ferrimagnetic ordering in chemically synthesized 2D Cr2S3 nanosheets. 2023, 133,

Magnetocaloric Effect in LA1.2R0.2CA1.6MN2O7 (R=Tb, Dy, Ho, Er) Perovskites Synthesized by Sol-Gel Method. 2022, 67, 9-16